THE IMPACT OF VEGETATION ON THE ATMOSPHERIC BOUNDARY LAYER AND CONVECTIVE STORMS

Tsengdar J. Lee

Roger A. Pielke, P.I.
NSF Grant # ATM-8915265
USGS Award # 14-08-0001-A0929

Colorado State University

DEPARTMENT OF ATMOSPHERIC SCIENCE

PAPER NO. 509

THE IMPACT OF VEGETATION ON THE ATMOSPHERIC BOUNDARY LAYER AND CONVECTIVE STORMS

Tsengdar J. Lee

Department of Atmospheric Science
Colorado State University
Fort Collins, Colorado
Fall, 1992

Atmospheric Science Paper No. 509

ABSTRACT

THE IMPACT OF VEGETATION ON THE ATMOSPHERIC BOUNDARY LAYER AND CONVECTIVE STORMS

The impact of vegetation on atmospheric boundary layer and convective storms is examined through the construction and testing of a soil-vegetation-atmosphere transfer (SVAT) model.

The Land Ecosystem-Atmosphere Feedback (LEAF) model is developed using an elevated canopy structure, an above–canopy aerodynamic resistance, two in–canopy aerodynamic resistances, and one stomatal conductance functions. The air temperature and humidity are assumed to be constant in the canopy whereas the wind and radiation follow a specified vertical profile. A simple dump-bucket method is used to parameterize the interception of precipitation and a multi-layer soil model is utilized to handle the vertical transfer of soil water. Evaporation from soil and wet leaves and transpiration from dry leaves are evaluated separately. The soil water uptake is based on soil water potential rather than on the length of roots. Separate energy budgets for vegetation and for the soil are used in order to remove unnecessary assumptions on energy partition between the vegetation and the substrate. Primary parameters are LAI, maximum stomatal conductance, and albedo. Secondary parameters include displacement height and environmental controls on stomatal resistance function.

Due to the complexity of the LEAF model, statistical methods are used to improve LEAF model performance. The Multi-response Randomized Block Permutation (MRBP) procedure is used to guide the choice of model parameter values. The Fourier Amplitude Sensitivity Test (FAST) is applied to better understand the model behavior in response to the changes in model parameters.

Finally, LEAF is used to study the growth of boundary layer and the local thermal circulations generated by surface inhomogeneities. Results show the atmospheric boundary layer is substantially cooler and more moist over unstressed vegetation than over bare dry soil. Thermally forced circulation can result from the juxtaposition of two vegetation types due to different biophysical characteristics. Results from three-dimensional simulations show that the surface spatial heterogeneities made by vegetation play an important role in generating local convective storms.

Tsengdar J. Lee
Department of Atmospheric Science
Colorado State University
Fort Collins, Colorado 80523
Fall 1992

To my parents

ACKNOWLEDGEMENTS

It is with gratitude and appreciation that I would first like to acknowledge Professor Roger A. Pielke, my thesis advisor, for his continuous guidance during the course of this study. His patient and unwavering support is deeply appreciated. Thanks are also due to my other Committee members, Professors Thomas B. McKee, Wayne H. Schubert, and Paul W. Mielke, Jr. Professor Thomas McKee is thanked for many suggestions on measuring and calculating the surface energy budget. He also helped me to better understand the physical controls of the climatic system and terrain effect on local weather. Professor Wayne Schubert is thanked for bringing me into the fascinating world of moist atmosphere and numerical weather prediction. Professor Paul Mielke is thanked for his help in many statistics questions. He also provided the computer code that is used to guide the choice of LEAF model parameters.

I would also like to thank Drs. Timothy Kittel and David Schimel of Natural Resource Ecology Laboratory for their help in ecology and plant physiology. Dr. David Schimel gave the acronym, LEAF, while I was developing the model. Dr. Roni Avissar of Rutgers University is specially thanked for considerable help in land-scape modeling and soil physics. Professor Lewis Grant introduced atmospheric water budget at various scales to me and answered many questions in landscape and agricultural practice, which is gratefully acknowledged.

This thesis work would not have made possible without many other people's help. I would like to thank Drs. Craig Tremback and Bob Walko for providing me the RAMS model code and answering numerous modeling questions. Dr. Marek Uliasz provided the FAST analysis program, which is grateful. My office mate Mike Moran is thanked for countless hours of consulting and his generosity of letting me access to his private

library. My former office mate Dr. Jennifer Cram answered many of my questions on data assimilation and I enjoyed our discussions on model development and management philosophy. Many discussions with my other office mates Cathy Finley and Dr. Xubin Zeng are certainly very helpful. Dr. Paul Wolyn, my former roommate, is thanked for discussions on complex flow over mountainous terrain and for his helpful reviews of the thesis. Tekmeng Wong helped answer many radiative transfer questions which is very appreciated. Mike Meyers is thanked for his advice in microphysics. Dr. Piotr Flatau and Bill Thorson are thanked for taking me into the UNIX world. Dallas McDonald is thanked for preparing part of the manuscript and answering many questions on word processing. Dr. Louis Steyaert and Ms. Jesslyn Brown of U. S. Geological Survey provided the land surface coverage and the NDVI data which have proven to be invaluable.

I received financial support during my stay at Colorado State University from the National Science Foundation Grants ATM-8616662 and ATM-8915265, the Office of Naval Research under Contract N00014-88-K-0029, and the U. S. Geological Survey (USGS), Department of the Interior, under Assistance Award No. 14-08-0001-A0929. The National Center for Atmospheric Research (NCAR) archive of NMC gridded data and upper air and surface observation data were used to initialize the RAMS model for the case study described in Chapter 6; NCAR is supported by the National Science Foundation. The USGS provided substantial support in the development, calibration and testing of LEAF (Chapters 4 and 5), the test and utilization of the USGS land cover characteristic data and in the performance of a case study (Chapters 6 and 7).

Finally, I would like to acknowledge Professor Len-Fu Chang of National Taiwan University for introducing me to the wonderful world of fluid dynamics. I decided my career soon after I took his fluid dynamic and turbulence classes. I wish to thank my wife, Serena, and my in-laws for their encouragement during the last several months of the work. It would be impossible to finish this thesis without Serena's full support at home. I am also grateful to my parents for their standing behind me throughout the years of this study. Their support was deeply appreciated.

TABLE OF CONTENTS

LIST OF TABLES

LIST OF FIGURES

LIST OF ABBREVIATIONS

ABL	Atmospheric Boundary Layer
APAR	Absorbed Photosynthesis Active Radiation
API	Antecedent Precipitation Index
AVHRR	Advanced Very High Resolution Radiometer
BATS	Biosphere-Atmosphere Transfer Scheme
CAPE	Convective Available Potential Energy
CSU	Colorado State University
DEM	Digital Elevation Model
ET	Evapotranspiration
FIFE	First ISLSCP Field Experiment
GIS	Geographic Information System
HAPEX	Hydrologic Atmospheric Experiment
IR	Infrared
ISLSCP	International Satellite Land Surface Climatology Project
LAI	Leaf Area Index
LCL	Lifting Condensation Level
LEAF	Land Ecosystem-Atmosphere Feedback Model
LFC	Level of Free Convection
LSAI	Leaf and Stem Area Index
MCS	Mesoscale Convective System
MRBP	Multi-responses Randomized Block Permutation procedure
NDVI	Normalized Difference Vegetation Index
NMC	National Meteorological Center
NOAA	National Oceanic and Atmospheric Administration
RAMS	Regional Atmospheric Modeling System
UTC	Universal Time Coordinate
USDA	United States Department of Agriculture
USGS	United States Geological Survey
VPD	Vapor Pressure Deficit

LIST OF SYMBOLS

C_H	heat or moisture exchange coefficient (dimensionless)
C_s	aerodynamic transfer coefficient (dimensionless)
c_p	specific heat of air at constant pressure ($J\,deg^{-1}\,kg^{-1}$)
d	displacement height (m)
d_s	stomatal conductance ($m\,s^{-1}$)
d_{smax}	maximum stomatal conductance ($m\,s^{-1}$)
d_{smin}	minimum stomatal conductance ($m\,s^{-1}$)
d_{rs}	relative stomatal conductance (dimensionless)
E	water vapor flux ($kg\,s^{-1}\,m^{-2}$)
E_c	canopy water vapor flux ($kg\,s^{-1}\,m^{-2}$)
E_{evap}	water vapor flux due to evaporation ($kg\,s^{-1}\,m^{-2}$)
E_g	ground water vapor flux ($kg\,s^{-1}\,m^{-2}$)
f_C	CO_2 stress function (dimensionless)
f_R	global solar radiation stress function (dimensionless)
f_{T_c}	temperature stress function in cold range (dimensionless)
f_{T_h}	temperature stress function in hot range (dimensionless)
f_V	vapor pressure deficit stress function (dimensionless)
f_Ψ	soil water stress function (dimensionless)
G	ground heat flux ($W\,m^{-2}$)
H	sensible heat flux ($W\,m^{-2}$)
H_c	canopy sensible heat flux ($W\,m^{-2}$)
H_g	ground sensible heat flux ($W\,m^{-2}$)
h	potential leaf-air transfer coefficient ($m\,s^{-1}$)
h	canopy height (m)
K	leaf-air transfer coefficient ($m\,s^{-1}$)
k	von Karman's constant (dimensionless)
LAI	leaf area index ($m^2\,m^{-2}$)
n	decay coefficient for wind profile in the canopy (dimensionless)
P_s	shelter coefficient (dimensionless)
Q_{sc}	absorbed short wave radiative energy by the canopy ($W\,m^{-2}$)
Q_{ss}	absorbed short wave radiative energy by the soil ($W\,m^{-2}$)
Q_{lc}	absorbed long wave radiative energy by the soil ($W\,m^{-2}$)
Q_{ls}	absorbed long wave radiative energy by the soil ($W\,m^{-2}$)
q	specific humidity ($kg\,kg^{-1}$)
q_a	specific humidity at the atmospheric reference level ($kg\,kg^{-1}$)
q_c	specific humidity of the canopy ($kg\,kg^{-1}$)
q_{eff}	effective surface specific humidity ($kg\,kg^{-1}$)
q_g, q_G	specific humidity of the ground ($kg\,kg^{-1}$)
q_{sat}	saturation specific humidity ($kg\,kg^{-1}$)
q_{sfc}	specific humidity at the lower boundary of the atmosphere ($kg\,kg^{-1}$)

q_{veg}	specific humidity of the vegetation ($kg\,kg^{-1}$)
q_*	surface layer humidity scale ($kg\,kg^{-1}$)
R_l	long wave radiative energy reaching the surface ($W\,m^{-2}$)
R_n	net radiation flux ($W\,m^{-2}$)
R_s	short wave radiative energy reaching the surface ($W\,m^{-2}$)
r_a	aerodynamic resistance ($s\,m^{-1}$)
r_b	bulk leaf boundary layer resistance ($s\,m^{-1}$)
r_{bare}	aerodynamic resistance for bare soil ($s\,m^{-1}$)
r_c	canopy resistance ($s\,m^{-1}$)
r_{closed}	aerodynamic resistance for closed canopy ($s\,m^{-1}$)
r_d	soil surface aerodynamic resistance ($s\,m^{-1}$)
r_{plant}	plant resistance ($s\,m^{-1}$)
r_s	stomatal resistance ($s\,m^{-1}$)
r_{soil}	soil surface resistance ($s\,m^{-1}$)
T	temperature (K)
T_a	temperature at the atmospheric reference level (K)
T_c	temperature of the canopy (K)
T_g, T_G	temperature of the ground (K)
T_{sfc}	temperature at the lower boundary of the atmosphere (K)
T_{veg}	temperature of the vegetation (K)
u, u_a	wind speed ($m\,s^{-1}$)
u_f	in canopy wind speed ($m\,s^{-1}$)
u_*	surface friction velocity ($m\,s^{-1}$)
W_{res}	water reservoir depth (m)
W_{max}	maximum water reservoir depth (m)
z_0	surface roughness length (m)
z_0'	soil surface roughness length (m)
z_{ref}	atmospheric reference height (m)
α_T	total surface albedo (dimensionless)
α_s	soil surface albedo (dimensionless)
α_v	vegetation albedo (dimensionless)
γ	psychrometric constant (K^{-1})
Δ	rate of change of saturated mixing ratio with temperature (K^{-1})
ϵ_g	ground surface emissivity (dimensionless)
ϵ_v	vegetation emissivity (dimensionless)
θ_{eff}	effective surface potential temperature (K)
θ_{veg}	potential temperature of the leaves (K)
θ_*	surface layer temperature scale (K)
λ	latent heat of vaporization ($J\,kg^{-1}$)
λE	latent heat flux ($W\,m^{-2}$)
ρ	agreement measure (dimensionless)
ρ_a	air density ($kg\,m^{-3}$)
σ	critical value of LSAI for closed canopy ($m^2\,m^{-2}$)
σ_f	shielding factor or fractional coverage of leaves (dimensionless)
σ_f'	relative contribution from the vegetation (dimensionless)
σ_{wet}	fractional coverage of wet leaves (dimensionless)
τ_v	vegetation transmittance (dimensionless)

Ψ	soil water potential (Pa)
Ψ_M	stability function for momentum transfer (dimensionless)
Ψ_M	stability function for heat and moisture transfer (dimensionless)
Ω	leaf age function (dimensionless)

Chapter 1

INTRODUCTION

It is well known that virtually all motions in the atmosphere are ultimately fueled by energy received from the sun. Incoming solar energy can be absorbed in the atmosphere directly by gases, clouds or aerosols. However, much of this energy is absorbed at the earth's surface and returned to the atmosphere as sensible and latent heat fluxes. In other words, energy is supplied into the atmosphere mainly through surface-to-atmosphere exchange processes. Obviously, the amount of energy exchange is highly dependent on the surface characteristics and their spatial distributions. Various scales of atmospheric motion have been found due to the spatial variation of the surface turbulent heat fluxes. Coherent structures, like Hadley and monsoon circulations on the larger scales; sea-breeze and mountain-valley breeze circulations on the smaller scales, are all driven by surface forced thermal contrasts. On the microscale, Hadfield et al. (1992a,b) and Walko et al. (1992) also find that organized thermals in the atmospheric boundary layer are influenced by even relatively small-scale surface inhomogeneities. It has been proposed that the predictability of atmospheric motions should increase when coherent structures exist (Pielke et al., 1991; Zeng, 1992).

Since most land surfaces are covered by vegetation, it is reasonable to assume vegetation should have an important impact on the atmospheric boundary layer. The existence of vegetation not only generates surface inhomogeneities but also modifies the structure of the atmospheric boundary layer. The evapotranspiration process extracts water from deep soil layers and transfers this moisture into the atmosphere which results in an enrichment of moisture in the atmospheric boundary layer. Convective clouds are found once parcels of air in the boundary layer are lifted to the lifting condensation level (LCL). If the air

parcel is lifted beyond the level of free convection (LFC), deep cumulus clouds can form. Depending on the atmospheric conditions, these deep cumulus clouds can further be organized into cumulus convective complexes. It can be seen from the above arguments that the existence of vegetation can provide moisture to the atmospheric boundary layer and lower the LCL and LFC. It also provides the potential to lift the boundary layer air parcel above the LCL through (a) enhanced vertical mixing due to the larger surface roughness length, and (b) surface convergence due to the thermal contrast between different surface covers. A recent study by Chang and Wetzel (1991) has demonstrated the importance of vegetation in modifying a pre-storm environment.

It has been proposed that the landscape created by the existence of vegetation is important in the structure of the atmospheric boundary layer and the onset of convective storms. Based on low level flight measurements, Segal et al. (1989) have shown that the atmospheric boundary layer is shallower, cooler, more moist and less turbulent over irrigated crop land than over adjacent bare soil surface. An observational study by Rabin et al. (1990) has shown that convective clouds are first formed over a harvested wheat field surrounded by growing vegetation. Clouds are also suppressed immediately downstream of lakes and forests. It has also been speculated that the observed precipitation peak in the growing season may be due, in part, to the recycling of water locally (Koster et al., 1986). In order to forecast the weather more correctly, a representation of the vegetated surface and a complete hydrological cycle are necessary in a numerical weather prediction model. In fact, it has also been hypothesized that the atmosphere is actually regulated by the biosphere (GAIA hypothesis; Lovelock, 1979). It is necessary, therefore, to understand biosphere-atmosphere interactions in order to understand climate change.

In this dissertation we will examine the impact of vegetation on the atmospheric boundary layer and convective storms through the construction and testing of a land surface Soil-Vegetation-Atmosphere Transfer (SVAT) model. Numerical experiments are performed to validate the model and the model results are compared between simulations with and without vegetation.

A review of previous observational and modeling studies of soil-vegetation-atmosphere exchange process is given in Chapter 2 of this study. A brief review of previous models

and technical studies is also provided. The history and formulation of the current Land Ecosystem-Atmosphere Feedback (LEAF) model used in this study is discussed in Chapter 3. The validation of the model and a sensitivity analysis of model parameters are reported in Chapter 4. Results from a number of two-dimensional model simulations are presented in Chapter 5. The sensitivity of atmospheric boundary layer structure and convective storms on the existence of vegetation is discussed in this Chapter while a case study over the Colorado eastern High Plain is reported in Chapter 6. Finally, Chapter 7 presents conclusions from the results of this study. A discussion of several modeling problems and future work is also presented.

Chapter 2

BACKGROUND

The momentum, heat and moisture exchange processes at the ground-surface and atmosphere interface are very complex especially when vegetation is present. The atmosphere responds to these energy and momentum exchanges and develops local circulations. In this Chapter, previous studies on the significance of vegetation on atmospheric circulations are briefly overviewed and followed by a discussion on modeling the soil-vegetation-atmosphere transfer processes.

2.1 Significance of Vegetation on Atmospheric Circulations

Atmospheric processes are sensitive to surface characteristics, since the Earth's surface is the boundary of the atmosphere at which momentum, energy, water, and other chemical substances are exchanged between the earth and the atmosphere. The surface characteristics play an important role in partitioning the incoming net radiation into turbulent energy fluxes returned to the atmosphere. Generally, the atmospheric boundary layer is deeper when the sensible heat flux is large and is shallower when the sensible heat flux is small. The significance of surface forcing to the weather and climate has long been well recognized, for example, in the famous work on numerical weather prediction, Richardson (1922) noted:

> *"The atmosphere and the upper layers of the soil or sea form together a united system. This is evident since the first meters of ground has a thermal capacity comparable with 1/10 that of the entire atmospheric column standing upon it, and since buried thermometers show that its changes of temperature are considerable. Similar considerations apply to the sea, and to the capacity of the soil for water."*

A simple sensitivity analysis (Pielke et al., 1991b), showed that a small change of surface albedo can result in a change of equilibrium atmospheric temperature as large as the

proposed greenhouse warming effect. Using a global GCM (General Circulation Model) equipped with a land-surface vegetation scheme, Mylne and Rowntree (1992) has shown the albedo feedback is important in tropical climate associated with deforestation. Thomas and Rowntree (1992) found that the multiple feedback between albedo, evaporation, and precipitation, in the boreal forest of North America, has a major climatic impact on the entire northern hemisphere.

Because these surface exchanges provide the primary source of energy for atmospheric motion, there has been numerous studies trying to understand these exchange processes and the atmospheric response to the surface characteristics. For the land surface, earlier experiments, including the Great Plains experiment (Lettau and Davidson, 1957), the Wangara experiment (Clarke et al., 1971), the Kansas experiment (Izumi, 1971), and the Minnesota experiment (Izumi and Caughey, 1976), address the momentum and heat fluxes in the surface layer. The surface layer similarity theory proposed by Monin and Obukhov (1954) was validated in these experiments. The formulation of exchange coefficient proposed by Businger et al. (1971) based on the Kansas experiment is one of the most widely used formulae to calculate atmosphere and land surface momentum and heat transfer. These experiments have addressed the problem of heat and momentum transfer over flat and homogeneous surface conditions. Lately, experiments have been designed to study more complicated surface conditions. The First ISLSCP (International Satellite Land Surface Climatology Project) Field Experiment (FIFE) has been designed to study the land surface climatology, including heat, moisture and trace gas exchange, biophysical and hydrological properties of the surface, using remote sensing techniques (Sellers et al., 1986). The HAPEX-MOBILHY (Hydrologic Atmospheric Experiment – Modélisation du Bilan Hydrique) program has been designed to study surface evaporation over a GCM grid area (André et al., 1986), which includes surface inhomogeneities. These experiments start to address the problem of inhomogeneous surface characteristics including (and perhaps the most important) the existence of vegetation.

The significance of vegetation on atmospheric circulations can also be see from Table 2.1 where the annual evaporation rate is measured using buried lysimeters. A surprising

Surface	Annual evaporation total (mm)
grass	1296
wet soil	939
water	1096

Table 2.1: Summary of annual evaporation data at Aspendale, Australia taken from Sellers (1965).

result is that the average evaporation total from grass covered lysimeters is the largest (even larger than what is from water filled lysimeters). This result shows that the existence of grass has increased the total evaporating surface and induced more turbulence due to the higher surface roughness length. When comparing to the evaporation measured from wet bare soil, the average evaporation from grass filled lysimeters is nearly 40 percent higher. By comparing many historical rain fall and run-off data, Brooks (1928) concluded that by replacing bare soil by forest, the local rainfall can be increased by as much as 2 percent. Using a coarse resolution GCM, Rind (1982) demonstrated that soil moisture availability at the beginning of the summer months has a great impact on the projected summertime climate. Numerical experiments performed by Walker and Rowntree (1977), and Rowentree and Bolton (1983) have shown that soil moisture anomalies can have a major impact on rainfall, humidity and temperature predictions. Similar results are also concluded by Manabe and Holloway (1975), Charney et al. (1977), and Shukla and Mintz (1982). Graetz (1991) studies the potential feedback on global atmospheric and climate change of climate-driven changes in terrestrial vegetation by relating the surface exchanges of energy, mass and momentum to two dimensions of vegetation structure and taxonomy. He concluded vegetation structure exerts the greatest influence on the exchange of momentum and radiation with the atmosphere. Using satellite and surface precipitation data, Otterman (1974, 1977) and more recently Otterman et al. (1990) show an increase rainfall in southern Israel following afforestation, increased cultivation and limitations on grazing. Garratt (1992) summarizes the sensitivity of climate simulations to land-surface characteristics and suggests the inclusion of vegetation ensures the combined impact of roughness, albedo and soil moisture availability upon simulated climate. He also suggests

that canopies tend to be rougher and less reflective than bare soil. They also prevent the near-surface region from drying out and can access the deep soil moisture. As a conclusion of his review, he lists the canopy effect and surface hydrology as a high priority need in general circulation models. Sud et al. (1992) study the amount of convective rainfall associated with increased surface roughness due to vegetation. They conclude that the higher surface roughness would increase convective rainfall not even considering the positive feedback from moisture convergence.

On the smaller scale, Anthes (1984) hypothesizes, using a linear model, that planting vegetation with 50 to 100 km bands in semi-arid regions could alter local atmospheric circulation and result in increases of convective precipitation. Three mechanisms are proposed to be responsible for this increase of rainfall: (1) increase of low-level moist static energy, (2) generation of a mesoscale vertical circulation by differential heating, and (3) increase of atmospheric water vapor through decreased runoff and increased evaporation due to the interception of precipitation by leaves. This hypothesis is later reconfirmed by numerous modeling studies including Yan and Anthes (1987).

It has been shown in modeling (e.g., Ookouchi et al., 1984; Segal et al. 1988; Avissar and Pielke, 1989; Pielke and Avissar, 1990; and Pielke and Segal, 1986) and observational studies (e.g. Segal et al. 1989; Pielke and Zeng, 1989; and Pielke et al. 1990) that the partitioning of sensible and latent heat fluxes into different Bowen ratios as a result of spatially varying landscape (e.g. soil moisture, and vegetation type) can significantly influence lower boundary layer structure and result in mesoscale circulations as strong as a sea breeze. Avissar and Pielke (1991) has also specifically demonstrated that sea–breeze–like circulation can be induced due to a spatial inhomogeneity in plant stomatal control. Over and adjacent to irrigated land in the semi-arid west, for example, enhanced cumulonimbus convection can result (Pielke and Zeng, 1989). Schwartz and Karl (1990) document how the appearance of transpiring leaves on vegetation in the spring has the effect of substantially cooling (and thus moistening) the lower atmosphere. In their observational study, Rabin et al. (1990) has shown that, when the lower atmosphere is less humid, convective clouds are formed first over a harvested wheat field surrounded by growing vegetation. Clouds are

also suppressed immediately downstream of lakes and forests. On the other hand, when the lower atmosphere is more moist, clouds are first form over lakes and forest where additional moisture for saturation condensation is available from evaporation. Pielke et al. (1991) present a procedure to represent this spatial landscape variability as a subgrid-scale parameterization in general circulation models. Recent evidence has suggested that vegetation and land-use pattern changes may have already altered the weather and climate on the local and regional scale as illustrated by Pielke et al. (1990), in which they illustrate observed variations in photosynthetically active vegetation, as measured by NDVI (Normalized Difference Vegetation Index) satellite imageries over the northern Great Plains of the U.S. Presumably, active vegetation is transpiring efficiently during the daytime while the other areas with very low vegetation cover or vegetation under water stress have most of their turbulent heat flux in sensible heat transfer. The satellite imageries confirm the existence of large spatial and temporal variability of photosynthetically-active vegetation, suggesting large corresponding variability in sensible heat flux.

The link between convective clouds and vegetation has also drawn considerable attention over the years. Using a mesoscale model with an explicit vegetation parameterization, Garrett (1982) suggests that surface parameters such as soil moisture, forest coverage and transpiration, and surface roughness may affect the formation of convective clouds and rainfall through their effect on boundary-layer growth. The sensitivity studies by Wetzel and Argentini (1990), and Argentini et al. (1992) have show that the daytime low level cloud amount is sensitive to vegetation cover, soil moisture and atmospheric stability. Schädler (1990) has shown that surface moisture inhomogeneities can trigger atmospheric circulation and form convective clouds. The fine scale boundary-layer cloud model study by Smolarkiewicz and Clark (1985) also shown that the low-level cumulus cloud formation is sensitive to surface soil moisture and vegetation coverage. The numerical model study by Chang and Wetzel (1991) has shown that realistic vegetation and soil moisture parameterization is necessary to best forecast storm precursor conditions.

2.2 Modeling of Soil-Vegetation-Atmosphere Interaction

After recognizing the importance of surface characteristics on atmospheric circulation and numerical weather prediction, Richardson (1922) went on to discuss the possible treatments of three principle surface covers, namely the sea, bare soil surfaces, and vegetation covered surfaces. For land surfaces, Richardson considered the motion of water in soil, the transfer of heat in soil, and evapotranspiration. He described the physics in the soil-vegetation-atmosphere transfer as:

> *"Leaves, when present, exert a paramount influence on the interchanges of moisture and heat. They absorb the sunshine and screen the soil beneath. Being very freely exposed to the air they very rapidly communicate the absorbed energy to the air, either by raising its temperature or by evaporating water into it. ... A portion of rain, and the greater part of dew, is caught on foliage and evaporated there without ever reaching the soil. Leaves and stems exert a retarding friction on the air, ..."*

It has been seventy years since Richardson published his book on numerical weather prediction and the idea of treating the exchange processes in the soil-vegetation-atmosphere continuum is still the same, except that many of the detailed physical and biophysical processes have become understood over the years. New model parameters have been introduced. For example, the relation between the leaf area index (LAI, which is the area of transpiring surface in a vertical column above a unit ground surface area) and the stomatal conductance (Jarvis and McNaughton, 1986) and between the root zone water stress and the evapotranspiration (ET) (Kramer, 1949) are parameterized in recent land surface models. It should be noted that even the ideas of introducing the LAI and the root zone water stress were briefly mentioned in Richardson's book.

2.2.1 Resistance/Conductance Functions

The primary goal of building a soil-vegetation-atmosphere transfer model is to provide a realistic boundary forcing to the atmosphere. This is accomplished through parameterizing the surface fluxes of momentum, sensible heat, and latent heat. A resistance (or conductance) function, when calculating these fluxes, is usually introduced analogous to

the Ohm's law in electricity:

$$\text{flux} = \frac{\text{potential difference}}{\text{resistance}}, \text{ or} \tag{2.1}$$

$$\text{flux} = \text{conductance} \times \text{potential difference}. \tag{2.2}$$

This concept of resistance/conductance function has generally been adopted in the communities of agricultural engineering and hydrology. For instance, analogous to the electric conductance, the rate of transpiration is proportional to the stomatal conductance and the vapor pressure difference between the intercellular space and the air within the canopy (henceforth referred to as the canopy-air). Depending on the complexity of the model, other resistance functions include aerodynamic resistance, canopy resistance, root resistance, soil surface resistance, *etc.* A simple relationship exists between the resistance and the conductance:

$$\text{conductance} = \frac{1}{\text{resistance}}. \tag{2.3}$$

For the rest of this dissertation, we will generally use "resistance" form except when discussing the measurement on stomatal conductance made by Avissar et al. (1985).

Stomatal Resistance Function

Consider a highly simplified soil-plant-atmosphere system as shown in Figure 2.1, in which the ground is completely covered by a horizontally homogeneous layer of vegetation. Unlike the direct transfer of heat between vegetation and the atmosphere (as shown on the left hand side of the Figure 2.1), two different processes are involved in transferring water vapor. First, water vapor escapes from the interior chamber (sub-stomatal cavity) of the vegetation to the surface of the leaf (i.e. from point A to point B shown in Figure 2.1) through a small opening (i.e. stoma) on the leaf surface. The amount of the water vapor flux (and hence the amount of latent heat flux) is controlled by the size of the stomatal opening. This process in turn regulates the temperature of the leaves and hence the sensible heat flux to the atmosphere.

Assuming this stomatal opening can be parameterized by a single stomatal resistance function, r_s, the water-vapor-flow to the leaf surface is:

$$E_{A \to B} = \rho_a \frac{q_{veg} - q_{sat}(T_{veg})}{r_s}, \tag{2.4}$$

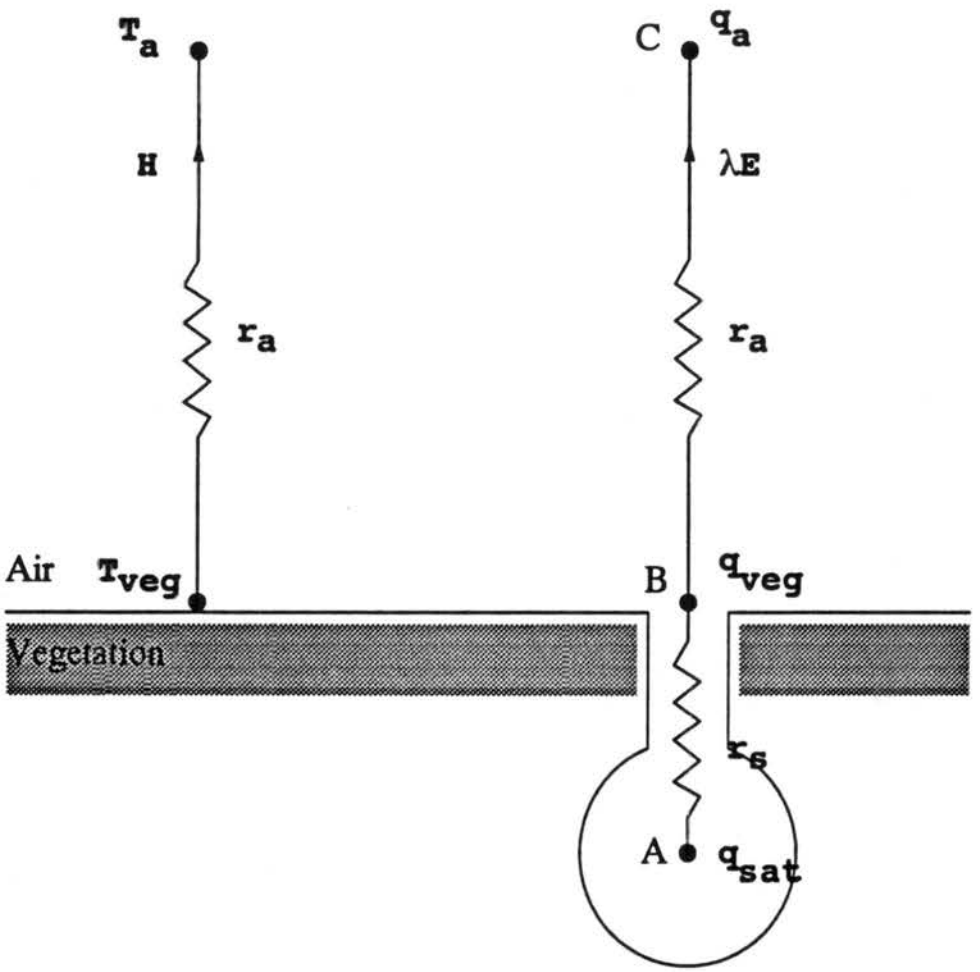

Figure 2.1: Schematic representation of a vegetated surface at uniform temperature T_{veg}. The latent heat flux λE must pass through the stomatal resistance r_s as well as an aerodynamic resistance r_a.

where q_{veg} is the specific humidity at the surface of the leaves, and $q_{sat}(T_{veg})$ is the saturation specific humidity at the intercellular space with the temperature of the leaves, T_{veg}. Variable ρ_a is the density of the air.

The stomatal resistance is regulated by the enzyme kinetic mechanism to optimize the gain of carbon and minimize the lose of water and other resources (Collatz et al., 1991; Sellers et al., 1992). The stomatal opening responses to the changing environment in the following ways

1. it opens only when the leaf receives enough photosynthetically active radiation (PAR);
2. it opens when the leaf-temperature is larger than a threshold value;
3. it opens when the CO_2 concentration in the air at the leaf-surface is large enough to permit CO_2 to diffuse into the leaf; and
4. it closes when the leaf suffers water stress.

Two forms of water stress, i.e. vapor pressure deficit (VPD[1]) and soil water potential (SWP) are usually considered. The stoma close when the leaf looses water faster than water can be supplied from the root. The VPD is directly proportional to the lose of water and the SWP determines the supply of water. When SWP[2] is too large, the plant is permanently wilted and a threshold value is called the permanent wilting-point. Figure 2.2 shows the response of stomatal resistance to the environmental variables.

Aerodynamic Resistance Function

Between points B and C in Figure 2.1, the water vapor flux is regulated by the stability and the turbulence of the air flow. An aerodynamic resistance, r_a, is usually

---

[1]Specifically, VPD is defined as the vapor pressure difference between the sub-stomatal cavity and the air immediately above the leaf surface.

[2]Actually, negative SWP is too large. SWP is negatively defined and is the amount of suction needed to extract water from a soil sample.

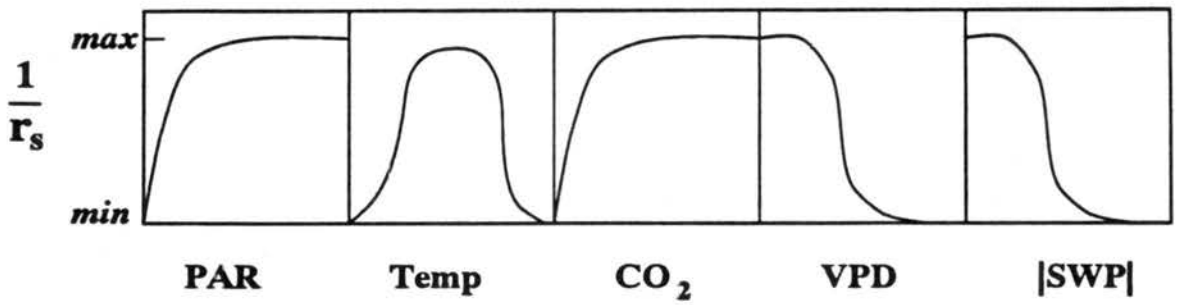

Figure 2.2: The response of stomatal resistances, r_s, to environmental variables. Variable PAR is photosynthetically active radiation, $TEMP$ is leaf temperature, CO_2 is the concentration of CO_2, VPD is vapor pressure deficit, and SWP is soil water potential.

used to parameterize this process so that the water vapor flow from the leaf-surface to the canopy-air is represented as

$$E_{B\to C} = \rho_a \frac{q_a - q_{veg}}{r_a}. \tag{2.5}$$

This aerodynamic resistance is also called boundary-layer resistance since it represents primarily a boundary-layer exchange process of air flow over a leaf.

If we further assume there is no accumulation of water vapor at the surface of the leaves (i.e. $E_{A\to B} = E_{B\to C}$), we obtain:

$$E = \rho_a \frac{q_a - q_{sat}}{r_a + r_s}. \tag{2.6}$$

In this equation E is the evaporation rate from the intercellular space to the canopy-air.

For the sensible heat flux, only the aerodynamic resistance function is important and the resulting heat flux between the leaf surface and the atmosphere is:

$$H = \rho_a c_p \frac{T_a - T_{veg}}{r_a}, \tag{2.7}$$

where H is the sensible heat flux and T_a is the temperature of the canopy-air.

Leaf and Bulk-Boundary-Layer Resistance Functions

Conceptually, the above stomatal and aerodynamic resistance functions are only for a small portion of a leaf which contains a single stoma. Depending on the location on a leaf and the impinging air flow direction, different stomatal and aerodynamic resistances can

be found on different portions of the leaf. However, it is extremely difficult to measure the exact stomatal resistance. Practically, at least one leaf is used in a leaf-chamber to measure an "integrated stomatal resistance" or "leaf resistance" and this leaf resistance is very often also called stomatal resistance instead. Notice that water vapor can actually escape from the leaves without going through the stomata. The resistance for this alternative pathway, i.e. from the epidermic cells via the cuticle, however, is orders of magnitude larger than the stomatal resistance and is often included in the leaf resistance. The value for the leaf resistance is species dependent and can be found in Rutter (1975). Typically, the leaf resistance is smaller (around 25 to 150 $s\,m^{-1}$) for herbaceous agricultural plants and larger (200 to 1000 $s\,m^{-1}$) for trees.

The aerodynamic resistance function also needs to be modified when considering a whole leaf. The size and the shape of the leaf must be taking into account. Usually, depending on the shape of the leaves, the aerodynamic resistance function is parameterized according to laboratory measurements of air flow around a cylinder or a plate (Thom, 1972; Dickinson et al., 1986) and the final "leaf-scale" aerodynamic resistance is sometimes called bulk-boundary-layer resistance (Sellers et al., 1986).

Canopy Resistance Function

When considering a whole canopy, the stomatal (leaf) resistance function must be scaled up again. A canopy resistance function, r_c, is often used to represent the scaled-up stomatal resistance function and is given by

$$r_c = \frac{r_s}{LAI}. \tag{2.8}$$

The canopy resistance represents the effective stomatal resistance per unit ground surface area.

2.2.2 Model Structures

Depending on the complexity of a soil-plant-atmosphere model, different model structures are used. A one-layer model treats soil and vegetation together as a single lower boundary of the atmosphere. The two-layer model treats soil and vegetation separately and the multi-layer model further divides vegetation into several layers.

The most well known example of the one-layer model is the Penman-Monteith (Penman, 1948; Monteith, 1965) model. Recognizing that heat must be supplied externally to convert water into water vapor and that diffusion must take place to transfer water vapor away from the evaporating surface. The Penman-Monteith model has the following form:

$$\lambda E = \frac{\Delta(R_n - G) + \rho_a c_p (q_a - q_{sat})/r_a}{\Delta + \gamma(r_c/r_a)} \tag{2.9}$$

where Δ is the rate of change of saturated mixing ratio with temperature, $\gamma = c_p/\lambda$ is the psychrometric constant, R_n is the net radiation absorbed by the surface, and G is the ground heat flux. A canopy resistance and an aerodynamic resistance functions are used to account for the diffusion between the leaf interior to the leaf surface, and between the leaf surface to the atmosphere, respectively. Many other modifications have been considered over the years so that the advection of energy and the effect of soil can be considered (e.g. Wallace et al., 1990; Shuttleworth and Wallace, 1985). This type of model is the most widely used and is also called the "big-leaf" model where the vegetation is simply represented as one big-leaf coverage of the surface. However, as pointed out by Goudriaan (1989), this type of model needs to parameterize the energy exchange at the soil surface (usually a fixed portion of the net radiation becomes ground heat flux) which is a major source of error. Recent examplesof this type of parameterization include Avissar and Mahrar (1988) and Noilhan and Planton (1989), who have implemented this approach into mesoscale atmospheric models and have shown reasonable success.

The multilayer model, also classified by Goudriaan (1989) as an "aerial gradient model", is the most complicated model. It has detailed in-canopy air properties (wind speed, temperature, moisture, and turbulence) and a profile of radiation through the canopy. Usually, many discrete layers are prescribed using information on canopy morphology. For the each layers, different stomatal resistances must be calculated based on the local environment. In an recent article by Raupach and Finnigan (1988) the usefulness and correctness of this approach are discussed in detail. They argue that the single-layer model is useful when only surface fluxes are needed. On the other hand, a multilayer model is useful when detail microclimate and hydrology are studied. The models proposed by Goudriaan and Waggoner (1972), and Chen (1984a,b) are typical examples.

For the purpose of atmospheric modeling, we need to know the surface fluxes to the atmosphere and the hydrology of the surface. Correct surface fluxes are needed for an accurated representation of the surface forcing on the atmosphere. The energy and water stored in the soil and vegetation provide a "delayed" forcing to the atmosphere. For the last decade, "two-layer models" have attracted most attention from atmospheric modelers. The two-layer model, also called "greenhouse canopy model" by Goudriaan (1989), consists of two separate energy budgets for vegetation and soil, uniform air temperature and moisture in the canopy, non-uniform vertical profiles of radiation and wind, complicated canopy transpiration through a feedback to the in-canopy vapor pressure deficit, and temperature-vapor pressure feedbacks. It takes advantage of the simplicity of the one-layer model but has separate energy budgets and hydraulic properties for the vegetation and soil. A recent study by Camillo (1991) has shown that two-layer models work significantly better than one-layer models. He also suggests that additional layers are not needed for evaporation estimation. Typical examples of the two-layer models are the Simple Biosphere Model (Sellers et al., 1986) and the Biosphere-Atmosphere Transfer Scheme (Dickinson et al., 1986).

Chapter 3

FORMULATION OF THE LAND ECOSYSTEM-ATMOSPHERE FEEDBACK (LEAF) MODEL

Since the Earth's surface is the only natural boundary where the atmosphere exchanges its momentum and energy with the solid earth, the Colorado State University (CSU) Regional Atmospheric Modelling System (RAMS) has traditionally had a separate surface module to calculate the exchange of momentum, energy and water through the bottom boundary. Relatively sophisticated multi-layer soil models (McCumber and Pielke, 1981; Tremback and Kessler, 1985) have been implemented into the RAMS. Lately, the need to parameterize vegetation control on atmospheric circulations has been better recognized, not only because vegetation is one of the essential elements that control the hydrological cycle but also because vegetation covers a large part of the land surface. Several types of mesoscale atmospheric circulations are induced by surface forcing (Pielke and Segal, 1986), thus, the inclusion of a vegetation model becomes necessary when a detailed partitioning of heat fluxes over land surface is desired. This Chapter will discuss the history and the formulation of the new CSU Land Ecosystem-Atmosphere Feedback (LEAF) model.

3.1 History

Due to the complexity of the surface exchange processes, a bulk surface layer representation is often chosen for numerical models. The sensible and latent heat fluxes are parameterized to be proportional to the temperature and moisture difference between the lowest level in the atmosphere and the ground surface. Typical bulk formulas are

$$H = \rho_a c_p C_H u_a (T_a - T_{sfc}), \tag{3.1}$$

$$\lambda E = \rho_a \lambda C_H u_a (q_a - q_{sfc}), \tag{3.2}$$

in which H is the sensible heat flux, λE is the latent heat flux (E is the water vapor flux and λ is the latent heat of evaporation), and variables ρ_a, u_a, T_a and q_a are air density, wind speed, air temperature, and specific humidity at the lowest model atmospheric level. Variables T_{sfc} and q_{sfc} are temperature and specific humidity at the lower boundary of the atmospheric model. Variables C_H and c_p are the heat (or moisture) exchange coefficient and the specific heat of air at constant pressure. It is obvious that, in addition to the exchange coefficient, C_H, the surface properties (i.e. T_{sfc} and q_{sfc}) are important in determining these turbulent heat fluxes. As a result, there have been many studies addressing the prediction of surface temperature and moisture (e.g. Deardorff, 1978; Dickinson et al., 1986; Sellers et al., 1986; Avissar and Mahrer, 1988).

Deardorff was the first one who introduced a vegetation parameterization into a meteorology model. He used the "big leaf" (see Section 2.2.2) or "bulk vegetation layer" representation to parameterize the vegetated surface. This "big leaf" concept is still one of the main types of existing vegetation parameterizations used in meteorological models (e.g. Noilhan and Planton, 1989). Following Deardorff's work, McCumber (1980) developed a vegetation model which was later adopted and modified by Avissar and Mahrer (1982, 1988). In 1989 this (Avissar and Mahrer, 1988; hereafter AM88) vegetation model was implemented into a test version of the RAMS. Using this implementation, it was found that this vegetation model is relatively insensitive to the LAIand quite sensitive to the soil moisture content. This surprising result (lack of sensitivity to the LAI) is now understood as a drawback of the AM88 model and is the primary reason of the current modified implementation which is referred to here as the Land Ecosystem-Atmosphere Feedback model (LEAF). The detailed formulation of the AM88 model and the LEAF model will be discussed in the following sections.

3.2 The AM88 Formulation

3.2.1 Relative Stomatal Conductance

The bulk transfer Equation 3.2 can be reformatted as

$$\lambda E = \rho_a \lambda K (q_a - q_{sat}). \tag{3.3}$$

In this expression, variable q_{sat} is the saturation specific humidity at the temperature T_{veg}, and K is the representative leaf-air transfer coefficient ($\mathrm{m\,s^{-1}}$). Comparing the Equations 3.2 and 3.3, it must be noted that

$$K \neq C_H u_a \tag{3.4}$$

since two different processes are involved in Equation 3.3 as described in Section 2.2.1. Thus, the transfer coefficient, K, actually describes the total conductance between the sub-stomatal chamber and the free atmosphere. Assuming these two processes are independent with each other, Avissar et al. (1985) defined

$$K = h \cdot d_{rs} \tag{3.5}$$

and measured the value of d_{rs} in a controlled chamber. In this equation, h is the potential leaf-air transfer coefficient in $\mathrm{m\,s^{-1}}$ and d_{rs} is the relative stomatal conductance function, which is a normalized real number between 0 and 1. Notice that the relative stomatal conductance is not the same as the inverse of the real stomatal resistance function, r_s (shown in Figure 2.1). Later, Avissar and Pielke (1991) have extended the work by Avissar et al. (1985) to account for the leaf age

$$d_{rs} = \Omega[d_{smin} + (d_{smax} - d_{smin}) f_C f_R f_{T_c} f_{T_h} f_V f_\Psi]/d_{smax} \tag{3.6}$$

where Ω is the leaf age function, d_{smin} is the minimum stomatal conductance which occurs only through the leaf cuticle when the stomata are completely closed, d_{smax} is the maximum stomatal conductance obtained when stomata are completely opened, and each of the f functions quantifies the influence of a specific environmental factor upon the conductance (C for ambient atmospheric carbon dioxide concentration, R for solar global radiation, T_c and T_h for leaf temperature at cold and hot ranges, V for vapor pressure deficit (VPD) between leaf and ambient air, and Ψ for soil water potential (SWP) in the root zone). The expression used for each of these functions is

$$f_i = \frac{1}{1 + \exp[-S_i(X_i - X_{b_i})]} \tag{3.7}$$

where the subscript i refers to the environmental factor, X_i is the intensity of the factor i, X_{b_i} is the value of X_i at $f_i = 1/2$, and S_i is the slope of the curve at this point. Constants

d_{smin}, d_{smax}, X_{b_i}, and S_i must be empirically determined. For a tobacco plant, Avissar et al. (1985) gave $d_{smin} = 0.0005$ m s^{-1}and $d_{smax} = 0.0093$ m s^{-1}and the environmental factors are listed in Table 3.1 and illustrated in Figure 3.1. The properties of the relative

Environmental factor	*Units*	X_{b_i}	S_i
CO_2 concentration	ppm	∞	–
Global radiation	Wm^{-2}	3.5	0.034
Temperature (cold range)	°C	8.9	0.41
Temperature (hot range)	°C	34.8	-1.18
Vapor pressure difference	Pa	2860	-0.0031
Soil water potential	Pa	12×10^5	5×10^{-6}

Table 3.1: Values of X_{b_i} and S_i for functions of stomatal response to environmental factors (after Avissar et al., 1985).

stomatal conductance function, d_{rs}, and its environmental influence functions, f_i's, are discussed by Avissar et al. (1985) and Avissar and Pielke (1991). Lynn and Carson (1990) also discussed in detail the external influence functions. Some of the intrinsic factors (e.g. position of stomata on the leaves, concentration and hormonal equilibrium of the leaves, and growing stages) are discussed briefly in Winkel and Rambal (1990), and Avissar (1992). A limitation of Equation 3.6 given by Winkel and Rambal (1990) is that there may be interactions between environmental factors. Strong correlations between environmental factors are sometimes shown in field data resulting in a bias in the estimation of the parameters. This effect has been ignored in Equation 3.6.

3.2.2 Latent Heat Flux

As can be seen in the previous section, K is a function of air passing the leaves (represented by h) and the stomatal controls (represented by d_{rs}). It is assumed that the two effects can be separated so that

$$\lambda E = \rho_a \lambda h d_{rs}(q_a - q_{sat}) \tag{3.8}$$

$$= \rho_a \lambda h (q_a - q_{veg}), \tag{3.9}$$

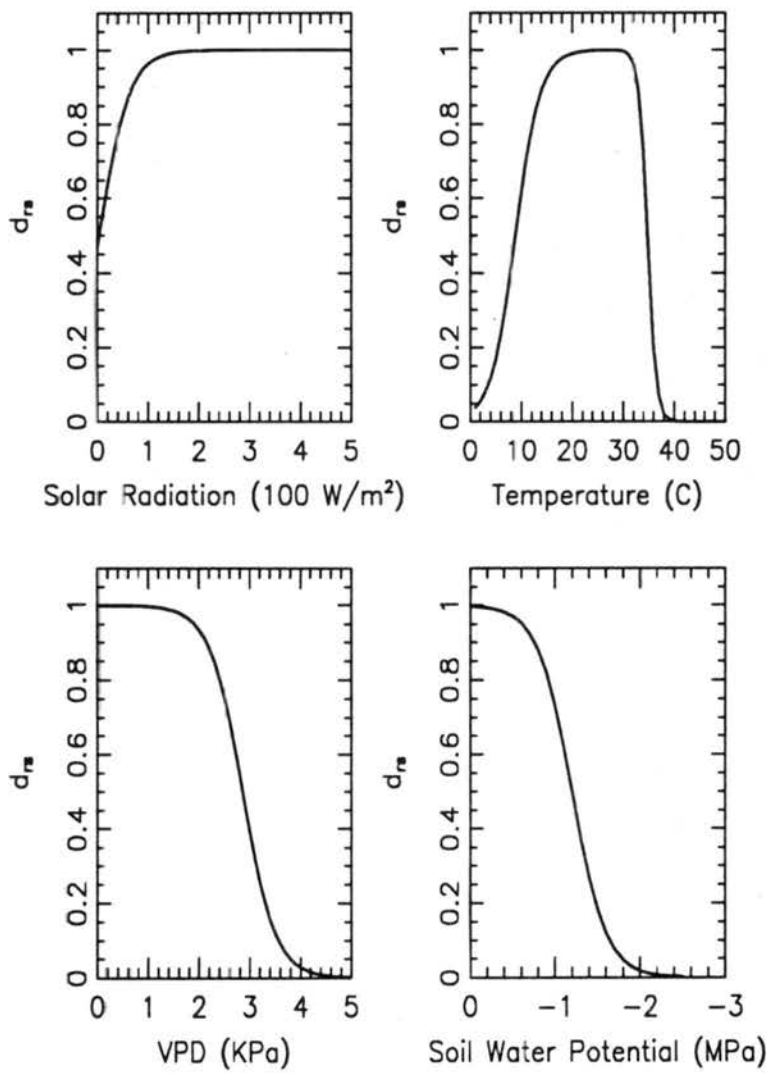

Figure 3.1: Schematic representation of the stomatal response to the environment as tabulated in Table 3.1. Adopted from Avissar and Pielke (1991).

where q_{veg} is the equivalent specific humidity near the leaf-atmosphere interface. Comparing equations 3.5 and 3.9, it is found that variable h is actually the aerodynamic conductance for this equivalent condition. The variable q_{veg} is easily deduced from equations 3.8 and 3.9, so that

$$q_{veg} = d_{rs} q_{sat} + (1 - d_{rs}) q_a. \tag{3.10}$$

This is the same equation as Eq. 53 in AM88 or Eq. 6 in Avissar and Pielke (1990, hereafter AP90) if we replace variable q_a by q_{z0} or q_G. Comparing Eq. 3.10 with Eq. 53 in AM88 and Eq. 6 in AP90, there is an obvious confusion. The three variables q_a, q_{z0}, and q_G represent specific humidities at three different locations (first atmospheric level, leaf-atmosphere interface, and surface of the ground). Several different representations have been proposed by various investigators where different weights are assigned to the specific humidity at the ground, the saturation specific humidity at the leaf temperature and the specific humidity at the first model atmospheric level. We will only point out the confusion for now and it will become more clear later.

While the other vegetation models were mainly designed for use in general circulation models, the AM88 model is designed for use in a mesoscale model (RAMS) in which the first atmosphere level is assumed to be at the top of the surface layer. The surface layer Monin-Obukhov similarity theory becomes very useful in calculating the surface fluxes. The bulk transfer equation for the latent heat flux can be rewritten into a surface flux form

$$\lambda E = \rho_a \lambda u_* q_*, \tag{3.11}$$

where u_* is the surface friction velocity and q_* is the surface layer humidity scale. Since this model is qualified as a Goudriaan's (1989) "big-leaf" model, the contributions from the vegetation and the ground to this total evapotranspiration must be artificially defined as

$$\lambda E = \lambda E_{veg} + \lambda E_g, \tag{3.12}$$

$$\lambda E_{veg} = \sigma_f' \rho_a \lambda u_* q_* \tag{3.13}$$

$$\lambda E_g = (1 - \sigma_f') \rho_a \lambda u_* q_* \tag{3.14}$$

$$\tag{3.15}$$

in which $\sigma_f^{'}$ is a weighting function defined as

$$\sigma_f^{'} = \frac{2\mathrm{LAI}\sigma_f}{1 + 2\mathrm{LAI}\sigma_f}. \tag{3.16}$$

The weighting function, $\sigma_f^{'}$, is actually a ratio between the total transpiring leaf surface and the total evapotranspiring surface. In the expression, value "1" represents the ground surface, $2\mathrm{LAI}\sigma_f$ is the total evapotranspiration active vegetation area and the factor 2 takes both sides of the leaves into account. For some vegetation having stomata on only one side of the leaves, this factor must be reduced to 1. Variable σ_f, a shielding factor, represents the fractional coverage of the ground by canopy. This factor can either be specified (e.g. Dickinson et al., 1986) or calculated based on an empirical formula. Kanemasu et al. (1977) suggested a relation between the leaf area index and the shielding factor for agricultural plants as

$$\sigma_f = 1 - \exp(-\mathrm{LAI} \times 0.4). \tag{3.17}$$

The surface value of q is required for the computation of q_*. Assuming that the air does not directly influence the specific humidity of the under-laying vegetation and ground surface, AM88 used a weighted effective surface specific humidity to represent the moisture of the canopy level air as

$$q_{eff} = \sigma_f^{'} q_{veg} + (1 - \sigma_f^{'}) q_G. \tag{3.18}$$

Recall that q_{veg} can be calculated according to Equation 3.10. Figure 3.2 shows schematically the vegetation surface where the relative stomatal conductance is absorbed into the effective specific humidity q_{eff}.

3.2.3 Sensible Heat Flux

Similar to the discussion in the previous section, the sensible heat flux can be written as

$$H = \rho_a c_p u_* \theta_*, \tag{3.19}$$

$$H_{veg} = \sigma_f^{'} \rho_a c_p u_* \theta_*, \tag{3.20}$$

$$H_g = (1 - \sigma_f^{'}) \rho_a c_p u_* \theta_*, \tag{3.21}$$

$$\tag{3.22}$$

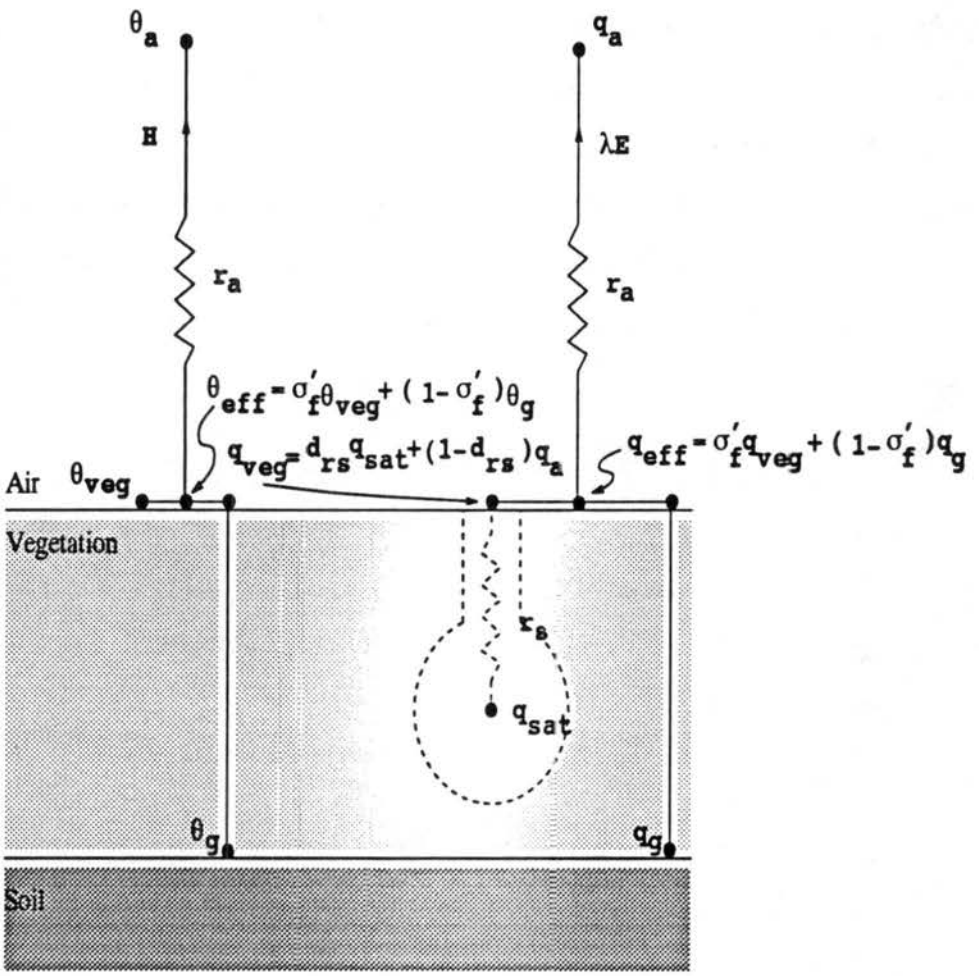

Figure 3.2: Same as Figure 2.1 except the stomatal conductance has been absorbed into an effective surface value of specific humidity, q_{eff}. The effect of the underlying soil surface is also taken into account.

where θ_* is the surface layer temperature scale. A weighted effective surface potential temperature is also required in order to calculate θ_*. Similar to the way the weighted effective surface specific humidity is calculated, the effective surface potential temperature is calculated in the following fashion

$$\theta_{eff} = \sigma_f' \theta_{veg} + (1 - \sigma_f')\theta_G \tag{3.23}$$

where θ_{veg} is the potential temperature of the leaves.

3.2.4 Discussion

It has been shown in the previous sections that the AM88 model has three assumptions. First, there is no canopy flow; each of the fluxes calculated are above the canopy. The model actually treats the canopy as the bottom boundary. Secondly, since the surface layer Monin-Obukhov similarity theory is used, the first model atmosphere level must be no higher than the top of the surface layer. The location of variable q_a in Equation 3.10 is not too important as long as it is in the surface layer. However, the use of q_G in Eq. 6, AP90 is not justified unless they assumed q_G is representative of the specific humidity in the canopy-air. The use of q_{z0} in Eq. 53, AM88 is preferred in case a formulation of canopy flow is used. In any case, there is no canopy flow in the current version of the RAMS so that the use of specific humidity at the lowest atmosphere level is preferred. Thirdly, since this is an one-layer model, the resultant latent and sensible heat fluxes have to be further separated into vegetation and soil surface components, which are assumed to be proportional to the effective coverage ratio (i.e. σ_f' for vegetation and $1 - \sigma_f'$ for the underlying soil). Using this assumption has highly simplified the system. The possible non-linear effect on modifying the contribution from the soil has not been considered. For example, consider a scenario in which the air temperature is between the leaf temperature and the soil temperature ($T_{veg} > T_a > T_G$) and the soil surface is fully covered by vegetation. The total sensible heat flux is from the surface to the atmosphere. Using σ_f' as a weighting function to partition the total sensible heat flux will then yield positive sensible heat fluxes from both the vegetation and soil surface and hence result in an even cooler soil temperature. However, since the effective surface potential temperature is also

weighted using σ_f' (i.e. Equation 3.23), the temperature of the soil is weighted less and the effective surface temperature may still be larger than the air temperature and so that sensible heat flux continues to leave the surface toward the atmosphere. Thus, the soil temperature becomes colder and colder when instead it should warm up due to a heat flux from the vegetation to the soil surface.

There are other problems with the AM88 model: (1) the way AM88 handles the contributions from the vegetation (i.e. E_{veg}, H_{veg}) is questionable. The philosophy behind Eqs. 3.13 and 3.20 is that once the total heat flux is obtained, the fractional contribution from the vegetation can be retrieved using the same weighting function, σ_f'. However, recall that since σ_f' has been used in Eq. 3.18 to calculate the effective surface specific humidity, the use of Eqs. 3.13 and 3.20 have erroneously doubly counted the effect of σ_f'. In order to use Eq. 3.18, an assumption has been made that the atmosphere only responds to the representative canopy-air but not the individual vegetation and ground surfaces. However, the atmospheric moisture actually is directly related to the vegetation moisture when calculating q_{veg} (i.e. Eqs. 3.8 and 3.9). This inconsistency in the assumptions has become a major difficulty in understanding the model; (2) the proposed relative stomatal conductance, d_{r_s}, does not consider the aerodynamic effect. Avissar et al. (1985) constructed the formula (i.e. Equation 3.6) based on their leaf-chamber measurements presumably at constant air flow. Otherwise, the maximum stomatal conductance has to be a function of wind speed. This shortcoming will be further demonstrated in Section 3.3.3. Because of the assumption that a representative canopy-air can be used, (3) the leaf area index (LAI) has only been applied in the weighting function for the contributions from the vegetation and the soil surface. It does not scale up the evapotranspiration from the leaf scale to the canopy scale. This is perhaps the reason AM88 is lacking a sensitivity to the LAI.

3.3 The LEAF Formulation

Knowing the weakness of the AM88 model, we developed a new and improved model. The LEAF formulation completely re-structures the AM88 model with an emphasis on the

scaling up of the evapotranspiration to the canopy scale and the removal of inconsistent assumptions. As suggested by Dickinson et al. (1986), evaporation and transpiration are evaluated separately, and leaf stem area index (LSAI) and the fractional area of wet surface are also introduced. Vegetation and the characteristics of the land surface are grouped into 18 categories (see Table 3.2) as described in the BATS (Biosphere-Atmosphere Transfer Scheme; Dickinson et al., 1986).

LEAF	BATS	Description	LEAF	BATS	Description
1	1	Crop/mixed farming	2	2	Short grass
3	3	Evergreen needleleaf tree	4	4	Deciduous needleleaf tree
5	5	Deciduous broadleaf tree	6	6	Evergreen broadleaf tree
7	7	Tall grass	8	9	Tundra
9	10	Irrigated crop	10	11	Semi-desert
11	13	Bog or marsh	12	16	Evergreen shrub
13	17	Deciduous shrub	14	18	Mixed woodland
15	8	Desert	16	12	Ice cap/glacier
17	14	Inland water	18	15	Ocean

Table 3.2: Land cover and vegetation type from Biosphere-Atmosphere Transfer Scheme (BATS; Dickinson et al., 1986). The order has been rearranged in LEAF for computational purpose.

3.3.1 Model Structure

As mentioned in Section 2.2.2, the land surface parameterization schemes currently used in atmospheric models have virtually the same model structure. Following Richardson's "vegetation-film" and Deardorff's (1978) "big-leaf" concept, LEAF introduces a layer of vegetation that interacts with the atmosphere. For this layer of vegetation, averaged quantities, such as wind speed, thermal capacity, exchange coefficients, radiative extinction coefficient, are utilized so that the detailed flow structure and the interception of radiation in the canopy are not resolved. However, prescribed wind profile and radiation distributions are used to calculate these averaged quantities. This type of model has been classified as a "greenhouse canopy" model by Goudriaan (1989) (see Section 2.2.2) so that in addition to the "big-leaf", the impact of the canopy-air is also parameterized. Figure 3.3 shows schematically the structure of the model. Variables H and λE are sensible

and latent heat fluxes, T is temperature, e is water vapor pressure, Ψ is water potential, and r indicates a resistance function. Subscripts a, c, g, and veg denote variables at different locations, namely the atmospheric reference level, the canopy-air at the zero plane displacement height, the ground surface, and the canopy respectively. Three aerodynamic resistance functions are used: r_b is a bulk boundary layer resistance, which is a resistance function between the leaves and the canopy-air, r_a is a resistance function between canopy-air and the atmospheric reference level, and r_d is a resistance between the ground and the canopy-air. In Figure 3.3, the resistance functions in parentheses indicate the functions which are implicitly embedded in other functions. For example, the resistance functions for water transport between the roots and the canopy, i.e. r_{plant} and r_{soil}, implicitly exist in the formulation of relative stomatal conductance d_{r_s}.

In this soil-vegetation-atmosphere transfer model, the canopy and the ground first exchange heat (radiative, sensible, and latent heat) with the surrounding air and then the canopy-air exchanges heat with the boundary layer atmosphere. We view this two step exchange process as a major improvement to the "big-leaf" model in that the surface heat and moisture fluxes from the vegetation to the atmosphere are regulated by the heat and moisture capacity of the canopy-air. Also, the water flow from the root zone to the surface of the leaves are regulated by the soil resistance, the plant resistance, and the bulk stomatal resistance.

3.3.2 Aerodynamic Resistances

The primary goal of the existing soil-vegetation models is to provide a realistic boundary forcing to the atmosphere. This is partly accomplished through parameterizing the surface momentum, sensible heat, and latent heat fluxes from the canopy-air to the atmospheric surface layer. Figure 3.4 shows schematically the model assumed mean wind structure of flow over and within a vegetation layer. It is assumed that the surface-layer logarithmic wind profile law is valid above the vegetation layer and a exponential decay law is valid within the canopy[1].

---

[1]The secondary local wind maximum observed in a forest stand cannot be modeled by this exponential decay law

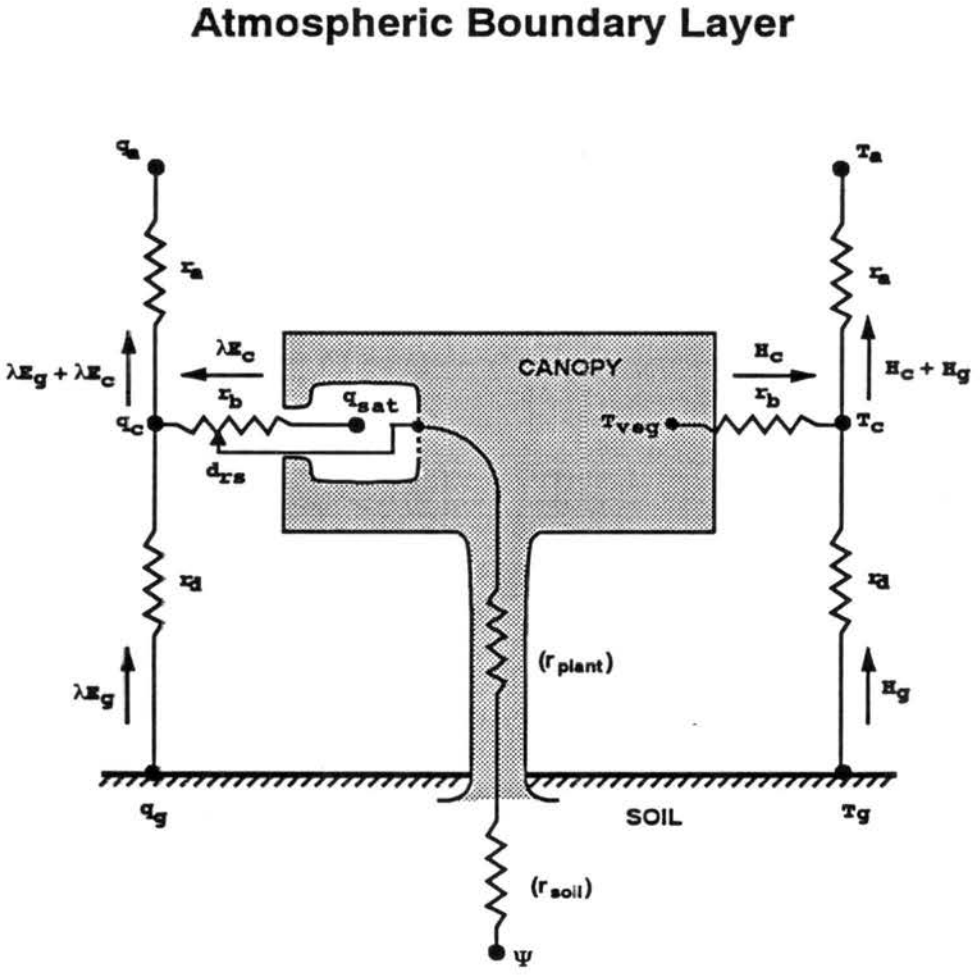

Figure 3.3: Framework of the Land Ecosystem-Atmosphere Feedback model (LEAF). The transfer pathways for latent and sensible heat flux are shown on the left and right hand sides of the diagram respectively (modified from Sellers et al. 1986). Symbols are described in the text.

Following the Monin-Obukhov surface-layer similarity theory, for flow above the canopy the logarithmic wind profile is

$$u(z) = \frac{u_*}{k}\left[\ln\left(\frac{z-d}{z_0}\right) + \Psi_M\right] \tag{3.24}$$

where u is the wind speed at a height z within the surface layer, u_* is the friction velocity, k is the von Karman's constant, d is the zero plane displacement height, z_0 is the surface aerodynamic roughness, and Ψ_M is a stability adjustment function for momentum transport. The momentum flux (or the shear stress) above the canopy is in the form of

$$\tau = \rho C_D u^2 = \rho u_*^2 = \rho\left[\frac{ku}{\ln\left(\frac{z-d}{z_0}\right) + \Psi_M}\right]^2 \tag{3.25}$$

where τ is the shear stress, ρ is the density of air, C_D is the drag coefficient. The displacement height, d, and the surface roughness length, z_0, are calculated in LEAF based on (Shuttleworth and Wallace, 1985) and (Monteith and Unsworth, 1990) so that

$$z_0 = 0.13\,h, \text{ and} \tag{3.26}$$

$$d = 0.63\,h, \tag{3.27}$$

It may not be physically consistent to hold d and z_0 fixed while varying the LAI. However, for short range weather forecasts where LEAF is been used, this may not be a problem and we can supply these variables as model parameters and hold them fixed during the period of the model simulation (usually no more than several days).

For the sensible and latent heat fluxes, the boundary layer aerodynamic resistance function, r_a, is used in LEAF, so that

$$H = \rho c_p \frac{T_a - T_c}{r_a}, \tag{3.28}$$

$$\lambda E = \rho\lambda \frac{q_a - q_c}{r_a}, \tag{3.29}$$

$$\frac{1}{r_a} = \frac{k^2 u}{\left[\ln\left(\frac{z_{ref}-d}{z_0}\right) + \Psi_M\right]\left[\ln\left(\frac{z_{ref}-d}{z_0}\right) + \Psi_H\right]}. \tag{3.30}$$

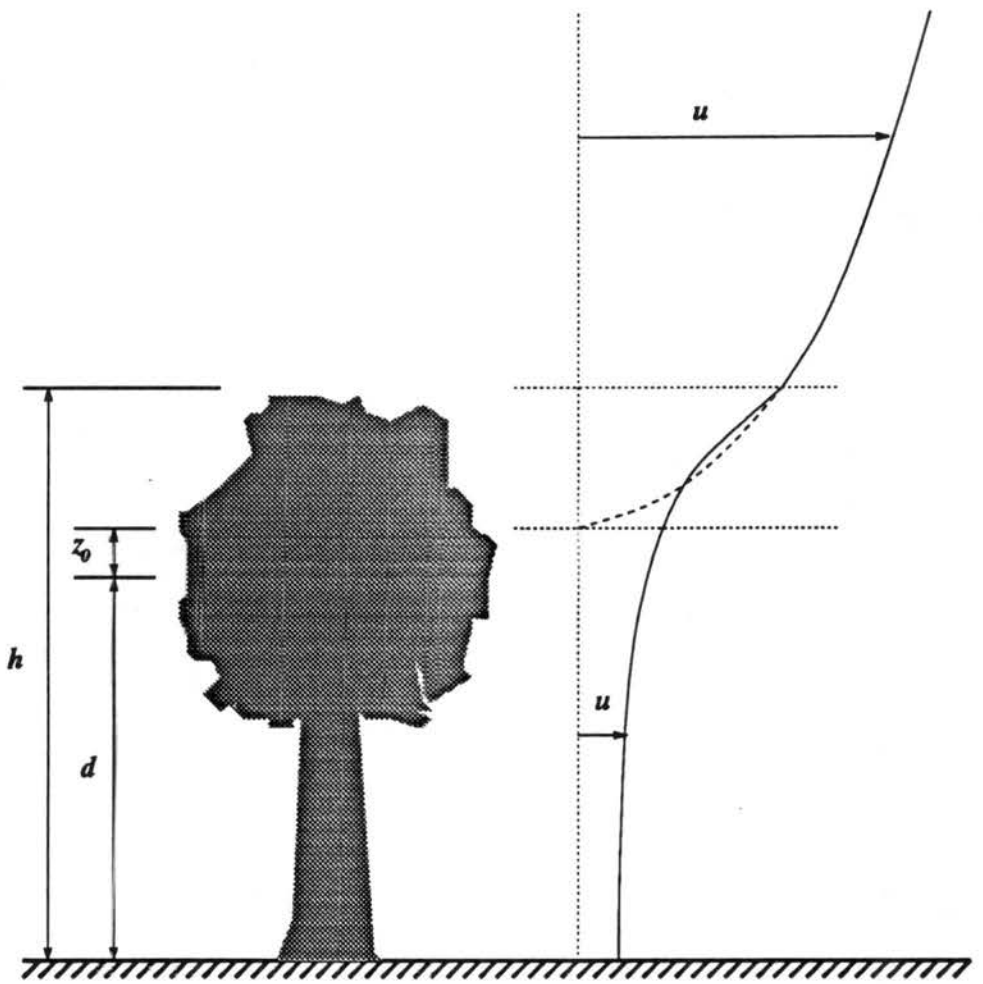

Figure 3.4: Wind profile above and within the canopy.

In these formulae, the variable Ψ_H is a stability adjustment function for heat and moisture transport, λ is the latent heat of vaporization, and z_{ref} is a reference height in the surface layer taken to be the first vertical grid level in the RAMS. Recall that the transfer pathways have been shown in Figure 3.3. The stability adjustment functions can be found, for example, in Paulson (1970), Businger et al. (1971), and Louis (1979). Louis's scheme is used in LEAF due to the fact that the latter scheme is non-iterative.

The bulk boundary layer resistance, r_b, should depend upon the morphology of the vegetation and take into account the fact of air flow around the leaves. Following the work by Goudriaan (1977), LEAF uses the form

$$\frac{1}{r_b} = \int_0^{\mathrm{LSAI}} \frac{\sqrt{u_f}}{C_s P_s} d\,\mathrm{LAI} \tag{3.31}$$

where u_f is an average wind speed in the canopy, C_s is a transfer coefficient which depends on the shape of the leaves, and P_s is a shelter coefficient. As noted by Sellers et al. (1986) the major difficulty in using this formula is the determination of the shelter coefficient, P_s. This coefficient is highly dependent on the morphology of the vegetation and can only be determined empirically. Following Thom (1972) and Sellers et al. (1986), P_s is specified as

$$P_s = \frac{1}{1 + 0.5\mathrm{LSAI}}. \tag{3.32}$$

It is assumed that the wind speed in the canopy, i.e. $z < h$, resembles an exponential decay form (e.g. Inoue, 1963) such as

$$u(z) = u(h) \exp\left[-n\left(1 - \frac{z}{h}\right)\right] \tag{3.33}$$

The values of n have been given by Ciono (1972) and Schädler et al. (1990): 0.4–0.8 for sparse rigid elements, 1–2 for corn, 2–4 for wheat, and 3 for dense vegetation. The averaged wind speed is calculated following Schädler et al. (1990) so that

$$h u_f^2 = \int_0^h u^2(z) d\,z, \tag{3.34}$$

which yields

$$u_f = u(h)\sqrt{(1 - \exp(-2n))/2n}. \tag{3.35}$$

The wind speed at the top of the canopy can be calculated using the logarithmic wind profile law to obtain

$$u(h) = \frac{u_*}{k}\left[\ln\left(\frac{h-d}{z_0}\right) + \Psi_M\right]. \tag{3.36}$$

Finally, since only one layer of vegetation is assumed in the model and the leaves are uniformly distributed vertically, Equation 3.31 is reduced to

$$\frac{1}{r_b} = \frac{0.01\,\mathrm{LSAI}}{P_s}\sqrt{\frac{u_f}{l}} \tag{3.37}$$

where l is a typical dimension of the leaves or the stems along the wind direction. The empirical constant 0.01 $\mathrm{m\,s^{-1/2}}$ has been determined using wind-tunnel data after Gates (1980) and used by Dickinson et al. (1986). Similar expression is also suggested by Jones (1983).

Knowing the bulk boundary layer resistance, the resultant sensible heat flux from the leaves to the canopy-air can be written as

$$H_c = \rho c_p \frac{T_a - T_c}{r_b}, \tag{3.38}$$

where T_a and T_c are the temperature of the canopy-air and the leaves, respectively. The resultant latent heat flux will be discussed later with the stomatal resistance function.

The surface aerodynamic resistance, r_d, should also depend on the morphology of the vegetation. For example, a constant stress profile may be used in a hardwood forest, where the wind profile may be logarithmic near the surface and below the elevated canopy. However, there may be no turbulent exchange of heat and moisture between the soil and the canopy-air beneath a dense grass canopy since the wind reduces to zero in the canopy. For sparse canopy, it is even more difficult to parameterize this effect. The relative contribution from the soil should be very important when the density of the canopy is small.

Due to the fact that this soil to canopy exchange process is not yet clearly understand, the form proposed by Shuttleworth and Wallace (1985) is used in LEAF, with some

variation

$$r_d = r_{bare}\max\left[\left(1-\frac{\mathrm{LSAI}}{\sigma}\right),0\right]+r_{close}\min\left[\frac{\mathrm{LSAI}}{\sigma},1\right], \tag{3.39}$$

$$r_{bare} = \ln(z_{ref}/z_0')\ln(z_{ref}+z_0)/z_0'/k^2u, \tag{3.40}$$

$$r_{close} = \frac{\ln(z_{ref}-d)/z_0}{k^2u}\times \left[\ln(z_{ref}-d)/(h-d)+\frac{h}{n(h-d)}[\exp[n\{1-(d+z_0)/h\}]-1]\right] \tag{3.41}$$

where r_{bare} is the resistance function when the surface is bare and r_{close} is the resistance when the surface is covered by a closed canopy. Variable z_0' is the roughness length when the surface is bare. It is assumed that there is minimum soil contribution when LSAI is larger than σ. The advantage of using this formula is that it utilizes a realistic wind profile law to calculate the resistance functions, r_{bare} and r_{close}. The resultant turbulent heat fluxes from the soil are

$$H_g = \rho c_p\frac{T_c-T_g}{r_d}, \tag{3.42}$$

$$\lambda E_g = \rho\lambda\frac{q_c-q_g}{r_d}, \tag{3.43}$$

where q_g, which is calculated according to Lee and Pielke (1992), is the specific humidity immediately above the surface with a surface temperature T_g.

3.3.3 Stomatal Resistance

The major difference between a vegetated and a bare soil surface is the access to water in the soil. Over a bare soil surface, water is available for evaporation only from the top soil layers. In the presence of vegetation, water is also available from deep soil layers where roots are present. Although the transfer of water in the plant is mostly passive (meaning that water is not directly used by the photosynthesis process; see, for example, Barry (1969)), it is responsible for the transport of nutrition from the root zone to the leaves where the photosynthesis process is taking place. The result of this transport process is

that water is lost to the atmosphere through the opening (stomata) on the leaves. Recall from Section 2.2.1 that water vapor pressure is at the saturation value in the intercellular space (Rutter, 1975). However, the vapor pressure at the surface of the leaves is regulated by the size of opening of the stomata which is a function of environmental variables (e.g. photosynthetically active radiation, water stress, temperature, and CO_2 concentration; e.g. see Figure 3.1).

Assuming the stomatal opening can be parameterized by a single resistance function, r_s, the water vapor flow from the intercellular space to the canopy-air, similar to what has been shown in Figure 2.1, is a two step process. First, water vapor is transferred to the leaf surface

$$\lambda E_1 = \rho\lambda \frac{q_{sfc} - q_{sat}}{r_c}, \tag{3.44}$$

where r_c is a canopy resistance function (or bulk stomatal resistance function) q_{sfc} is the specific humidity at the surface of the leaves, and q_{sat} is the saturation specific humidity pressure at the intercellular space with the temperature of the leaves, T_{veg}. Following Jarvis and McNaughton (1986), r_c is defined as

$$\frac{1}{r_c} = \frac{\mathrm{LAI}}{r_s}. \tag{3.45}$$

Notice that, by using this relationship, the stomatal resistance has been scaled-up to become the canopy resistance. Secondly, water vapor is transferred to the canopy-air

$$\lambda E_2 = \rho\lambda \frac{q_c - q_{sfc}}{r_b}. \tag{3.46}$$

Assuming no accumulation of water vapor at the surface of the leaves (i.e. $E_1 = E_2$), then

$$\lambda E_c = \rho\lambda \frac{q_c - q_{sat}}{r_b + r_c}. \tag{3.47}$$

In this equation E_c is the evaporation rate from the intercellular space to the canopy-air. This equation is widely used in many micrometeorological models and is an absolute approach, where the magnitude of the stomatal resistance function is parameterized.

LEAF, on the other hand, adopted a relative approach, where the "potential evaporation" (maximum evaporation rate when there is no stomatal resistance) is evaluated

first and then adjusted by a "relative stomatal conductance". This approach has been referred to as the "threshold concept" by Avissar and Mahrer (1988), so that

$$\lambda E_c = \rho\lambda \frac{d_{rs}}{r_b}(q_c - q_{sat}), \tag{3.48}$$

where d_{rs} is the relative stomatal conductance. This can conceptually be seen in Figure 3.3 where the actual boundary aerodynamic resistance r_b is adjusted by a dial (i.e. d_{rs}).

Comparing Equations 3.47 and 3.48, it is found that

$$d_{rs} = \frac{r_b}{r_b + r_c}. \tag{3.49}$$

Obviously, the leaf resistance, r_c, still has to be determined. Since transpiration is controlled by the stomata, a realistic parameterization of the stomatal opening is necessary in order to correctly estimate the amount of latent heat flux. Past studies showed that the stomata opening is affected by environmental variables (Allaway and Milthorpe, 1976; Jarvis, 1976; Avissar et al., 1985) and is parameterized in LEAF with a form modified from Equation 3.6 and Equation 3.45

$$\frac{1}{r_c} = \mathrm{LAI}\,[d_{smin} + (d_{smax} + d_{smin}) f_R f_{T_c} f_{T_h} f_V f_\Psi], \tag{3.50}$$

where f_{T_c} and f_{T_h} are adjustment factors for leaf temperature at cold and hot ranges respectively, f_V is an adjustment factor for water vapor pressure deficit, f_R is an adjustment factor for total solar radiation, and f_Ψ is an adjustment factor for soil water potential. Subscripts *min* and *max* indicate the minimum and maximum values. Note that both the absolute leaf resistance, r_c, and aerodynamic resistance, r_b, are used in calculating the relative stomatal resistance function, d_{rs}, to correct the error in the stomatal resistance calculation used in AM88 (see the discussion in Section 3.2.4).

Although LEAF is realistic in describing the stomatal response to environmental variables, a major difficulty in applying the model is to define these plant related functions. Recently, Sellers et al., (1991) , using enzyme kinetic theory, has modified the formulation of the stomatal conductance function to account for the rate of photosynthesis explicitly.

3.3.4 Interception and Re-evaporation of Precipitation

One important impact of vegetation on land-surface hydrology is that the vegetation canopy intercepts some precipitation and re-evaporates the intercepted water back to the atmosphere. This process prevents some water dripping to the ground and suppresses transpiration. It has been shown by Deardorff (1978), Dickinson et al. (1986) and more recently Lakhtakia (1991) that this interception and re-evaporation process has a great impact on short term local environments and thus the weather. Following Deardorff's (1978) work, a maximum depth of water film of 0.0002 m can be stored on the leaves. The fraction of wet leaf, when it is not completely wet, is defined as

$$\sigma_{wet} \equiv \left(\frac{W_{res}}{W_{max}}\right)^{\frac{2}{3}} \tag{3.51}$$

where the maximum storage on the leaves is $W_{max} = 0.0002 \times LSAI$, and the variable W_{res} is the actual water "reservoir" depth. Note that the existence of dew is treated the same as intercepted precipitation.

The depth of the water reservoir can vary with time so that

$$\frac{\partial W_{res}}{\partial t} = P - \sigma_{wet} E_{evap} \quad 0 \leq W_{res} \leq W_{max}, \tag{3.52}$$

where variable P is the precipitation reaching the leaves and E_{evap} is the evaporation rate. Similar to the latent heat flux by transpiration (i.e. Eq. 3.48) the evaporation rate when the leaves are completely wet is

$$E_{evap} = \rho \frac{1}{r_b}(q_c - q_{sat}). \tag{3.53}$$

Since there is no transpiration through the wet portion of the leaf, the total evapotranspiration becomes

$$\lambda E_c = \rho\lambda \left[(1 - \sigma_{wet})\frac{q_c - q_{sat}}{r_b + r_c} + \sigma_{wet}\frac{q_c - q_{sat}}{r_b}\right], \tag{3.54}$$

where the first term on the right-hand-side is the contribution of latent heat flux from transpiration and the second is from evaporation.

3.3.5 Model Equations

If we can relate the resistance function to some environmental variables, as shown in the previous two sections, and assume that the atmospheric condition is predicted, then the only unknown becomes the corresponding surface value. For example, the wind speed, air temperature, and water vapor pressure at the displacement height are required in order to estimate the amount of momentum, sensible heat, and latent heat fluxes. Since the surface roughness length and the displacement height are prescribed in LEAF, the momentum flux is immediately obtained by employing surface layer similarity theory. Sensible and latent heat fluxes, on the other hand, are still to be resolved.

As mentioned before, LEAF also prescribes wind profiles in the canopy. This will leave two variables to be determined, namely the water vapor pressure and the temperature of the canopy-air (i.e. q_c and T_c in Figure 3.3). Assuming the canopy-air has minimum heat and moisture storage, the turbulent heat fluxes gained from the soil and vegetation must be balanced by the loss to the atmosphere, so that

$$H = H_c + H_g, \text{ and} \tag{3.55}$$

$$\lambda E = \lambda E_c + \lambda E_g. \tag{3.56}$$

Substituting Equations 3.28, 3.29, 3.38, 3.54, 3.42, and 3.43 into Equations 3.55 and 3.56, we can solve for the temperature (T_c) and the specific humidity (q_c) of the canopy-air to obtain

$$T_c = \frac{T_{veg}/(r_b + r_c) + T_g/r_d + T_a/r_a}{1/(r_b + r_c) + 1/r_d + 1/r_a}, \tag{3.57}$$

$$q_c = \frac{(1 - \sigma_{wet})q_{sat}/(r_b + r_c) + \sigma_{wet}q_{sat}/r_b + q_g/r_d + q_a/r_a}{(1 - \sigma_{wet})/(r_b + r_c) + \sigma_{wet}/r_b + 1/r_d + 1/r_a}. \tag{3.58}$$

However we still need to determine the surface temperatures T_{veg} and T_g. This is done by solving the surface energy budget equation. Assuming a very small heat capacity in the canopy layer and the top soil layer, LEAF uses a prognostic equation for the energy balance

$$C_c\frac{\partial T_{veg}}{\partial t} = Rn_c + H_c + \lambda E_c, \tag{3.59}$$

$$C_g \frac{\partial T_g}{\partial t} = Rn_g + H_g + \lambda E_g + G, \tag{3.60}$$

where C_c and C_g are heat capacity, in J m^{-2} K^{-1}, of the canopy and the top soil layer, respectively. Variables Rn_c and Rn_g are the net radiation absorbed in the canopy and by the soil, and G is the ground heat flux to the deep soil layers. This is different than McCumber's (1980) and AM88 models in which the balance equation at the vegetation surface is solved as

$$0 = Rn_c + H_c + \lambda E_c. \tag{3.61}$$

The surface temperature must, however, be solved iteratively in Equation 3.61. However, Tremback and Kessler (1985) have shown that the iterative scheme not only increases the computational time requirement but the model can fail to converge because the coupling between the surface and the atmosphere is a highly nonlinear process, as shown in Clapp and Hornberger (1978). Solving the prognostic equations, as in LEAF, has the advantage of saving computation time but is less accurate (Dickenson, 1991; personal communication) and it also introduces new parameters, namely the heat capacities C_c and C_g. Fortunately these heat capacities are usually small so that the prognostic equations can still simulate the fast response of the surface temperature to the radiative forcing, especially for very small time steps ($<$ 60 sec) as generally used in LEAF.

3.3.6 Radiation Fluxes

Equations 3.59 and 3.60 show that the surface energy budget is mainly forced by radiation. A correct representation of the radiative flux in the canopy is necessary. The optical properties of the canopy are summarized by Sellers et al. (1986) so that three radiation bands should be considered

1. Visible or PAR (0.4 – 0.72 μm): Most of the energy in this region is absorbed by the leaves.

2. Near Infrared (0.72 –4μm): Radiation is moderately reflective in this region.

3. Thermal Infrared (> 4 μm): Leaves behave like a black body in these wavelengths.

For the visible and near infrared regions, the direct and diffuse radiation should also be treated separately. This is because the radiative transfer in the canopy for these short waves is highly dependent on the angle of the incident flux. For this reason, the change of surface albedo with solar angle should be considered and the values are higher in the morning and evening when the solar angle is low (e.g. Sellers et al., 1986).

The vegetation surface albedo, in LEAF, is not varying with time and there is no distinction between direct and diffuse radiation. Consider the reflectance and transmittance of the canopy are α_v and τ_v, respectively. The soil surface has an albedo (reflectance) of α_s. The short wave radiative flux absorbed by the canopy and the soil are

$$Q_{sc} = R_s(1-\alpha_v-\tau_v)(1+\tau_v\alpha_s) \tag{3.62}$$

$$Q_{ss} = R_s\tau_v(1-\alpha_s+\alpha_s\alpha_v) \tag{3.63}$$

where variable R_s is the total downward short wave radiative flux at the surface, and Q_{sc} and Q_{ss} are absorbed short wave radiative energy of the canopy and of the soil, respectively. The short wave radiation is reflected once between the soil and the canopy.

For the long wave radiative energy, if the emissivity of the canopy and the soil are ϵ_v and ϵ_s and the total downward atmospheric long wave radiative energy is R_l, the absorbed long wave energy by the canopy and the soil are expressed as

$$\begin{aligned} Q_{lc} &= R_l\sigma_f\epsilon_v - 2\sigma_f\epsilon_v\sigma T_{veg}^4 \\ &\quad +\sigma_f\epsilon_v\left[R_l(1-\sigma_f)(1-\epsilon_g)+\sigma_f\epsilon_v(1-\epsilon_g)\sigma T_{veg}^4+\epsilon_g\sigma T_g^4\right] \end{aligned} \tag{3.64}$$

$$Q_{ls} = \epsilon_g\left[R_l(1-\sigma_f)+\sigma_f\epsilon_v\sigma T_{veg}^4+\epsilon_s\sigma_f(1-\epsilon_v)\sigma T_g^4-\sigma T_g^4\right] \tag{3.65}$$

where the reflectance, absorptance, and transmittance of the canopy are $\sigma_f(1-\epsilon_v)$, $\sigma_f\epsilon_v$, and $(1-\sigma_f)$; the reflectance and absorptance of the soil are $(1-\epsilon_s)$ and ϵ_s,respectively. Recall that variable σ_f is the fractional coverage of vegetation (see Section 3.2.2). The long wave radiation is also reflected once between the soil and the canopy. Among the variables used in Equations 3.62, 3.63, 3.64, and 3.65, the downward short and long wave radiative fluxes, R_s and R_l, are diagnosed using the two-stream methods proposed by Chen and

Cotton (1983b) or Mahrer and Pielke (1977). Variables ϵ_v and ϵ_s are user specified. The soil surface albedo, α_s is calculated based on soil moisture content (Idso et al., 1975; McCumber, 1980). The fractional vegetation coverage is defined, in LEAF, as

$$\sigma_f = 1 - \tau_v. \tag{3.66}$$

The variables α_v and τ_v are calculated using α_s, LAI and user specified variable α_T, which is the total surface albedo. For the vegetation albedo, α_v, it is calculated as

$$\alpha_v = \alpha_T - \tau_v^2 \alpha_s \tag{3.67}$$

while, based on observations during the FIFE (Sellers et al., 1988) experiment, the transmittance of vegetation is calculated as

$$\tau_v = \exp(-0.75\ \mathrm{LAI}) \tag{3.68}$$

and is shown in Figure 3.5.

3.3.7 Soil Representation

The major difference between the "greenhouse canopy" and the "big-leaf" model is that vegetation is treated separately from the ground surface in the first approach. In order to close the surface energy budget equations in the previous section (e.g. Equations 3.59, 3.60), a soil model must be used to obtain the soil surface temperature, T_g and also the soil heat flux, G. LEAF uses a multi-layer soil model (McCumber and Pielke, 1981) and has a detailed description for the transfer of moisture and temperature (Tremback and Kessler, 1985).

Soil moisture flux (liquid and gas) is a function of soil water potential gradient and the soil hydraulic conductivity (McCumber and Pielke, 1981) and both are related to soil moisture. Soil water potential can vary over several orders of magnitude from wet to dry and it is very difficult to describe the appropriate average thermal and hydrological behaviors of the soil using a coarse resolution soil model. It is also interesting to note (Avissar, 1991; personal communication) that during sunlight hours, since the soil surface temperature is warmer than the deep soil temperature below and the air temperature

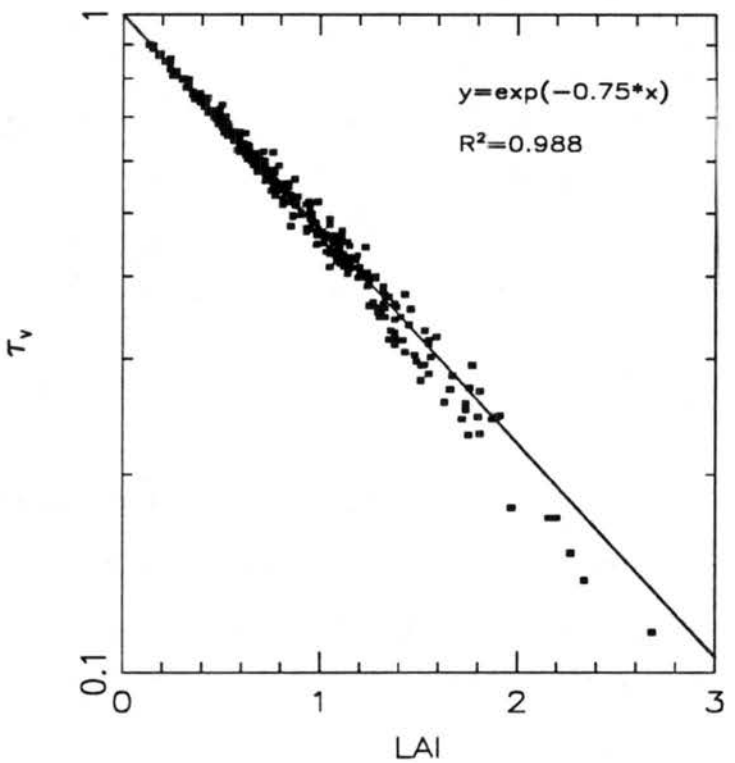

Figure 3.5: The transmittance of grass canopy as a function of LAI. Data were obtained during FIFE89 experiment.

above, the soil moisture flux is away from the surface into the deep soil and the atmosphere, causing a rapid drop of surface soil moisture content. This phenomena would not be possible to resolve using a bulk soil layer approach. It is also difficult to represent the soil water stress (a function of soil water potential) on vegetation correctly using a low resolution soil model. However, it is extremely difficult to initialize the multi-layered soil model because of the lack of observations. Special measurement must be performed to obtain the needed information on soil moisture and temperature profiles. Recently, Mahfouf (1991) has attempted to obtain soil moisture using a data assimilation technique.

The numerical method for solving the multi-layer soil model has been described in Tremback and Kessler (1985) and is not repeated here. Although the number of layers and the grid increment are user specified in RAMS, LEAF assumes a certain configuration has been followed. The soil layers are divided into three zones: the surface layer, the root zone, and the recharging zone. The surface layer consists of one *thin* soil layer and the soil moisture is subjected, beside vertical transport, to evaporation only. The root zone has half of the rest of the layers and the soil moisture is subjected to transpiration and vertical transport only. Finally, the recharging zone is only responsible for vertical water transport. Due to the large soil water potential gradient often observed at the soil surface during sunlight hours, the top soil layers must be thin (2 to 10 cm with the highest soil layer no more than 5 cm thick). However, the soil layers in the root zone cannot be too thin to prevent numerical problems (i.e. drying out the whole layer in one model time-step). Usually, several 10 to 30 cm thick layers are placed in the root zone with finer soil layer increments on top.

3.3.8 Water Uptake

The water transpired through vegetation to the atmosphere has to be taken out from the soil. Since the time-step used in RAMS is usually less than several minutes, water uptake is done at every time-step by finding the soil layer in the root zone that has the lowest (wettest) soil water potential and taking all the needed water from that layer. This procedure is quite different than what has been used by AM88 in which water is taken from the soil layers according to the length of the roots. Water stress calculated in LEAF is a

function of the lowest soil water potential in the root zone comparing to an averaged root-length weighted soil water potential used in AM88 model. As discussed in the previous Section, it is very difficult to find a reasonable average soil water potential and the AM88 approach often results in negative soil water content. Consider, for example, a dry soil layer mixed in with wet soil layers, the water stress is low due to the average between wet and dry layers and the transpiration out of the dry soil layer is high since its weighted by the root-length.

3.3.9 Infiltration

Soil water can be recharged from precipitation. A simple dump-bucket method is used for the infiltration process. The precipitation can only fill-up the top soil layer at any one model time-step. Any water excess above the porosity of the soil runs off immediately. The vertical soil water diffusion process then takes place to remove water from the top soil layer to the deep soil layers. Note that this procedure is dependent on the thickness of the top soil layer and the model time-step and needs to be subjected to further testing and improvement.

3.4 Solution Procedure

Figure 3.6 summerizes the solution procedure. For each RAMS model atmospheric time-step, a small time-step is started for the LEAF model (this is required for solving Equations 3.59 and 3.60). The RAMS model first advances the atmospheric variables to time level t then calls LEAF to advance the surface condition and surface fluxes to time level $t + \Delta t$ before returning to the RAMS to update atmospheric variables to time level $t + \Delta t$.

3.5 Summary

A new and extended vegetation model for use in a mesoscale meteorological model has been developed based on Avissar and Mahrer (1988). The current version of the model, called the Land Ecosystem-Atmosphere Feedback (LEAF) model, corrects two major shortcoming in the AM88 formulation. These are the underestimation of the effect

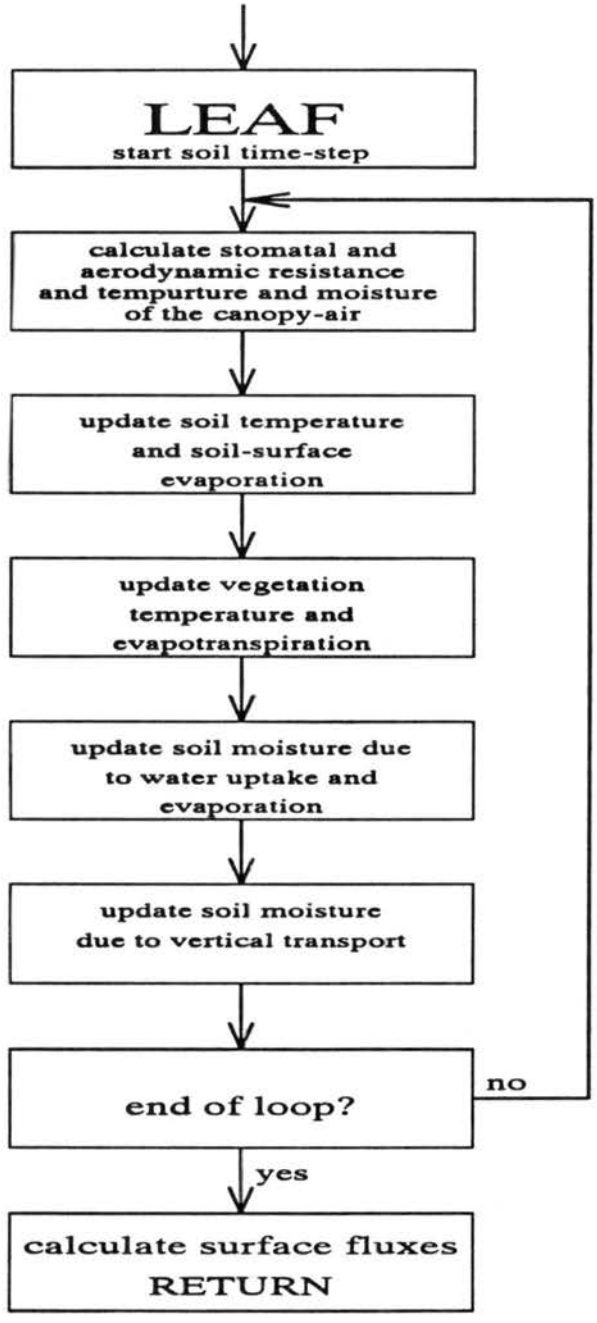

Figure 3.6: Solution flow-chart for the LEAF model.

of the leaf area index (LAI) and erroneously retrieving components of both the vegetation and soil surface sensible and latent heat fluxes from the total surface values. New features have been incorporated into the model including the introduction of SAI and LSAI, and the separation of vegetation and soil surface energy budgets. The model is thought to be an improved one. Validation and sensitivity studies using LEAF are reported in the next Chapter.

Chapter 4

IMPLEMENTATION AND SENSITIVITY STUDIES

Because of the large number of model parameters involved in describing the complex soil-vegetation-atmosphere system, it is difficult to prescribe the values for these parameters as well as the sensitivity of the atmospheric response to changes in these parameters. This is even more complicated when considering the real situation in which the surface is far from homogeneous in a model grid area, which usually consists of different surface coverages (e.g. vegetation, bare soil, and water body) and different species of vegetation. Traditionally, these parameters are prescribed using laboratory measurements of one dominant type of vegetation. However, it has been shown by Avissar (1992) that, even in a relatively homogeneous field, the vegetation parameters vary considerably due to different biophysical states. The deterministic approach simply becomes impossible.

In this chapter, the Multi-response Randomized Block Permutation (MRBP) procedure (Mielke, 1984, 1991) is used to improve LEAF model performance. Then, the Fourier Amplitude Sensitivity Test (Uliasz, 1988) is used to better understand the sensitivity of model results to the model parameters. Finally, several simulations with slightly perturbed model parameters are performed to understand some model behavior.

4.1 Improving LEAF Using MRBP

4.1.1 Initial Calibration

Thirteen LEAF model parameters (i.e. the ten parameters listed in Table 3.1 plus d_{smax} in Eq. 3.50, n in Eq. 3.33, and σ in Eq. 3.39) were optimized using the MRBP procedure. Specifically, MRBP randomly permutes the observed vector of values ($\mathbf{x}$)

relative to the model predicted vector of values ($\tilde{\mathbf{x}}$) and the agreement measure, ρ, is defined by

$$\rho = \frac{\mu_\delta - \delta}{\mu_\delta} \tag{4.1}$$

where $\delta = \frac{1}{n}\sum_{i=1}^{n} |\mathbf{x}_i - \tilde{\mathbf{x}}_i|$ and μ_δ is the average value of δ over all n! permutations. Notice that the Euclidean distance between vector value pairs is used to evaluate the agreement measure.

Two days during the FIFE 1987 experiment (Sellers et al., 1988), including both unstressed (June 6) and stressed (October 11) environmental conditions, were chosen so that the parameters are optimized to give better predictions with respect to three response values comprising $\mathbf{x}$ (net radiation, latent heat flux, and sensible heat flux) under these conditions. The half-hourly observations of these fluxes are interpolated to 5 minutes intervals and averaged over all the available sites, and a total of $n = 96$ groups of data are used by the MRBP procedure. The LEAF model is run with the observed atmospheric forcing, i.e. wind speed, atmospheric temperature, humidity, incoming long wave and short wave radiation, as shown in Figures 4.1 and 4.2. The initial soil (temperature and moisture) and vegetation (LAI, albedo, and height) conditions are also specified using averaged observed values. Note that the USDA soil class is silty clay loam for this tall grass prairie of eastern Kansas. Nine soil levels are used in the simulation and the soil temperature and volumetric moisture for the two days are listed in Table 4.1. Other surface conditions are listed in Table 4.2.

The model is first run with the default values described in Section 3.2.1 and the result shows poor model predictions, especially under the unstressed (summer) condition (Figure 4.3) with measure of agreement of $\rho = 0.699$ and the P-value of 3.1×10^{-186}. After the initial run, an integer frequency is assigned for each of the parameters so that the parameters were sampled differently within their specified ranges for an additional 695 model runs. Note that there are "gaps" between samples since integer frequencies were used. In the 695 model realizations, a number of runs provide agreement measures $(\rho) \geq 0.8$ with the best one being $\rho = 0.856$. However, it is quickly discovered that the

	Jun 6		Oct 11	
Z (m)	T (°C)	θ ($m^3 m^{-3}$)	T (°C)	θ ($m^3 m^{-3}$)
0.0	19.8	0.2	9.9	0.136
-0.015	19.8	0.248	9.9	0.136
-0.025	20.7	0.248	11.7	0.136
-0.05	20.1	0.273	15.5	0.170
-0.1	20.9	0.254	14.6	0.193
-0.3	20.5	0.346	23.1	0.264
-0.5	20.5	0.368	30.0	0.298
-0.75	20.5	0.360	30.0	0.295
-1.0	20.5	0.346	30.0	0.311

Table 4.1: Initial soil temperature and moisture profiles for June 6 and October 11, 1987 during the FIFE experiment.

Variable	Jun 6	Oct 11
Leaf Area Index	1.03	0.226
Stem Area Index	0.1	0.3
Total Surface Albedo	0.24	0.2
Vegetation Height (m)	0.31	0.25
Surface Roughness (m)	0.02	0.02

Table 4.2: Some surface parameters for June 6 and October 11, 1987 during the FIFE.

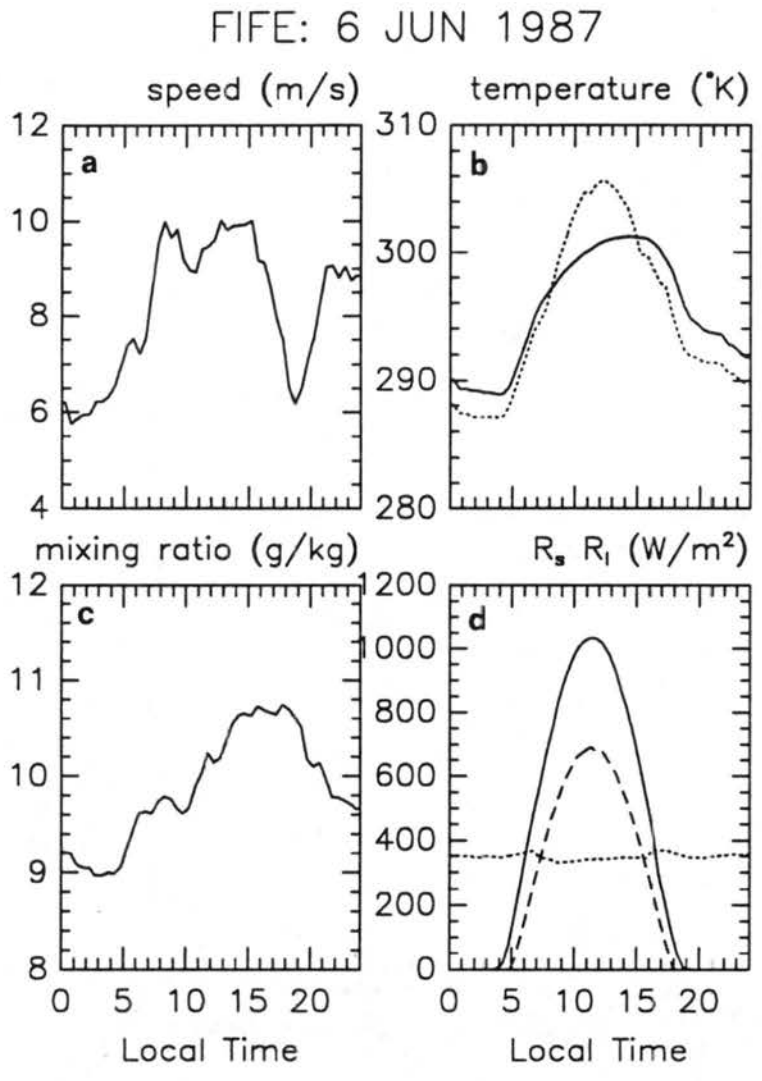

Figure 4.1: Atmospheric forcing to the LEAF model for June 6, 1987 during the FIFE experiment. (a) wind speed at 5.4 m, (b) temperature (solid line is screen height air temperature and dotted line is surface infrared radiation temperature), (c) mixing ratio, and (d) radiative forcing (solid line is downward short wave radiation, dashed line is downward long-wave radiation, and dotted line is observed net radiation).

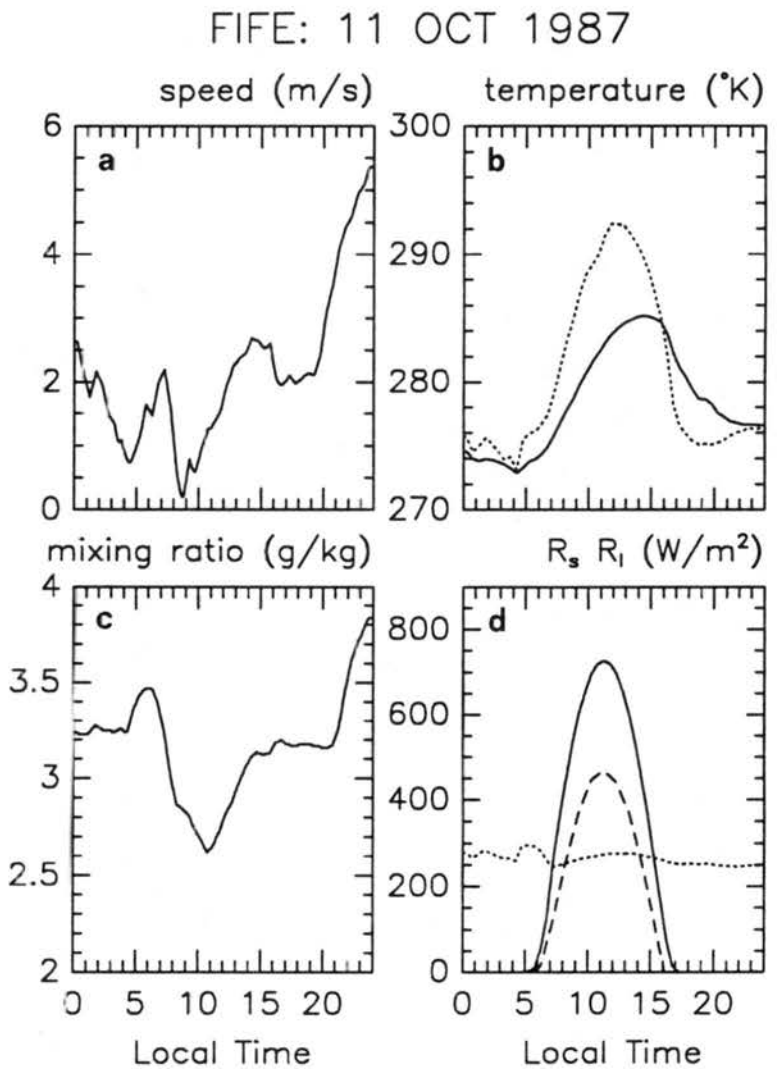

Figure 4.2: Same as Figure 4.1 except for October 11, 1987.

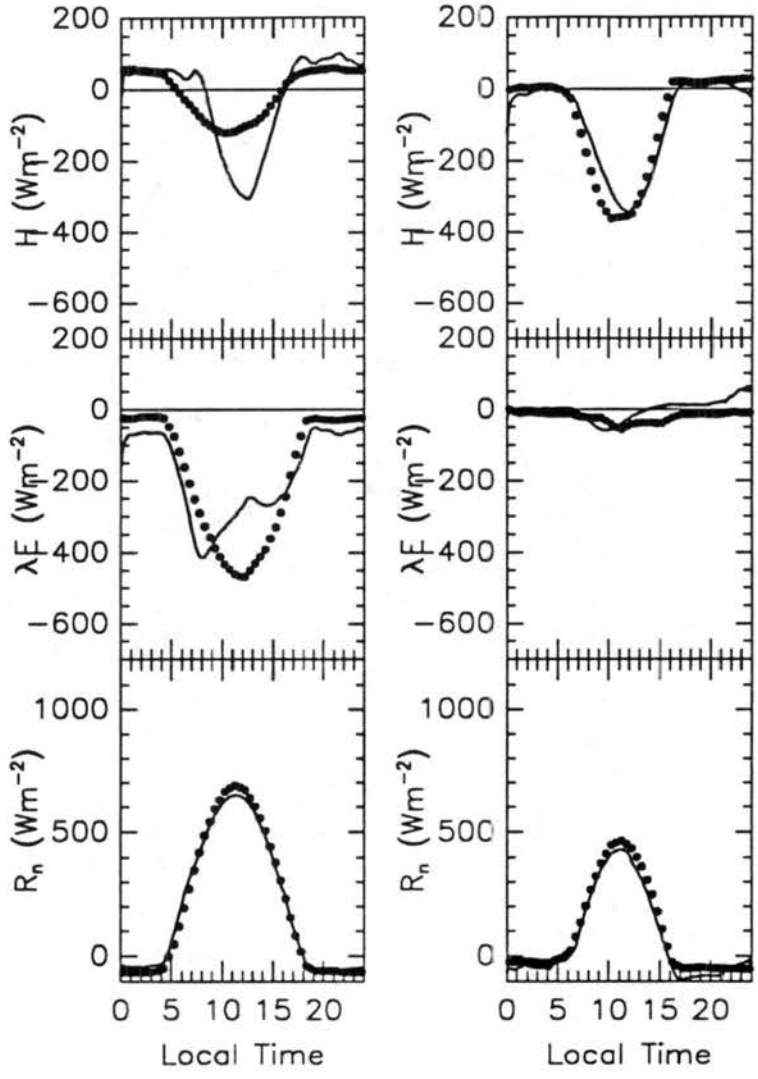

Figure 4.3: Comparison between model predictions and observations on sensible (H), latent (λE) heat fluxes and net radiation (R_n). Observations are shown in filled circles and model predictions are in solid lines. Left-hand side is for June 6 and right-hand side is for October 11 case.

parameter set that yields the best measure of agreement may be physically unsound or simply too different from our understanding of the mechanisms of atmosphere-vegetation exchanges of heat and moisture. In other words, the solution is not unique and scientific judgement must be used to choose a set of parameters. Figure 4.4 shows the result with $\rho = 0.840$ and the P–value is 1.74×10^{-195}. Table 4.3 and Figure 4.5 shows the resultant parameters for this set with $d_{smax} = 0.0072\ \mathrm{m\,s^{-1}}$, $n = 3.48$, and $\sigma = 2.17$.

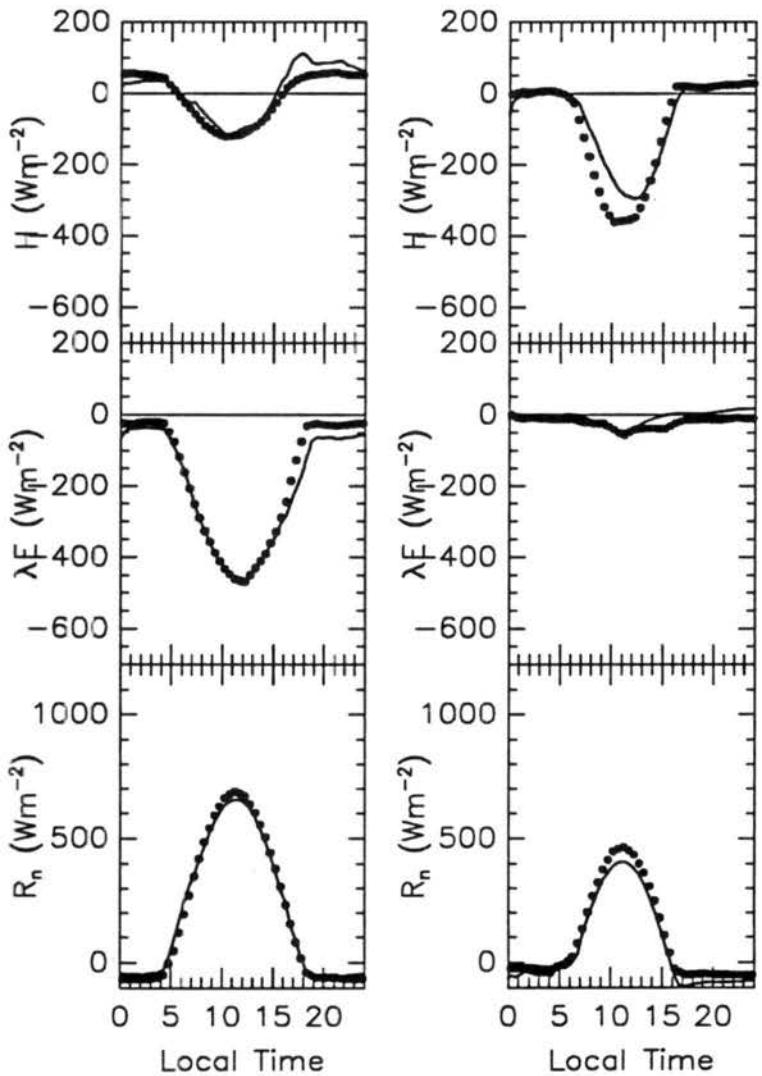

Figure 4.4: Same as Figure 4.1 but for the result from optimized LEAF simulation.

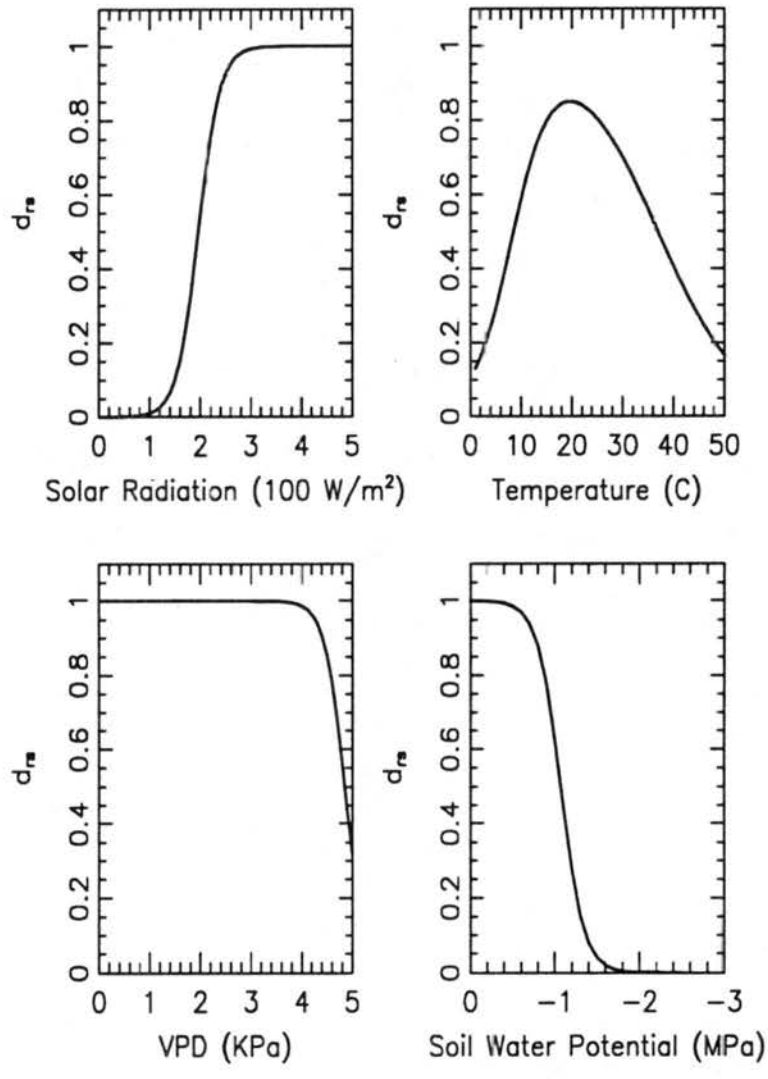

Figure 4.5: Same as Figure 3.1 but for environmental variables tabulated in Table 4.1.

Environmental factor	*Units*	X_{b_i}	S_i
Global radiation	Wm^{-2}	196	0.047
Temperature (cold range)	°C	8.33	0.258
Temperature (hot range)	°C	36.97	-0.124
Vapor pressure difference	Pa	4850	-0.0051
Soil water potential	Pa	1.1×10^6	7.42×10^{-6}

Table 4.3: Same as Table 3.1 but shows the parameters that produce better results.

4.1.2 Independent Test

In the last section the Multi-response Randomized Block Permutation procedure has been used to optimize a complicated vegetation–to–atmosphere exchange model (Land Ecosystem-Atmosphere Feedback model–LEAF). It is shown the procedure dramatically improved the model predictions for three responses (i.e. net radiation, sensible, and latent heat fluxes). Since some parameters are highly coupled, the solution is not unique and trained judgement must be involved to select a physically sound solution set. After the selection, two independent data sets are used to cross-validate the optimizing procedure. The first case is still from the FIFE experiment but for a different year. The data from August 3, 1989 is intentionally chosen due to the more complicated radiative forcing. As can be seen in Figure 4.6 the short wave radiation is far from a smooth clear day forcing as shown in Figures 4.1 and 4.2. The appearance of cloud is evident in the Figure. The soil temperature and moisture profile is shown in Table 4.4 and other surface conditions are shown in Table 4.5. The results using data before and after the optimization procedure are shown in Figure 4.7. The agreement measure is $\rho = 0.48$ and the P–value is 3.26×10^{-66} when using the old input data and $\rho = 0.623$ and the P–value is 3.27×10^{-62} when using the new input data.

The second independent data set is for July 30, 1986 which is reported by Verma et al. (1989). The data was taken at the same site that was later used by the FIFE experiment so the same biophysical processes were expected and our previous optimization exercise should still be valid. It was an extremely hot summer day as can be seen in Figure 4.8. Again, the soil temperature and moisture profiles are listed in Table 4.6 and other surface conditions are listed in Table 4.5. The results using data before and after the optimization

Aug 3, 1989		
Z (m)	T (°C)	θ ($m^3 m^{-3}$)
0.0	26.2	0.318
-0.015	26.5	0.318
-0.025	27.3	0.318
-0.05	27.7	0.318
-0.1	25.5	0.270
-0.3	25.7	0.309
-0.5	25.9	0.302
-0.75	25.9	0.281
-1.0	25.9	0.276

Table 4.4: Initial soil temperature and moisture profiles for August 3, 1989 during FIFE experiment.

Variable	Aug 3	Jul 30
Leaf Area Index	1.35	1.98
Stem Area Index	0.16	1.32
Total Surface Albedo	0.24	0.2
Vegetation Height (m)	0.35	0.31
Surface Roughness (m)	0.02	0.02

Table 4.5: Some surface parameters for the August 3, 1989 and July 30, 1986 cases.

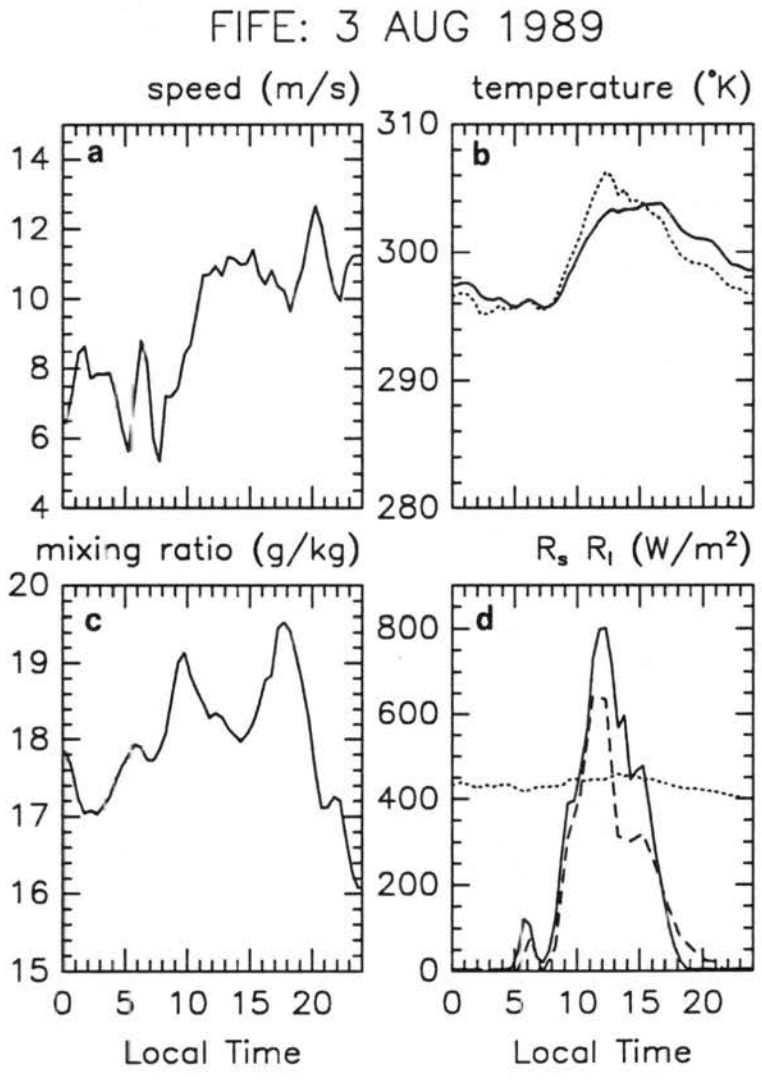

Figure 4.6: Same as Figure 4.1 except for August 3, 1989.

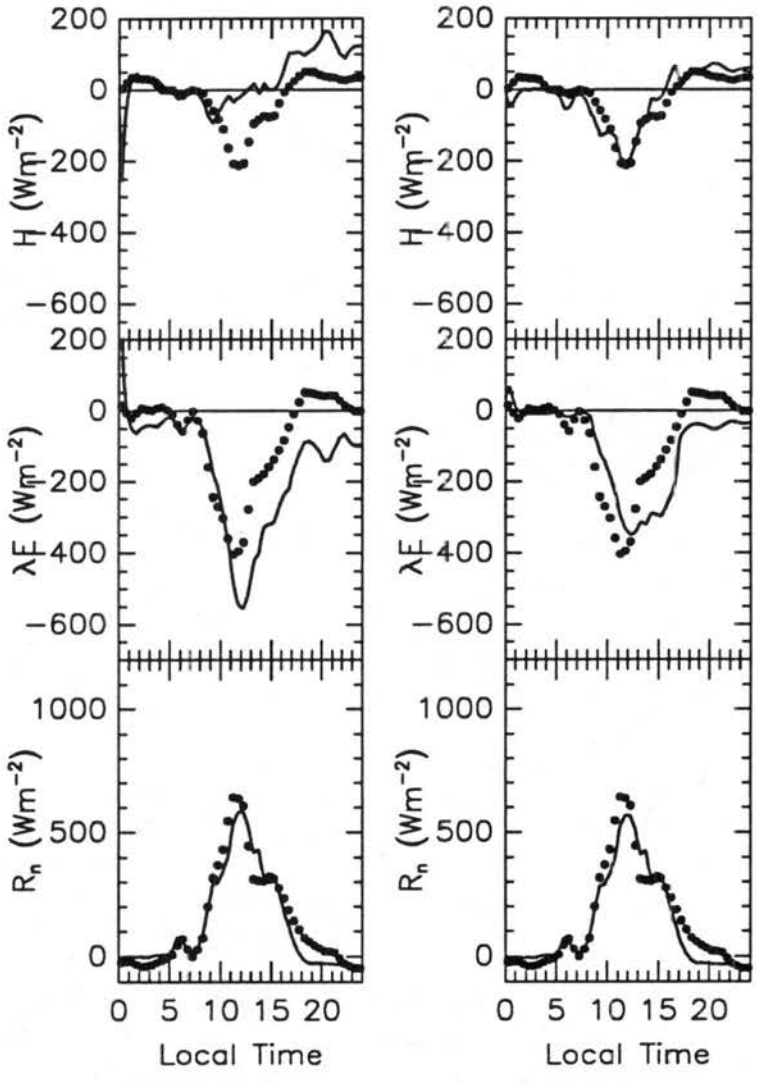

Figure 4.7: Comparisons between observation and simulation for the August 3, 1989 FIFE experiment using input model parameters before (left panels) and after (right panels) the optimization.

procedure are shown in Figure 4.9. The agreement measure is $\rho = 0.25$ and the P–value is 7.22×10^{-24} when using the old parameters and $\rho = 0.76$ and the P–value is 2.22×10^{-36} when using the new parameters.

Jul 31, 1986		
Z (m)	T (°C)	θ ($m^3 m^{-3}$)
0.0	29.3	0.2
-0.02	29.3	0.26
-0.25	28.7	0.26
-1.0	26.8	0.32
-1.5	25.6	0.32

Table 4.6: Initial soil temperature and moisture profiles for July 30, 1986 taken from Verma et al. (1989).

In summary, the MRBP procedure is used to improve the LEAF model performance. The procedure randomly permutes observed values relative to the model predictions and the agreement measure is based on the Euclidean distance. Half-hourly data interpolated to 5 minutes intervals from June 6 and October 11, 1987 of the FIFE experiment are used as dependent data (total of 578 groups). Half-hourly data interpolated to 5 minutes intervals from August 3, 1989 of FIFE (total of 289 groups) and hourly data during daylight hours from July 30, 1986 (total of 97 groups) are used as independent data sets. The independent data sets are chosen to have very different environmental conditions than the dependent data set. Thirteen parameters are optimized. Out of the thirteen parameters, eleven control the magnitude of the stomatal conductance and two control the aerodynamic conductances. The results are tabulated in Table 4.7.

4.2 Fourier Amplitude Sensitivity Test (FAST)

In the Section 4.1, the MRBP procedure is used to guide the selection of a certain set of parameters that are associated with the stomatal and aerodynamic resistance functions. However there are other parameters that are specified using field data (e.g. total surface albedo, leaf area index, stem area index, vegetation height). This raises a question: *How sensitive is the model solution to uncertainties in the parameters of the model?* In some

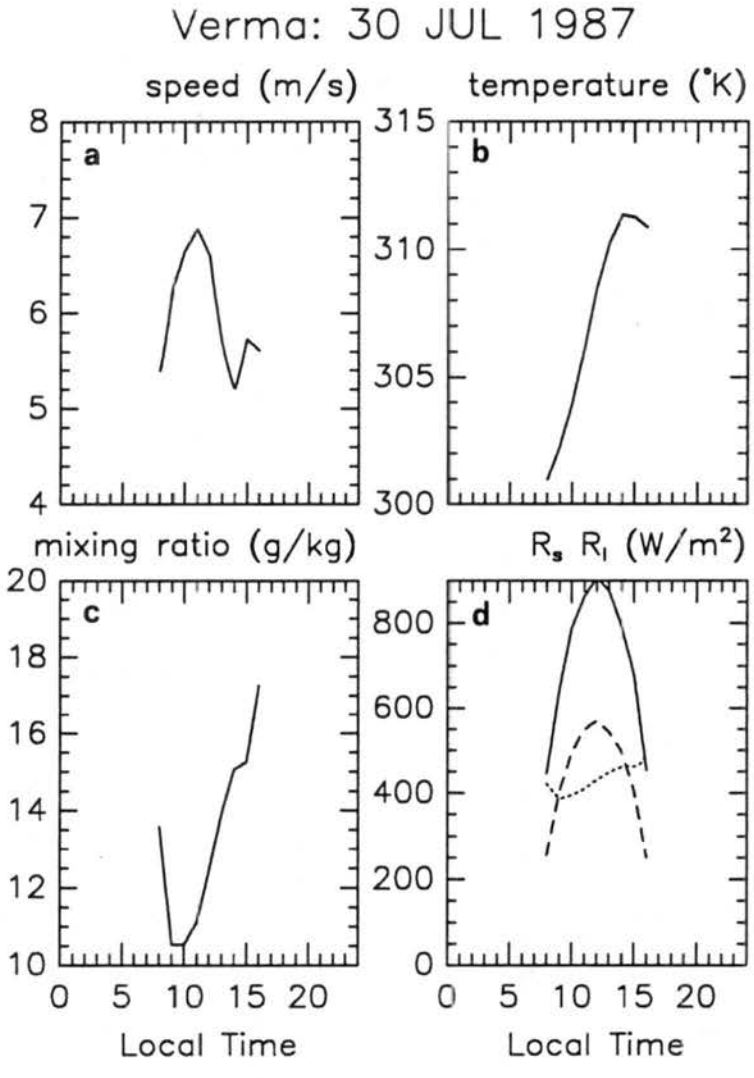

Figure 4.8: Same as Figure 4.1 except for July 30, 1986. Scott Denning of the Atmospheric Science Department at Colorado State University originally provided the data.

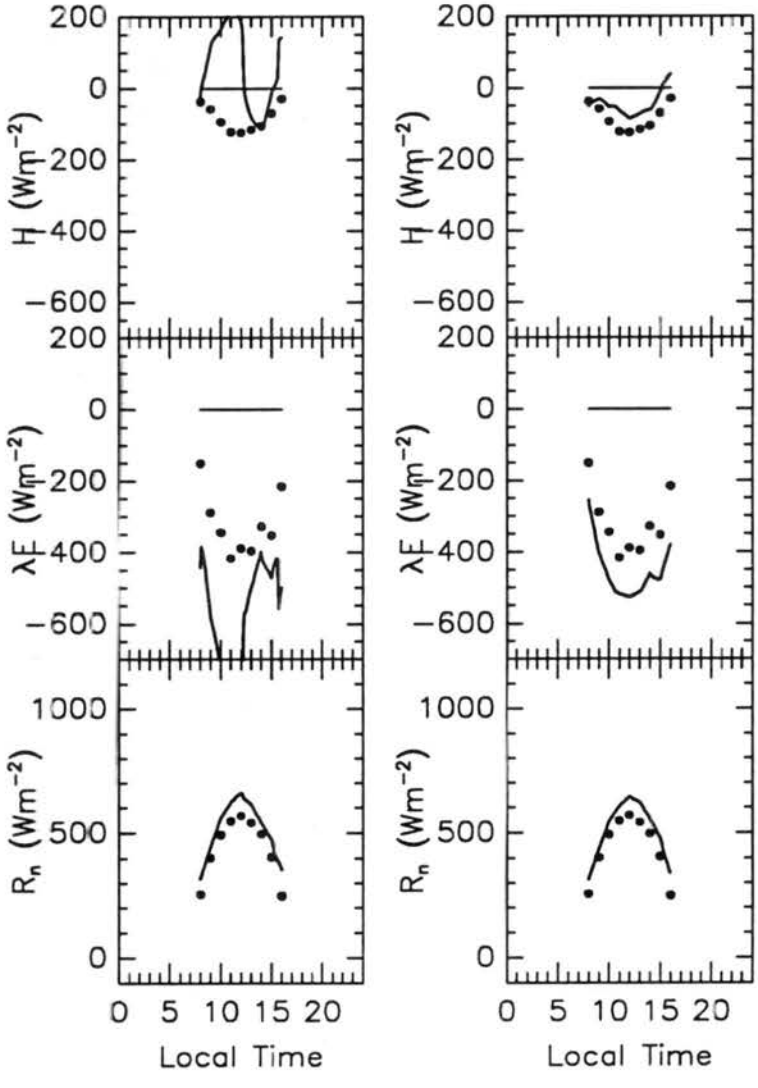

Figure 4.9: Same as Figure 4.7 but for July 30, 1986.

Tests		ρ	$P-value$	remark
Jun 6 and Oct 11, 1987	before	0.699	3.1×10^{-186}	Clear days
	after	0.840	1.7×10^{-195}	
Aug 3, 1989	before	0.48	3.3×10^{-66}	cloudy day
	after	0.623	3.3×10^{-62}	
Jul 30, 1986	before	0.25	7.2×10^{-24}	hot and dry
	after	0.76	2.2×10^{-36}	

Table 4.7: Summary of the LEAF's performance before and after the MRBP procedure.

cases a totally different solution might result from a slight change to the model input parameters. Due to the nonlinearity of the system, it is difficult to isolate the effect of a single parameter on the final solution. A model solution should, therefore, always be considered questionable until we fully understand the model sensitivity to various input parameters and the physics behind this sensitivity.

One traditional model sensitivity test has been to use the extreme values of a parameter as inputs for two model runs and then to compare the results. This procedure can tell us if there is a difference between the results but fails to tell the probable range of variation of the final solutions as a result of uncertainties in the input parameters. Also, only one parameter can be tested at a time with this approach. If more statistics are desired, the model has to be run over and over again for a set of different combinations of input parameters. The number of model runs required will be equal to mz^n, where m is the number of model output variables to be examined, z is the number of different input values for each parameter, and n is the number of parameters to be tested. This simple approach is obviously impractical when z and n are large.

Fortunately, a more efficient procedure has been developed to perform such a nonlinear sensitivity analysis of multi-parameter model systems (Cukier et al., 1978). This Fourier Amplitude Sensitivity Test (FAST) has been applied to a Lagrangian long-range transport model (Uliasz, 1988) and has proven to be accurate and objective.

4.2.1 Description of FAST

Consider a simple model:

$$Y = F(X) \tag{4.2}$$

where $X = \{x_i, i = 1, ..., m\}$ is an input vector of model parameters, F is an operator acting on X, and $Y = \{y_j, j = 1, ..., n\}$ is a output vector. Due to the uncertainties of the input parameters, the first moment statistic (the ensemble mean) of the output vector becomes:

$$\langle y_i \rangle = \int ... \int y_i(x_1, ..., x_m) p(x_1, ..., x_m) dx_1 ... dx_m \tag{4.3}$$

where p is the probability function for X. Assuming the input parameters are uncorrelated, the FAST method first finds a search curve, s, in this multi-dimensional parameter space. This is done by the transformation:

$$x_i = G_i(sin\, \omega_i s), \tag{4.4}$$

in which G_i's are transformation functions and ω_i are a set of incommensurate frequencies (i.e., $\sum_{i=1}^{m} \gamma_i \omega_i = 0$, γ_i are integers) assigned to each input parameters, x_i. The functions G_i are chosen so that the arc length, ds, is proportional to the probability $p(x_1, ..., x_m)dx_i$ for all i. Thus, Equation 4.3 becomes a one-dimensional integral over the search curve s:

$$\langle y_i \rangle = \lim_{T \to \infty} \frac{1}{2T} \int_{-T}^{T} y[x_1(s), ..., x_m(s)]\, ds. \tag{4.5}$$

Practically, integer frequencies are assigned to different input variables and the search curve is a closed loop in s that optionally samples each of the parameters of interest. Since the loop is closed, the model outputs become periodic in s and can be analyzed to obtain their Fourier coefficients. The mean value and the variance of the model outputs can then be written in terms of Fourier coefficients. The application of the FAST method is straightforward and a suggested three-step scheme can be found in Uliasz (1988). In the first step of the analysis different frequencies are assigned to input parameters and calculate input parameter combinations as sampling points from the search curve s. The second step is to run multiple model solution for provided parameter combinations. The final step uses the model results from the second step and performs Fourier amplitude analysis to obtain output statistics. As a summary, the FAST analysis requires frequency distributions of model input parameters as input data and the output will be:

1. mean values of model outputs;

2. variances of the model outputs due to the uncertainties in input parameters;

3. partial variances of the model output due to the uncertainty in each input parameter.

4.2.2 Results from FAST

Since FAST is designed to test model error due to uncertainty of model parameters which are treated constant in time or space, uncertainties in the external forcing to the model (e.g. wind, temperature, humidity, radiation, and precipitation) and initial conditions (e.g. soil moisture and temperature) should not be included. In this Section, two tests are performed using the same atmospheric forcing from June 6, 1987 of the FIFE experiment but with different soil moisture. It is intentional to keep the external forcing simple to reduce the uncertainty. The June 6, 1987 case of the FIFE experiment was a clear early summer day, and we do not expect much measurement error in the atmospheric forcing variables. The reason to make soil moisture variable is that we expect that LEAF is very sensitive to the uncertainty in soil moisture. By making soil moisture variable, we can observe the interaction between model parameters (boundary conditions) to the initial condition.

Like many other surface schemes used in atmospheric models, the primary responsibility of the LEAF model is to correctly partition the net radiation into sensible and latent heat fluxes. For this reason, the average and maximum sensible and latent heat fluxes are chosen as model output variables. Seven model parameters are chosen: maximum stomatal conductance (d_{smax} in Eq. 3.50); the exponent of the wind profile law in the canopy (n in Eq. 3.33); the threshold value of LAI for sparse canopy (σ in Eq. 3.39); the leaf area index (LAI, Eqs. 3.31, 3.50, 3.68); the total surface albedo (α_T in Eq. 3.67); the height of vegetation (h in Eq. 3.26, 3.27); and the soil surface roughness (z_0' in Eq. 3.40). For these input model parameters, a uniform distribution among a specified range is used (see Table 4.8) since we do not know the actual distribution. A total number of 175 model runs (Uliasz, 1988) are performed for each (i.e. wet and dry) cases. Figure 4.10 illustrates how the seven parameters are sampled.

Table 4.9 shows the result of a test with observed soil moisture content (see Table 4.1). Recall that the soil moisture is relatively wet for this early summer day and the vegetation

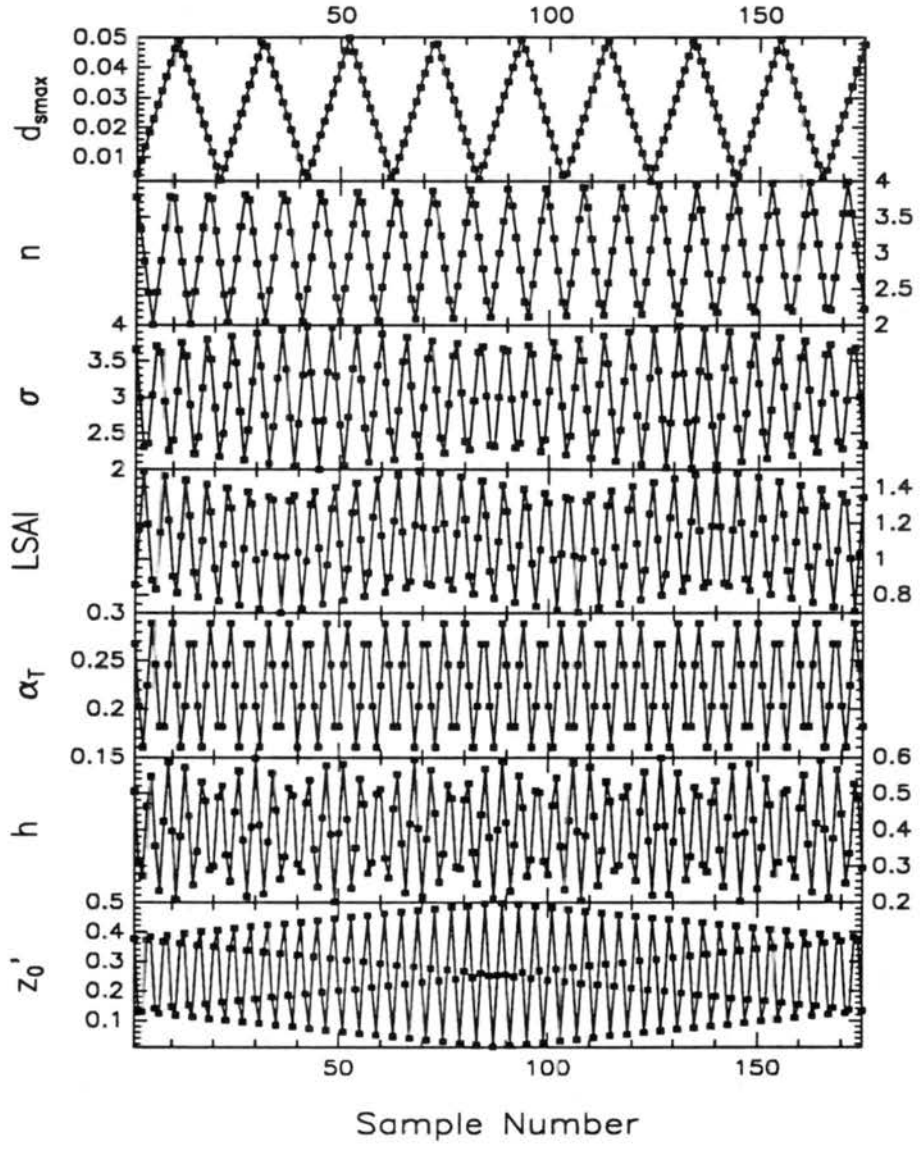

Figure 4.10: Coverage of the seven parameters within the specified ranges. A total of 175 samples are shown in the Figure.

Parameter	min	max
d_{smax} ($\mathrm{m\,s^{-1}}$)	0.002	0.05
n	2.0	4.0
σ	2.0	4.0
LAI	0.7	1.5
α_T	0.15	0.3
h (m)	0.2	0.6
z_0' (m)	0.01	0.5

Table 4.8: Input parameters and their maximum and minimum values for a uniform distribution.

does not experience water stress. The results show the mean and the maximum latent heat flux, denoted by $\lambda\bar{E}$ and λE_{max}, are the most sensitive to albedo and the maximum stomatal conductance, d_{smax}. This is because vegetation does not suffer water stress and most of the absorbed radiative energy turns into latent heat flux. The maximum stomatal resistance becomes less important than the total surface albedo, which determines the amount of solar energy which is absorbed by vegetation. On the other hand, the mean and the maximum sensible heat flux, denoted by $\bar{H}$ and H_{max}, are more sensitive to the maximum stomatal conductance than the surface albedo since the maximum stomatal conductance actually determines the specific amount of absorbed radiative energy that is turned into sensible heat flux. The exponent of wind profile law in the canopy, n, is the next parameter to which LEAF is sensitive. This is because n determines the wind speed in the canopy and thus the aerodynamic resistances of leaf-to-canopy-air and ground-to-canopy-air transport processes. The threshold value of LAI for sparse canopy, σ, spans a range between 2 and 4 and determines the relative contribution of the canopy to the ground-to-canopy-air aerodynamic resistance. As expected, this is a secondary parameter and the model is not too sensitive to the uncertainties of this parameter. The actual height of the canopy, h, determines the surface roughness and the displacement height of the canopy. For the specified range (0.2 to 0.6 meters), the vegetation surface roughness varies between 0.026 and 0.078 m and the displacement height varies between 0.126 and 0.378 m. Both are insignificant changes when the heat fluxes are linearly proportational

to the logarithm of surface roughness (c.f. Eqs. 3.28, 3.29, and 3.30). The same reason applies to the soil surface roughness length, z_0', when the specified range is too small to allow significant changes in heat fluxes.

output	mean	total variance	partial variances (%)						
	$W\,m^{-2}$	$W\,m^{-2}2$	d_{smax}	n	σ	LAI	α_T	h	z_0'
$\lambda\bar{E}$	-158.0	156.2	26.3	14.6	2.7	6.2	34.1	1.7	.5
$\bar{H}$	-44.86	38.40	60.5	6.8	1.1	2.1	10.2	.4	.3
λE_{max}	-499.7	1605.	24.7	18.9	3.6	9.8	28.0	1.9	.6
H_{max}	-158.3	389.9	60.7	6.3	1.0	1.9	8.8	1.9	.3

Table 4.9: Mean, total variance, and partial variances due to uncertainties in input model parameters.

Instead of using the observed soil moisture, which is relatively wet, the second test initializes the model with a uniformly dry soil. The soil moisture content is 0.2 $m^3\,m^{-3}$and is considered to be dry for heavy (high clay content) soil commonly observed over the Great Plains. We choose this soil moisture content because it is below the wilting point for vegetation to extract water and is still moist enough to allow evaporation from the soil (Lee and Pielke, 1992). The result from the FAST analysis is demonstrated in Table 4.10. A significant change in sensitivity to model parameters is found by comparing Tables 4.9 and 4.10. As expected, the model is no longer sensitive to the changes in stomatal conductance, d_{smax}. The exponent, n, of the wind profile law in the canopy becomes the most sensitive parameter since it controls the wind speed in the canopy and thus the sub-canopy exchange process (c.f. Eq. 3.41). The model is also sensitive to the total albedo and LSAI. The mean and maximum latent heat flux is more sensitive to the changes in LSAI, and the mean and maximum sensible heat flux is more sensitive to the changes in total albedo. These results show an interesting model behavior: Since the soil surface albedo is determined using soil moisture content and zenith angle only (Idso et al., 1975; McCumber, 1980), the total albedo actually defines the vegetation albedo and thus the sensible heat flux from the vegetation (assuming transpiration is minimum). The LSAI on the other hand determines the amount of energy transmitted through the canopy and available for evaporation from the soil.

output	mean	total variance	partial variances (%)						
	$W\,m^{-2}$	$W\,m^{-2}2$	d_{smax}	n	σ	LAI	α_T	h	z_0'
$\lambda\bar{E}$	-117.3	87.78	.1	44.9	9.2	21.9	11.4	.4	.7
$\bar{H}$	-86.10	70.59	.0	36.9	7.9	2.9	35.8	2.8	.6
λE_{max}	-406.6	2209.	.0	46.3	9.4	31.2	7.6	.4	1.1
H_{max}	-255.6	1149.	.0	49.9	9.3	12.6	12.4	1.0	.9

Table 4.10: Mean, total variance, and partial variances due to uncertainties in input model parameters. Same as Table 4.8 except the soil is relatively dry.

Using the FAST technique, the question on "How sensitive is the LEAF model solution to uncertainties in the parameters of the model?" can be answered. Unfortunately, it is demonstrated that the model is sensitive to different parameters in different environmental conditions. In other words, it is difficult to find a generalized parameter set that will work all the time. Among the seven tested parameters, less care is needed to specify the vegetation height and the soil surface roughness. Parameters d_{smax}, n, and σ can be determined using the technique shown in Section 4.1. The parameters LSAI and α_T must be specified with care while special attention is needed to specify the total albedo during both wet and dry conditions. Notice that the assumption has been made that each parameter can only vary within its specified range.

4.3 Further Tests

Sometimes knowing the importance of each model parameter on the model results is not enough. We also wish to know the model tendencies with respect to changes in model parameters. This information is not provided by the FAST experiments. The traditional sensitivity test is used here by changing one parameter at a time (Schadler et al., 1990; Martin et al., 1989) while holding the other six parameters constant. Again, the June 6, 1987 case of the FIFE experiment and the actual soil moisture profile is used. The reference parameter set has been mentioned in the previous Sections and is tabulated in Table 4.11 as a summary. The seven parameters are perturbed by 10 percent around their reference values and the same outputs, namely the mean and maximum sensible and latent heat fluxes, are examined. Figure 4.11 shows the qualitative response of this test.

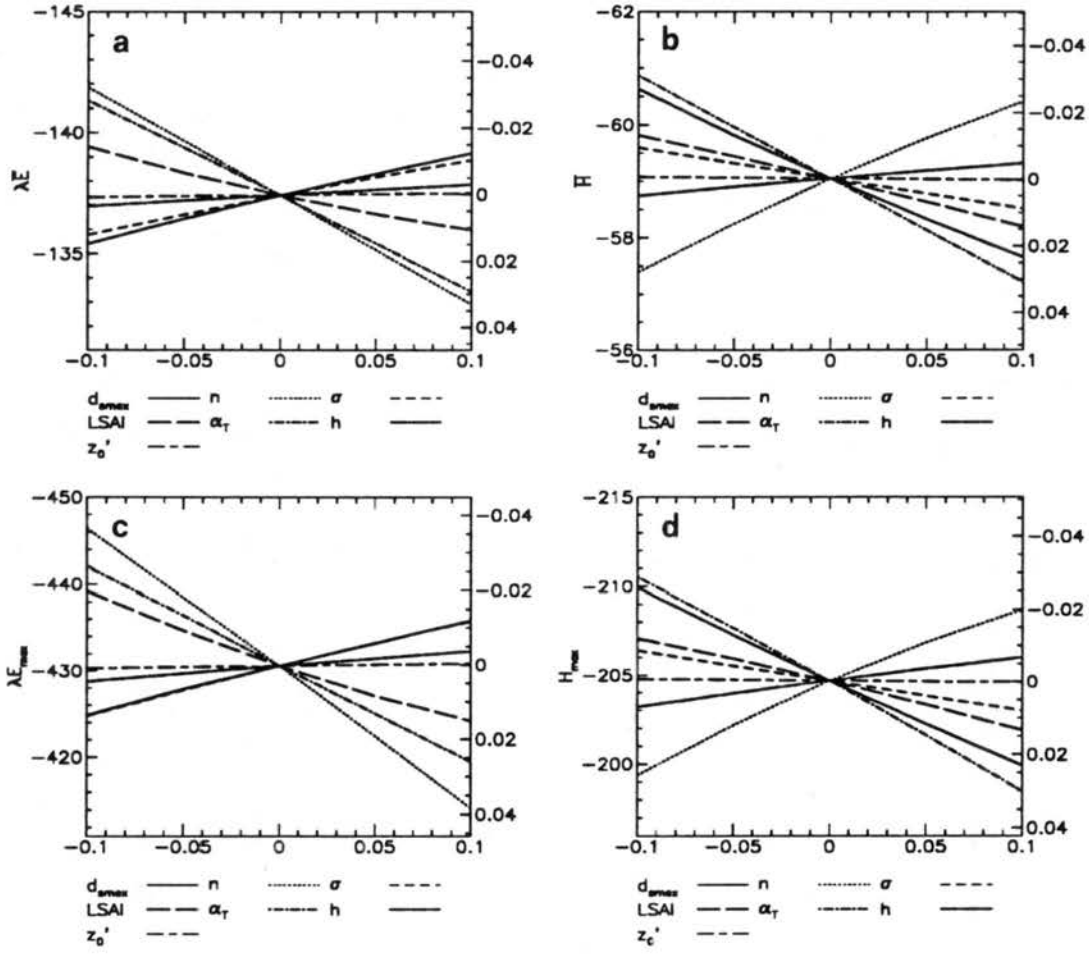

Figure 4.11: Sensitivity of (a) mean latent, (b) mean sensible, (c) maximum latent, and (d) maximum sensible heat fluxes to changes in model parameters. Labels are in relative changes (horizontal and right vertical axes) and $\mathrm{W\,m^{-2}}$(left vertical axis).

Parameter	reference
d_{smax} (m s^{-1})	0.0072
n	3.48
σ	2.17
LAI	1.13
α_T	0.24
h (m)	0.31
z_0' (m)	0.02

Table 4.11: Input reference parameters for the case of June 6, 1987 of the FIFE experiment.

As discussed before, this test does not show the real model sensitivity on input parameters. Nevertheless, it does show the model sensitivity around a pre-chosen set of parameter values. This is helpful especially when a model provides a set of default values (i.e. the reference values) for its input parameters. Since the same trend can be observed between the maximum and the average quantities (e.g. $\lambda\bar{E}$ and λE_{max}), only the quantities themselves are referred to. Table 4.12 summerizes the tendency of changes in latent and sensible heat fluxes as a response to changes in the seven input parameters around their reference values.

Parameter	tendency in parameter	tendency in λE	tendency in H
d_{smax}	↑	↑	↓
n	↑	↓	↑
σ	↑	↑	↓
LAI	↑	↓	↓
α_T	↑	↓	↓
h	↑	↑	↑
z_0'	↑	↑	↑

Table 4.12: Trend of changes in latent and sensible heat fluxes as response to changes in seven input parameters.

When the maximum stomatal conductance, d_{smax}, increases, the water vapor flow from the interior to the surface of the leaves becomes easier and results in an increase in latent heat flux and a decrease in sensible heat flux. When the exponent, n, increases the mean wind speed in the canopy decreases and the in-canopy aerodynamic resistances (i.e.

r_b and r_d) increase resulting in a decrease of latent heat flux. At first glance, the sensible heat flux should also decrease for the higher aerodynamic resistance. However, sensible heat flux actually increases as a result of the reduced latent heat flux. At the beginning, both sensible and latent heat fluxes should decrease due to a higher aerodynamic resistance and cause the leaf and soil temperature to rise. This raise of temperature promotes sensible heat flux and suppresses latent heat flux due to a higher stomatal resistance.

When the threshold coverage, σ, increases the latent heat flux increases and the sensible heat flux decreases while when the LSAI increases both the sensible and latent heat fluxes decrease. These two results show that the contribution from the soil is large. Recall that, from Equation 3.39, the aerodynamic resistance for transfer below the canopy is weighted between the bare soil value and the closed canopy value by $(1 - \mathrm{LSAI}/\sigma)$ and LSAI/σ), respectively. When σ becomes large the effect from the canopy becomes small and the soil contribution becomes large. When LSAI becomes large the effect from the canopy becomes large and the soil contribution becomes small. The fact that λE increases following the increase of σ and decreases following the decrease of LSAI shows that the evaporation from the soil is large compared to the transpiration by vegetation in this case. On the other hand, H decreases following both the increase of σ and LSAI. This can be understood by realizing taht the soil temperature is higher than the vegetation temperature in this very sparse canopy. When σ becomes large, the contribution from the soil becomes small and the sensible heat flux decrease. When LSAI increases, the contribution from the soil becomes small and the sensible heat flux decreases.

When the total surface albedo, α_T, increases, the absorbed radiative energy decreases, and both the sensible and latent heat fluxes decrease, as expected. The vegetation height, h, and the soil surface roughness, z_0', are used in calculating the aerodynamic resistances. When the surface is rough (higher values of h and z_0'), the aerodynamic resistance becomes small and both the sensible and latent heat fluxes increase. Although, as discussed earlier, 10 percent changes in h or z_0' are very small and the heat fluxes change little as a response to these small changes in surface roughness.

4.4 Summary

The LEAF model has been implemented into the CSU-RAMS as an optional surface module. The LEAF model is first "calibrated" using field observations and then tested against two independent data sets. The result shows the model can realistically re-produce the observed latent and sensible heat fluxes with small error. Sensitivity studies are then performed to understand the model behavior (or characteristics) when changing the values of model parameters. The most important conclusion from the FAST experiments is that the model responds to the changing environment quite differently for different situations (e.g. wet soil versus dry soil) which implies that a unique set of parameters can not be used for any environmental conditions. As recently suggested by Camillo (1991), some of the parameters may need to be re-evaluated on a daily basis. Nevertheless, when the observational data record is long enough, the model can be calibrated to work most of the time.

Finally, a conventional "perturbation" sensitivity study is performed to understand the model behavior for a fixed environment. It is found, for example, that the contribution of heat fluxes from the soil below the canopy of a tall grass prairie cannot be ignored. The evaporation from the soil can be larger than that of the canopy.

Chapter 5

SENSITIVITY OF ATMOSPHERIC BOUNDARY STRUCTURE ON VEGETATION

The sensitivity studies presented in the last Chapter were performed using prescribed atmospheric forcing. There was no feedback between the atmosphere and the surface. In reality, the atmospheric boundary layer changes its structure and characteristics in response to the change in surface forcing, while, at the same time, the surface fluxes changes their magnitude in response to the changes in turbulence intensity and moisture content in the atmospheric boundary layer. For example, during daylight hours, the atmospheric boundary layer grows and destabilizes after gaining sensible heat from the surface. Turbulent mixing helps to redistribute momentum, heat and water vertically resulting in a warmer and dryer boundary layer which, in turn, promotes additional surface heat and moisture fluxes. In this Chapter, the sensitivity of the atmospheric boundary layer to different surface cover is studied.

5.1 RAMS Model Setup

As mentioned previously, LEAF is implemented in the RAMS as an optional surface module. RAMS is a highly versatile atmospheric modeling *system*. It is based on a merger of a nonhydrostatic cloud model (Tripoli and Cotton, 1989a,b) and two hydrostatic mesoscale models (Mahrer and Pielke, 1977; Tremback et al., 1985) . RAMS consists of an ISentropic ANalysis package (ISAN), a Visualization and ANalysis package (VAN), and the RAMS atmospheric model (Walko and Tremback, 1991; Pielke et al., 1992). It has been used for numerous studies including a mesoscale convective system (Tremback, 1991), a pre-frontal squall line (Cram, 1990), passive tracer experiments (Moran, 1992) and the predictability on thermally-induced circulations (Zeng, 1992).

There are a number of options available in the RAMS. A user can configure the RAMS specifically for the problem that is studied by choosing the desired options from an input menu. These options have been described in Walko and Tremback (1992), Cram et al. (1992), Pielke et al. (1992) and more recently in Moran (1992). The options include the choice of model dynamic (hydrostatic or non hydrostatic), model physics (radiation schemes, turbulence parameterizations, moist processes, surface parameterizations), and model numerics (spatial grid structures, time differencing schemes, model initial and boundary conditions, input/output controls). The options used in this study are: non-hydrostatic; Chen and Cotton (1983b, 1983a) radiation parameterization; deformation K (Tremback, 1991) turbulent diffusion parameterization; condensation of cloud water vapor to cloud water when supersaturation occurrs; and the LEAF surface parameterization. A second order leapfrog time-split scheme described in Tripoli (1988) is used to integrate the model forward in time. The time step is 15 seconds. The model domain is discretized into 5(x)×40(z) and 80(x)×40(z) atmospheric grid points with 7 soil vertical levels for the quasi-one-dimensional[1] atmospheric boundary layer simulations and for the two-dimensional simulations, respectively. The grid-increments are 5 km Δx and 100 m Δz with a vertical grid stretch ratio of 1.1 up to a grid-increment of 800 m. The Klemp and Durran (1983) model top boundary condition with 10 Rayleigh friction damping layers (Arritt, 1985; Cram, 1990) is utilized to prevent upward propagating gravity waves from reflecting back downward. A cyclic lateral boundary condition is used for quasi-one-dimensional simulations while the Klemp and Wilhelmson (Klemp and Wilhelmson, 1978) radiative lateral boundary condition with a propagating gravity wave speed of 20 $m\,s^{-1}$is used in two-dimensional simulations to prevent lateral boundary reflections. The model is initialized with the Denver sounding observed at 1200 UTC, June 6, 1990 (Figure 5.1) and integrated forward in time for 24 hours.

---

[1]The manner in which RAMS is coded makes it easier to perform 1-D experiments with a uniform 2-D cyclic boundary condition formulation, rather than an actural 1-D vertical configuration.

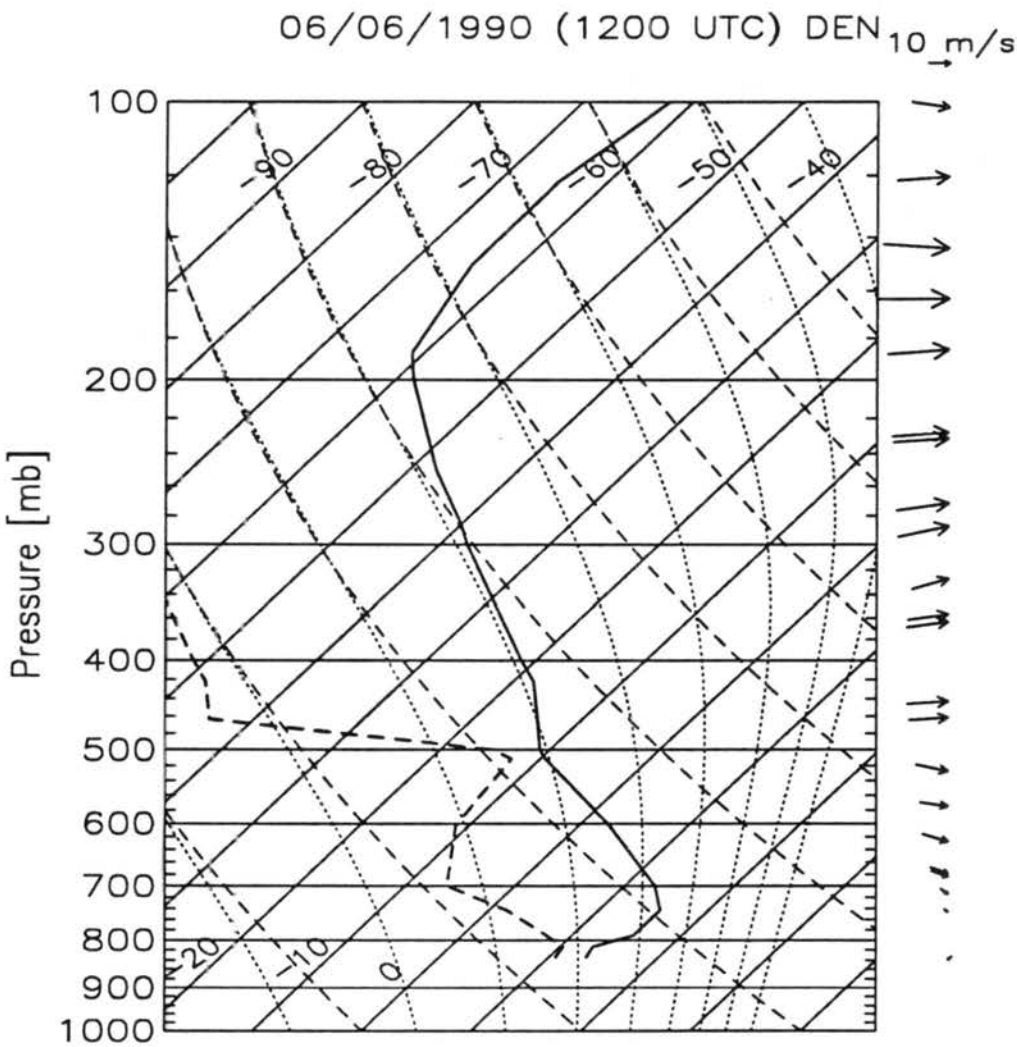

Figure 5.1: Denver sounding at 1200 UTC, June 6, 1990.

5.2 LEAF Model Configurations

There is other information needed in order to start LEAF model. First of all, the soil temperature and moisture need to be initialized. Seven soil layers are used with one top soil layer, three root-zone soil layers, and three recharging soil layers. The soil grid increments are variable with thiner soil layers near the surface. Table 5.1 shows the soil layer structure and initial soil temperature and moisture profiles. The soil temperature profile interpolated from soil temperature observations at the Colorado State University Main Campus Weather Station (Odelia Bliss, personal communication, 1992) is used in the following simulations with the top soil temperature replaced by 10.6 °C (3 °C lower than the observed screen height temperature). Three soil moisture profile are used in the following studies. The soil moisture profile S1 is interpolated from the soil moisture profile of the June 6, 1987 case of the FIFE experiment. This soil moisture profile represents a common spring-time wet soil profile. The soil moisture profile S2 simply replaces the profile S1 by a drier top soil moisture. This moisture profile mimics a soil that has been severely desiccated by the solar radiation from the previous days. The third soil moisture profile, S3, simply replaces the profile S1 by a dryer root-zone moisture. The value 0.2 of volumetric soil moisture is near the wilting point for the silty clay loam soil type commonly observed in the central Great Plains.

		S1	S2	S3
Z (m)	T (°C)	θ ($m^3 m^{-3}$)	θ ($m^3 m^{-3}$)	θ ($m^3 m^{-3}$)
0.00	10.6	0.200	0.100	0.200
-0.05	15.4	0.273	0.273	0.200
-0.10	17.4	0.254	0.254	0.200
-0.25	17.6	0.346	0.346	0.200
-0.50	15.8	0.368	0.368	0.368
-0.75	15.2	0.360	0.360	0.360
-1.00	14.4	0.346	0.346	0.346

Table 5.1: Initial soil temperature and moisture profiles.

Beside soil temperature and moisture profiles, LEAF requires a vegetation class (Table 3.2) as an input. A set of pre-defined parameter values are used according to the assigned

vegetation class. The vegetation temperature is assigned to be the same as the top soil temperature initially. Table 5.2 lists vegetation types and their pre-defined parameter values and the soil moisture profiles that are used. The environmental adjustment factors are the same for each different vegetations and have been tabulated in Table 4.3.

Inputs	SOIL1	SOIL2	GRASS1	GRASS2	CROP1	CROP2	TREE
LEAF class	15	15	2	2	1	9	3
d_{smax}	–	–	0.01	0.01	0.01	0.002	0.002
n	–	–	3.48	3.48	3.48	3.48	3.48
σ	–	–	2.17	2.17	2.17	2.17	2.17
LAI	–	–	1.0	1.0	2.0	6.0	6.0
$LSAI$	–	–	1.1	1.1	2.2	6.6	6.6
α_T	–	–	0.26	0.26	0.20	0.18	0.10
h	–	–	0.63	0.63	1.19	1.58	23.8
z_0'	0.01	0.01	0.01	0.01	0.01	0.01	0.01
soil type	7	7	7	7	7	7	7
soil moisture	S1	S2	S3	S2	S1	S1	S1

Table 5.2: LEAF parameters and initial soil moisture profile for seven model simulations.

Among the seven different surface covers, SOIL1 is a desert (bare soil) with dry top soil moisture, SOIL2 is also a desert but with wet top soil, GRASS1 is a stressed (dry root-zone soil moisture) short grass, GRASS2 is unstressed short grass, CROP1 is crop/mixed dry-land farming, CROP2 is irrigated crop, and TREE is evergreen needle-leaf tree. As mentioned previously, the soil class 7 is silty clay loam.

5.3 Boundary Layer Developments

Seven simulations with different surface cover are performed. The RAMS model is integrated for 24 hours and the boundary layer temperature and moisture profiles at different time (10, 12, 14, 16, and 18 LST) are show in Figures 5.2 to 5.8. The growth of the atmospheric boundary layer is evident in these Figures. When the surface moisture supply is small (cases SOIL1 and GRASS1), most of the absorbed radiative energy is converted into sensible heat and returned to the atmosphere. The more sensible heat that goes into the atmospheric boundary layer the higher the potential temperature is and, hence, the

atmospheric boundary layer is more turbulent and the depth is higher. Meanwhile, when the atmospheric boundary gradually erodes into the more stable layer aloft, drier air is entrained into the atmospheric boundary layer, resulting in a dryer boundary layer.

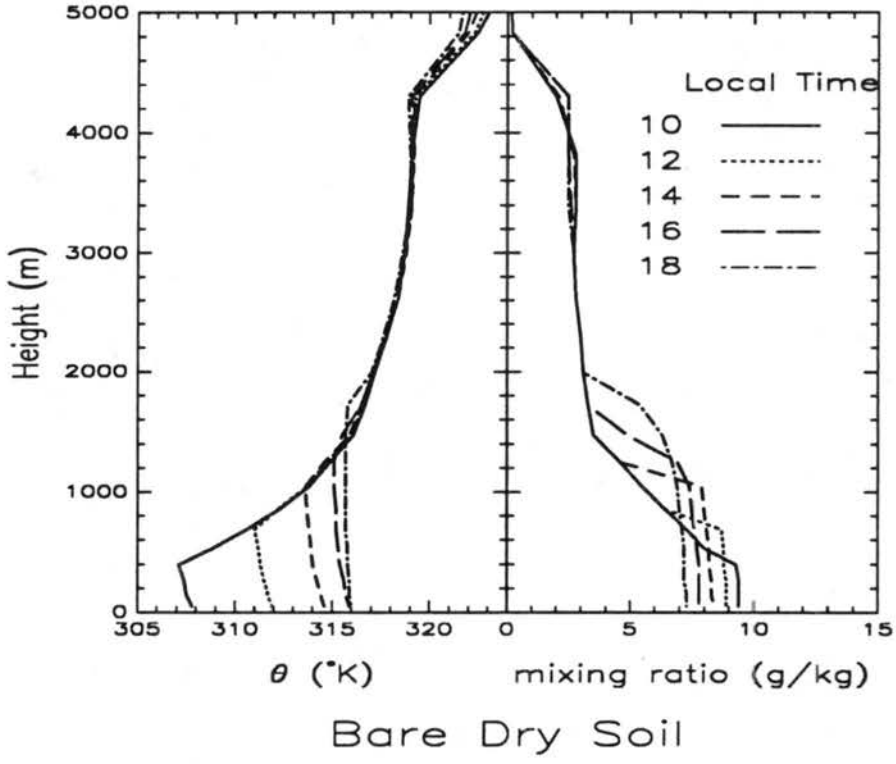

Figure 5.2: Atmospheric boundary layer potential temperature and water vapor mixing ratio at 10, 12, 14, 16 and 18 LST respectively. The surface cover is SOIL1.

When the surface moisture supply is abundant (cases SOIL2, GRASS2, CROP1, CROP2, and TREE), on the other hand, most of the absorbed radiative energy is converted into latent heat flux return to the atmosphere and results in a more moist and shallower atmospheric boundary layer. Note that CROP2 (irrigated crop) has a lower latent heat flux and higher sensible heat flux than CROP1 (crop/mixed farming) which is consistent to the discussion in Section 4.3 in which the higher LAI actually reduceds the evaporation from the soil.

Figures 5.9 and 5.10 summarizes the sensible and latent heat fluxes from the seven surface covers at different time during the day. Generally, the sensible heat flux is large

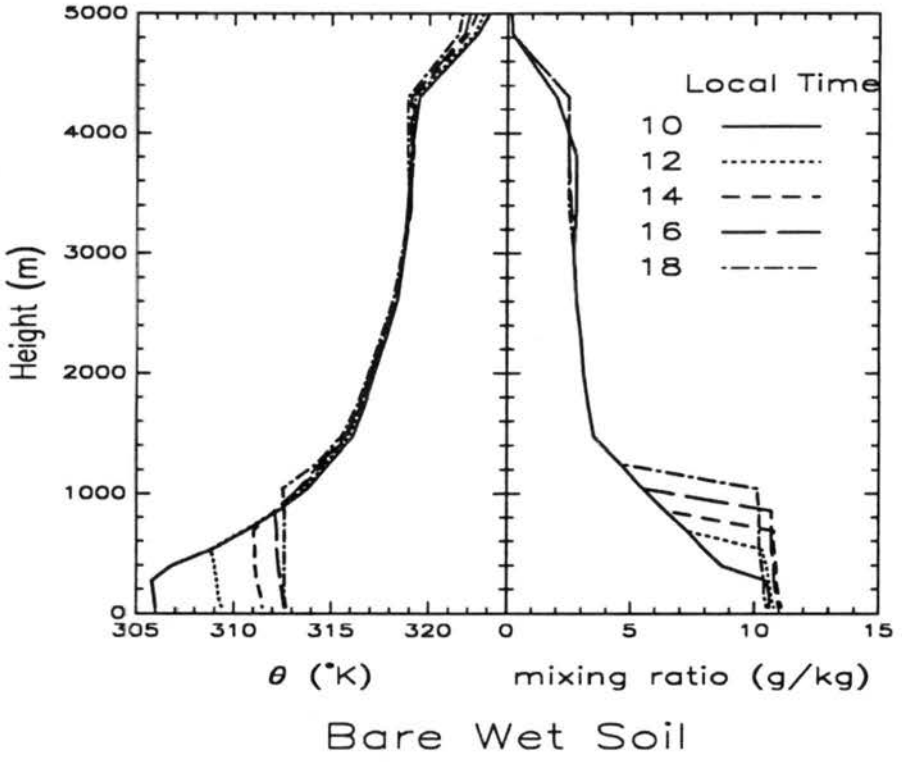

Figure 5.3: Same as Figure 5.2 except the surface cover is SOIL2.

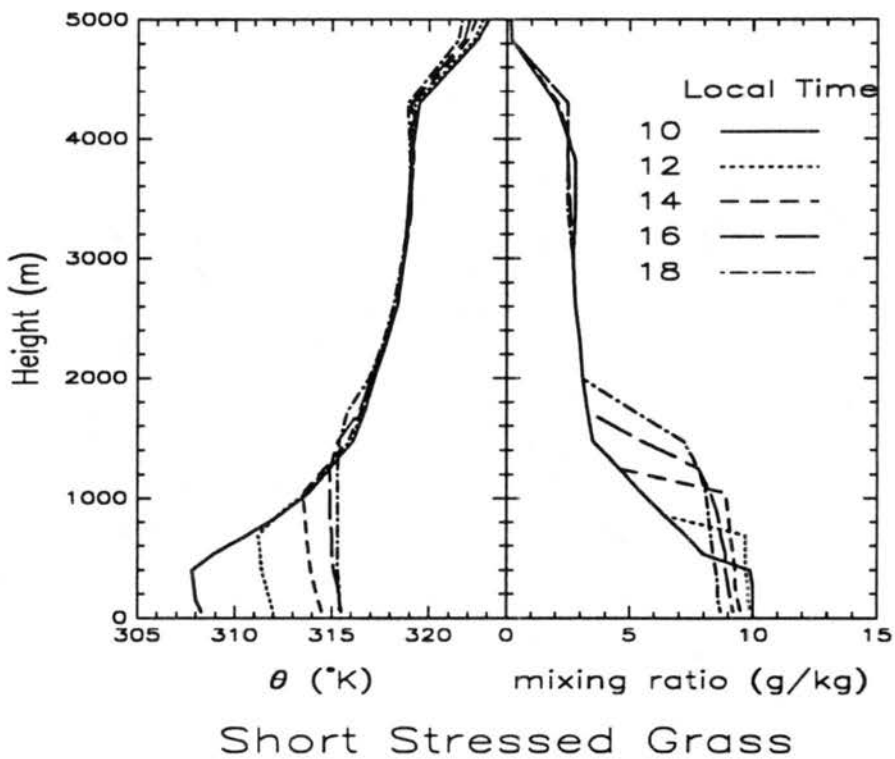

Figure 5.4: Same as Figure 5.2 except the surface cover is GRASS1.

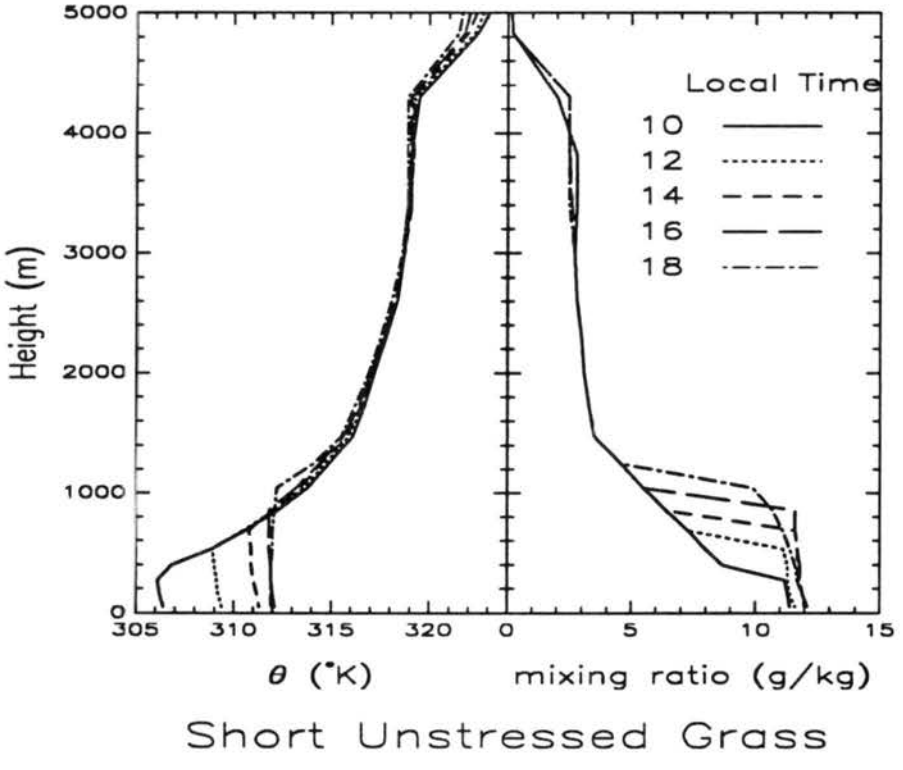

Figure 5.5: Same as Figure 5.2 except the surface cover is GRASS2.

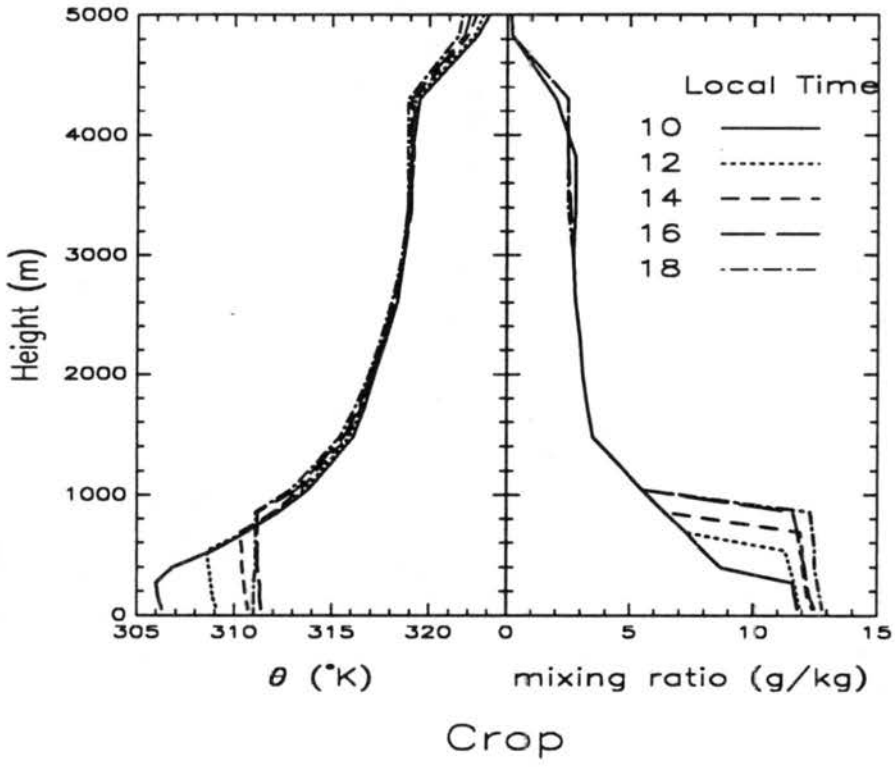

Figure 5.6: Same as Figure 5.2 except the surface cover is CROP1.

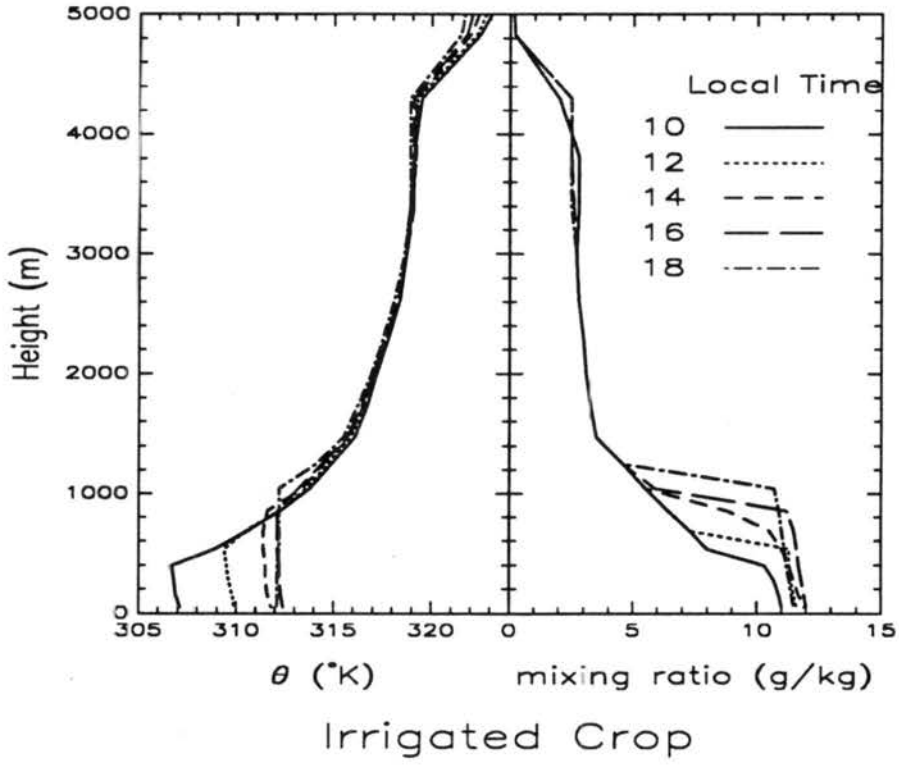

Figure 5.7: Same as Figure 5.2 except the surface cover is CROP2.

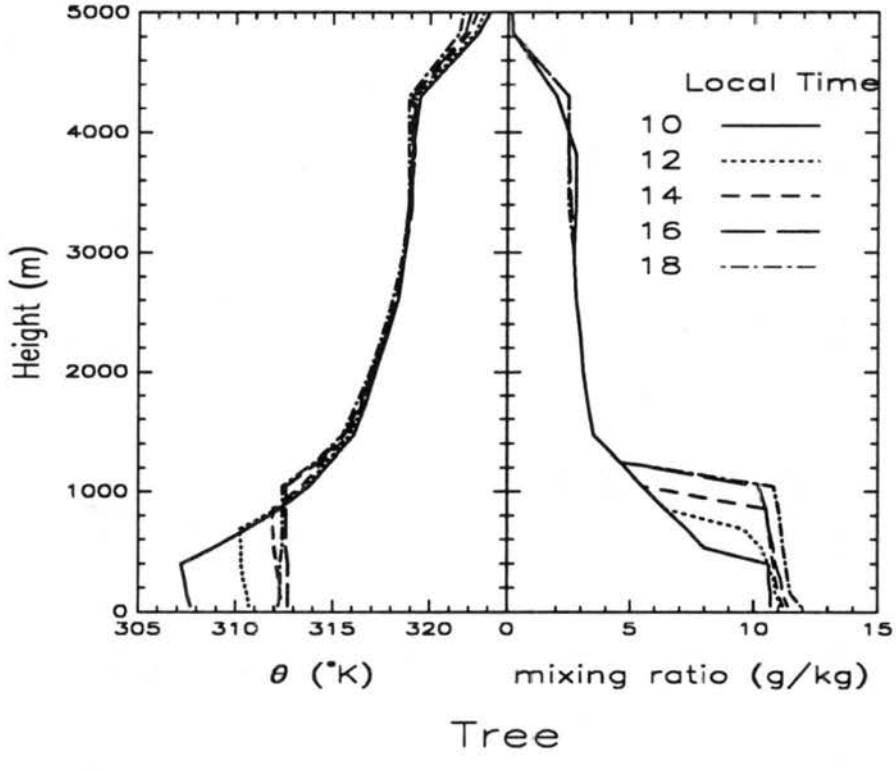

Figure 5.8: Same as Figure 5.2 except the surface cover is TREE.

when the surface moisture availability is small; the latent heat flux is large when the surface moisture availability is large. Bare dry soil has generally the largest sensible heat flux and lowest latent heat flux while the tree and crop simulations have the largest latent heat flux and smallest sensible heat flux.

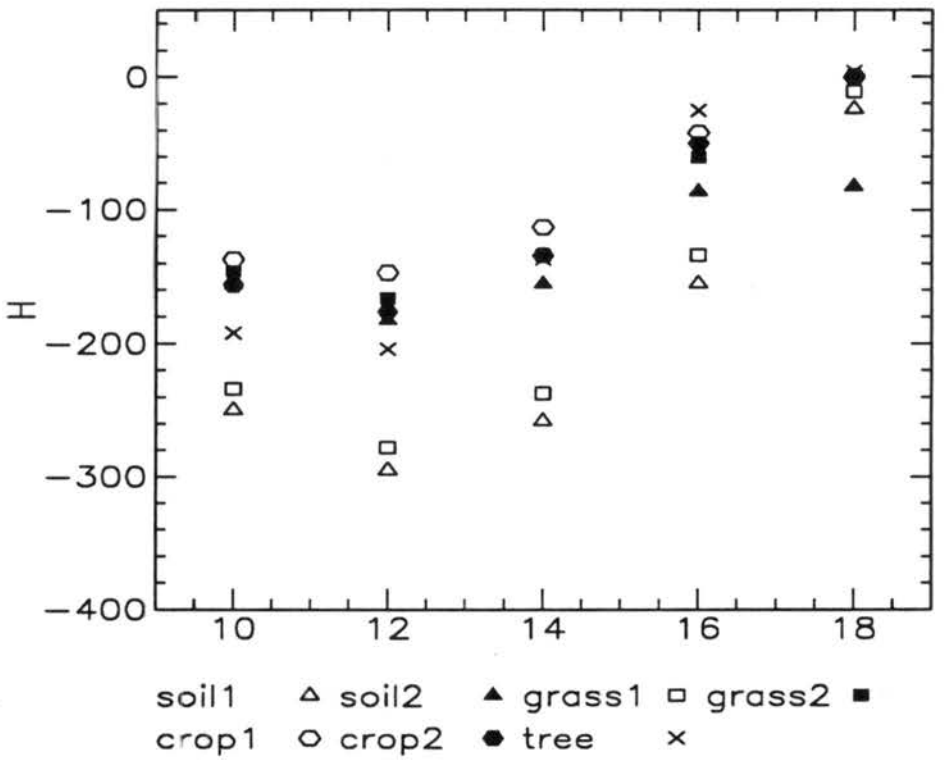

Figure 5.9: Scatter diagram of sensible heat flux at 5 different times for different surface covers.

5.4 Atmospheric Circulations Generated by Different Surface Covers

When two different types of surface covers are placed next to each other, due to their different thermal inertia, atmospheric circulations can be generated. Based on numerical experiments, Pielke (1984) concluded that a local wind pattern can be detected statistically when a horizontal difference on the order of 100 $W\,m^{-2}$ per 33 km is input into the atmosphere, whereas a 1000 $W\,m^{-2}$ difference will create significant obvious local wind patterns. Recently, Mahfouf et al. (1987) suggests that local atmospheric circulations

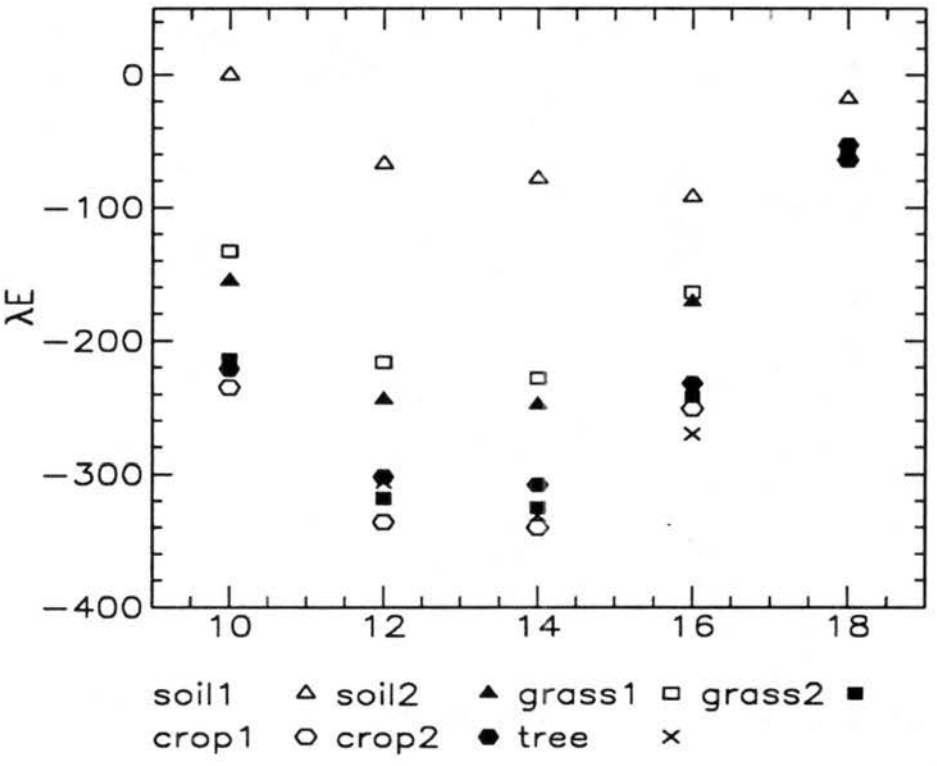

Figure 5.10: Same as Figure 5.9 except for latent heat flux.

can be generated by differences in soil moisture availability and soil texture. Knowing the one-dimensional simulation results shown in the previous Section, different surface covers can be placed together to induce local circulations. Table 5.3 shows seven two-dimensional model configurations where a 80 by 40 model domain is divided into two equal size sub-domains each one with a different surface cover contrast. Recall that the model is initialized with the Denver sounding shown in Figure 5.1.

	Surface Coverage	
Experiments	left	right
C1	SOIL1	SOIL2
C2	GRASS1	GRASS2
C3	SOIL1	GRASS2
C4	SOIL2	GRASS2
C5	GRASS1	SOIL2
C6	GRASS1	TREE
C7	GRASS2	TREE

Table 5.3: Two-dimensional model configurations where a 80 by 40 model domain is divided into two equal size sub-domains each one with a different surface cover contrast.

Figures 5.11 to 5.14 illustrate the results at 1400 LST for the seven simulations. Thermally forced local circulations are generated in response to the different surface covers. The local wind pattern is from the cooler surface to the warmer surface with return flow aloft. The surface latent and sensible heat fluxes approach their equilibrium value (simulated using the quasi-one-dimensional model) far away from the interface of the two surfaces. The over- and under-shooting of surface turbulent heat fluxes from their equilibrium values near the surface discontinuity is due to the local circulation generated by the meso-scale surface contrast.

In summary, the LEAF model is reasonably simulating a surface thermal contrast due to different surface moisture availability. Sea-breeze like local atmospheric circulations can be generated in response to this thermal contrast. The atmospheric boundary layer is shallower and more moist when above an unstressed vegetation surface while it is deeper and drier when above a stressed vegetation or a bare dry soil surface. When the turbulence in the atmospheric boundary layer is strong enough and the moisture is high enough,

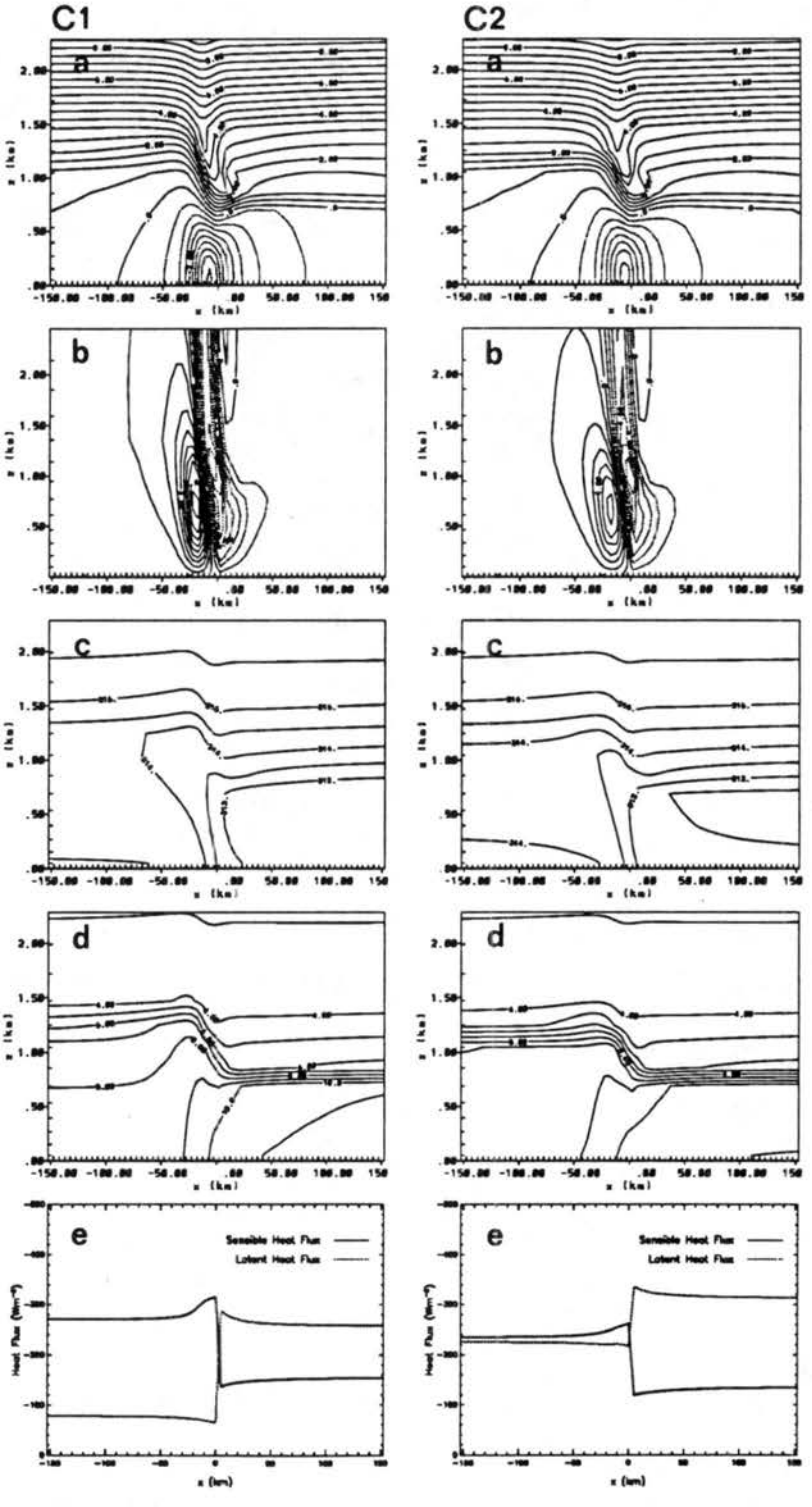

Figure 5.11: Two-dimensional simulations of cases C1 and C2 at 1400 LST. Panels (from top to bottom) are (a) horizontal wind component, u; (b) vertical wind component, w; (c) potential temperature, θ; (d) water vapor mixing ratio, r; and surface latent and sensible heat fluxes.

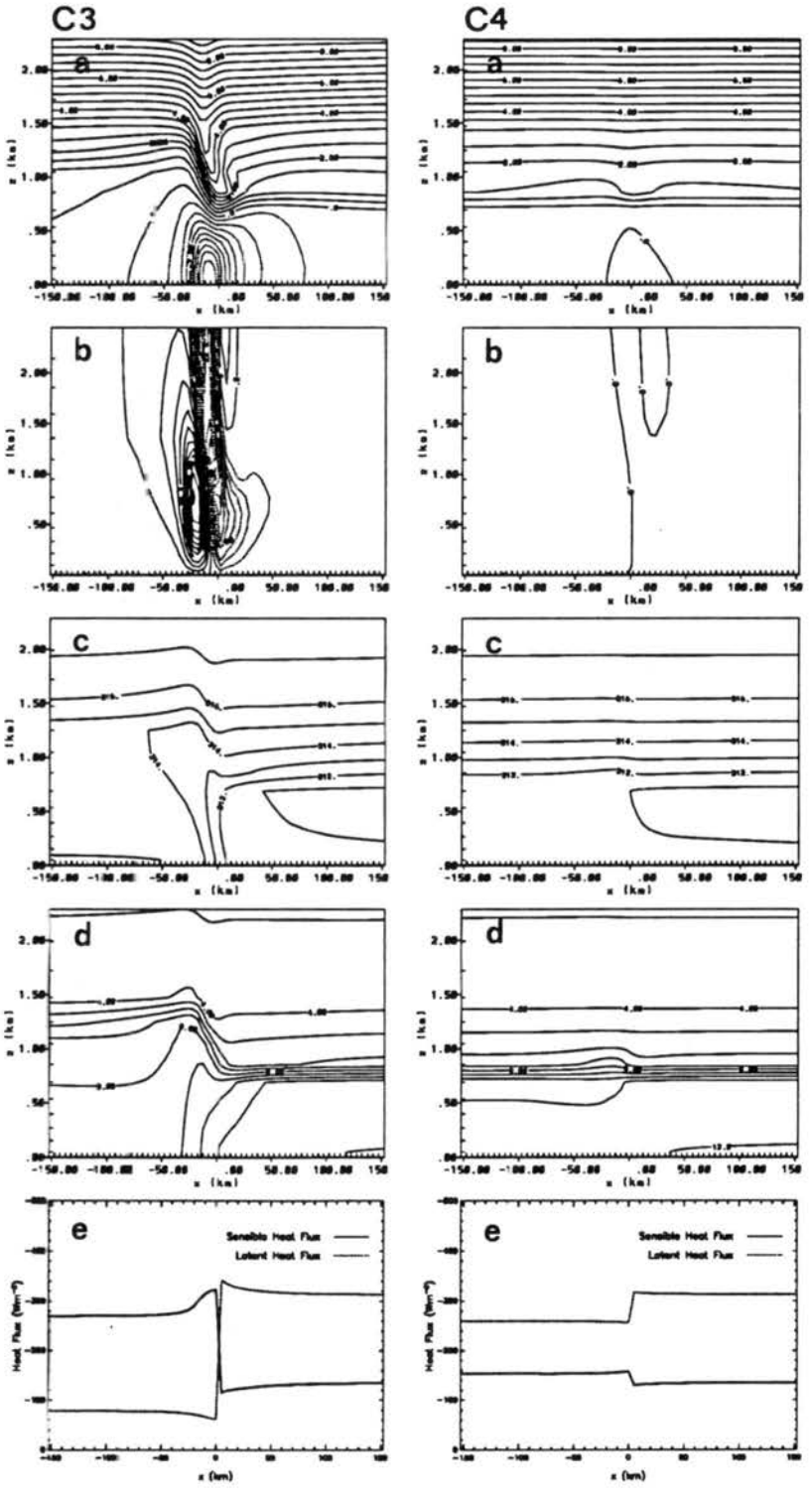

Figure 5.12: Same as Figure 5.11 but for cases C3 and C4.

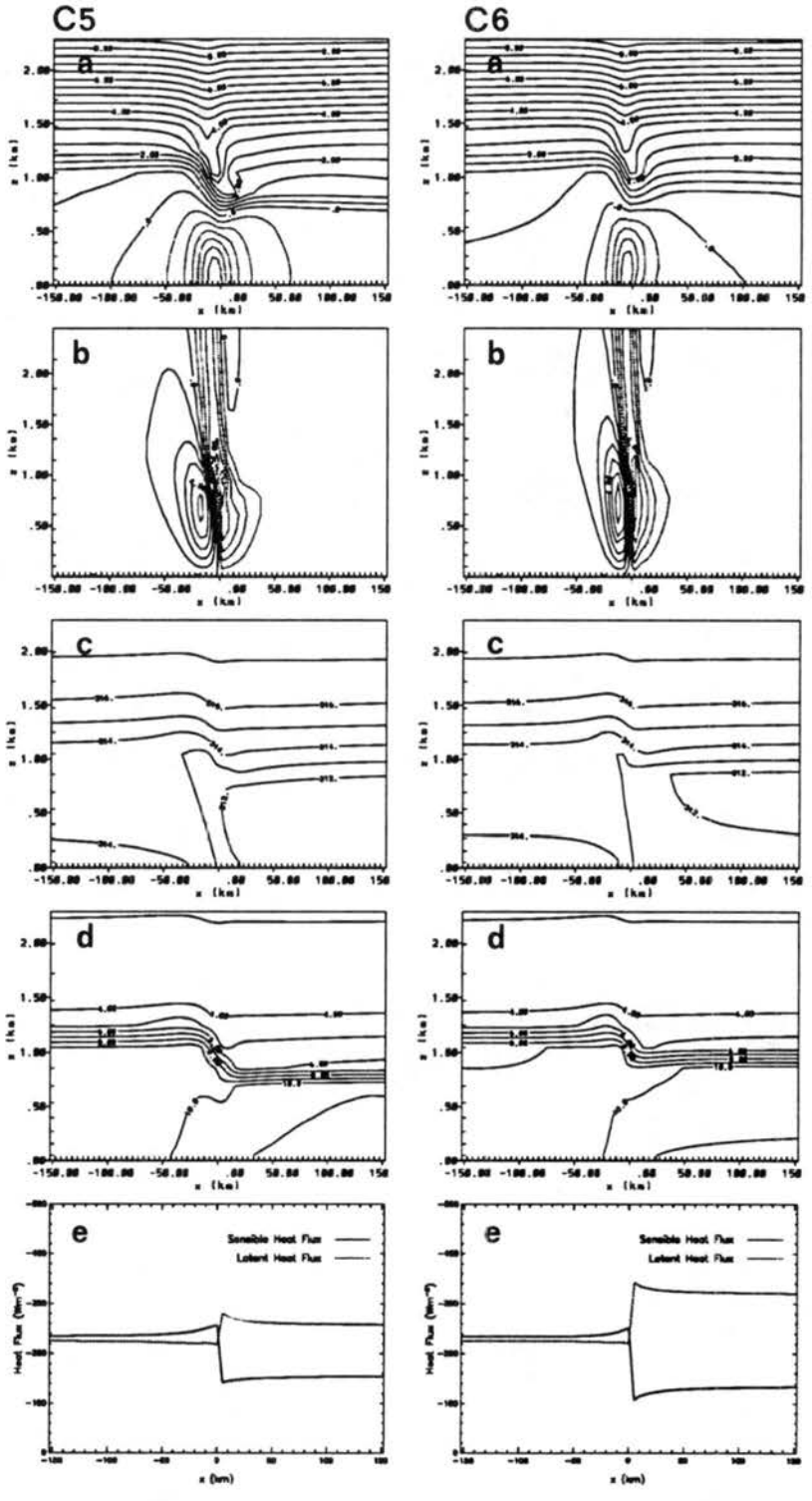

Figure 5.13: Same as Figure 5.11 but for cases C5 and C6.

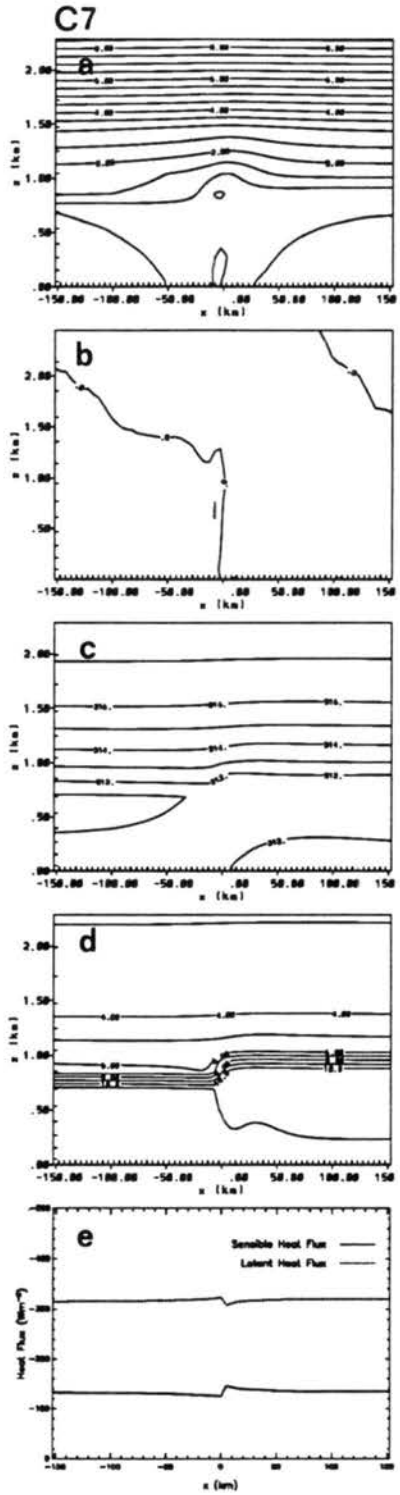

Figure 5.14: Same as Figure 5.11 but for case C7.

cumulus cloud are expected to form in response to the enhanced vertical mixing. Moreover, if the atmospheric is convectively unstable, cumulus convective clouds are also expected to form and to be particularly enhanced within convergence zones of the local thermal circulation which result from the juxtaposition of the different land surfaces.

Chapter 6

CASE STUDY

It is shown in the last Chapter that the existence of vegetation has modified the characteristics of the atmospheric boundary layer. When two different surface cover are placed next to each other in a mesoscale area, a local mesoscale thermally forced circulation can form associated with the biophysical and hydrological characteristics of the surfaces. This landscape generated circulation has been linked to the initiation of convective storms as discussed in Chapter 2. In this Chapter, it is attempted to replicate a real severe storm episode and examine the possible landscape effect.

6.1 Case Description and Experiment Design

A series of full three dimensional simulations are performed to replicate the June 6, 1990 tornado outbreak for Limon, Colorado. This case is chosen since the synoptic scale forcing over eastern Colorado on this date was relatively weak and it happened near the boundary of agricultural and wild short grass prairie. A detail observational study has been reported by Weaver et al. (1992). During this event series of tornado producing thunderstorms developed over the eastern plains of Colorado. One of the tornados struck the town of Limon causing 12.8 million dollars of damage and injuring 14 people. The surface, 75 kpa, and 500 kpa analysis at 1200 UTC on that date are shown in Figure 6.1. As described in Weaver et al. (1992) a cold front had pushed through the state of Colorado early on the previous day. The morning sounding at Denver (Figure 5.1) showed the atmosphere to be cool and moist near the surface. A storm out-flow boundary produced by a mesoscale convective system (MCS) over Kansas migrated westward during the day. As argued by Weaver et al. (1992) this out-flow boundary played an important role in producing the tornadoes later on that day.

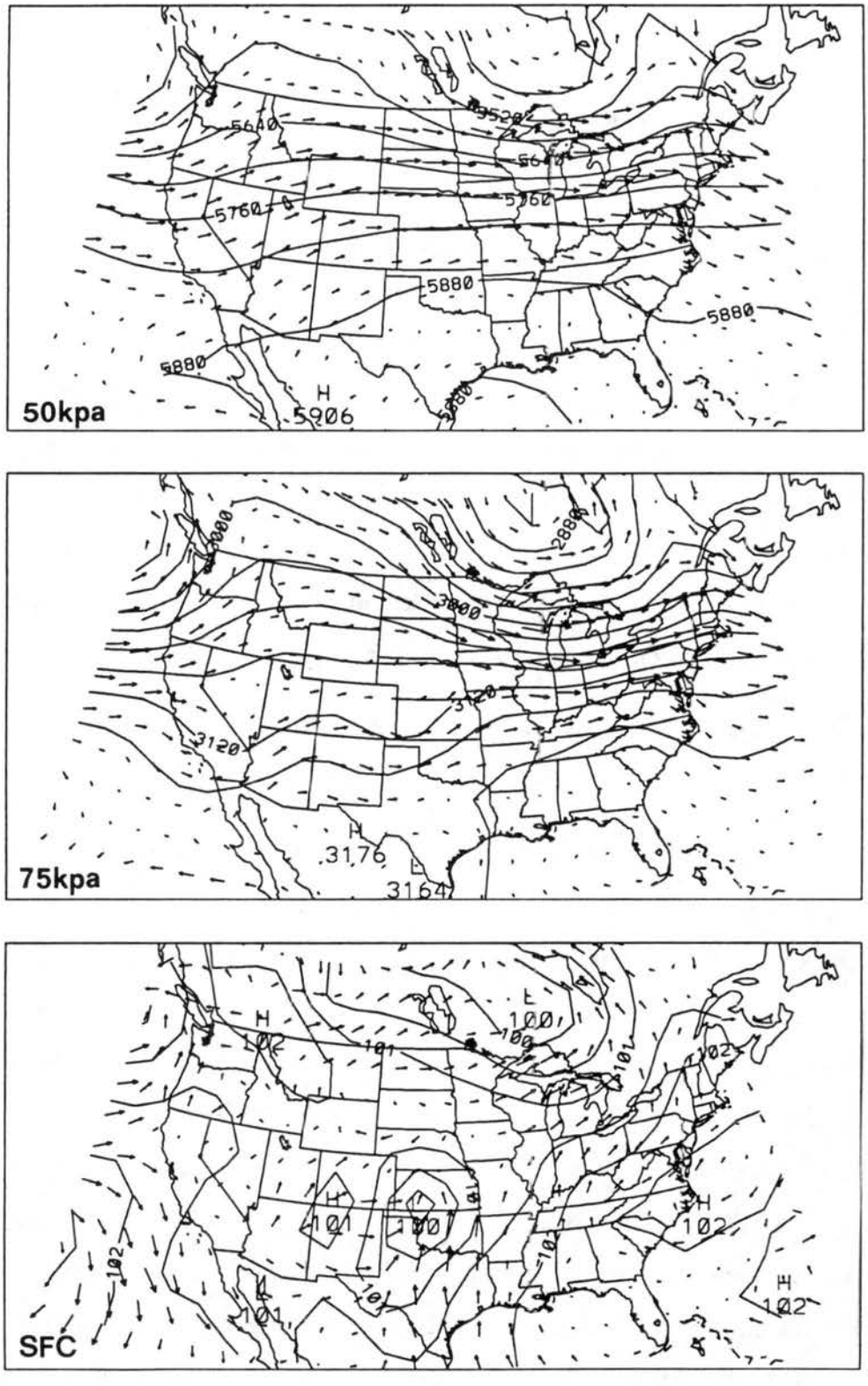

Figure 6.1: Surface, 75 kpa, and 50 kpa analysis at 1200 UTC on June 6, 1990.

In order to examine the possible landscape effect on this storm, three-dimensional numerical experiments were performed with and without surface heterogeneities in vegetation cover. Specifically, experiments with all bare soil, observed vegetation cover, and a homogeneous vegetation cover were compared. The RAMS model is set up with two nested grids. The coarse grid has a horizontal grid increment of 40 km and covers most of the central Great Plains (Figure 6.2) with $40 \times 40 \times 40$ grid points. The reasons to use such a large coverage are (a) to resolve the MCS that is suggested to be important in the storm development; and (b) to resolve the large scale gradient in surface moisture availability. The finer grid is designed to resolve the mesoscale surface heterogeneities. The finer grid has a 10 km grid increment and covers most of the Colorado eastern Plains, the State of Kansas and part of the state of Nebraska (see also Figure 6.2). The RAMS model is integrated forward in time for 14 hours starting at 1200 UTC (0500 LST) June 6, 1990. The variable initialization and the Davis lateral boundary condition described in Cram (1990) is utilized so that the boundary is relaxed toward a prescribed condition. The top boundary was a viscous damping layer described in Heckman (1991) to remove vertically propagating gravity waves. The cumulus parameterization is activated to remove sub-grid scale convective instability. Although the modified Kuo scheme (Tremback, 1991) is not designed to be used on the grid scale of this study, this was the only option that was currently available in the RAMS version 2C. Results that follow demonstrated, however, that this cumulus parameterization appeared to be realistic for this case study.

6.2 Initial Conditions

In order to integrate the RAMS atmospheric model forward in time, initial and boundary conditions must be provided. For the initial conditions, RAMS requires the state of the atmosphere, which includes winds, temperature, pressure, humidity, and the state of soil, which includes soil moisture and temperature.

The state of the atmosphere is initialized using NMC gridded data (e.g. see Figure 6.1). Rawinsondes and surface observations archived at the National Center for Atmospheric Research (NCAR) are ingested into the RAMS isentropic analysis package to produce

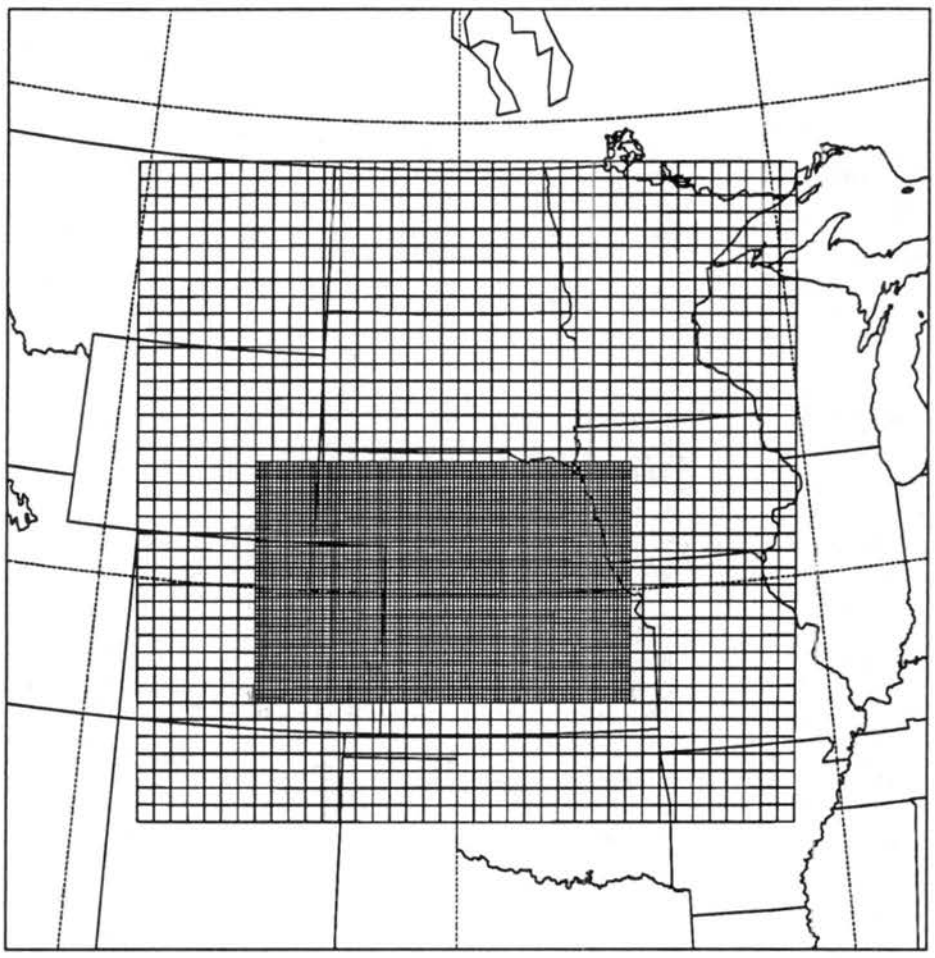

Figure 6.2: Model grid locations.

model initial fields for the atmosphere. The soil temperature was initialized based on the soil temperature profile observed at the Colorado State University Main Campus Weather Station. Knowing the air temperature and the soil temperature profile at this station, a soil temperature off-set from the screen height air temperature is obtained. The model initial soil temperature profiles are then initialized using the same off-set from the atmospheric temperature of the lowest model level at every horizontal grid point. Since the soil moisture is not a routinely observed variable, it has to be inferred using other information. For example, the standard RAMS initializes the soil surface relative humidity the same as the atmospheric relative humidity at the screen height and increases this value linearly to twice the surface value to a depth of 20 cm. This procedure is completely arbitrary and does not consider precipitation. Using a simple water budget, Chang and Wetzel (1991) relate the soil moisture to the antecedent precipitation index (API) from the rain gauge data.

Unfortunately, the rain gauge data was not available until recently and an alternative way to estimate soil moisture was used. The short term crop moisture (NOAA/USDA Weekly Weather and Crop Bulletin, Volumn 77, No. 22 and 23) were utilized to define the initial soil moisture. Using a conversion tabulated in Table 6.1, the initial soil moisture in the root zone and the recharging zone is defined as shown in Figure 6.3. Notice that the fraction field capacity[1] of 0.4 is near the wilting point for the soil commonly observed in the central Great Plains. The soil surface moisture is initialized as 0.25 of the field capacity.

6.3 Surface Data

For the surface boundary conditions, surface roughness and thermal and hydrological properties are essential. Soil texture, vegetation leaf area index (LAI), land-use and land-cover data are necessary in order to estimate the surface thermal and hydrological properties. The percentage of surface coverage by different vegetation and landscape are

---

[1]Field capacity is defined as the maximum amount of water a soil sample can hold against the gravitational drainage.

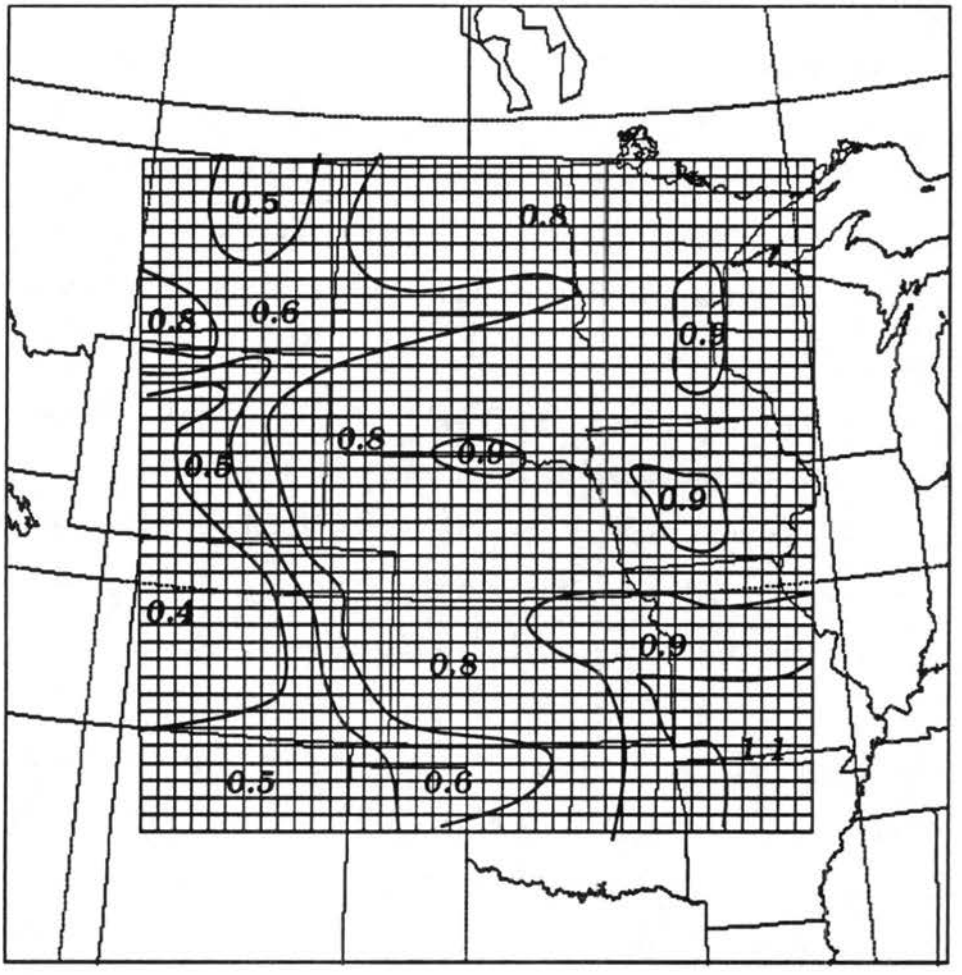

Figure 6.3: Initial soil moisture fraction of field capacity in the root zone and recharging zone.

Soil Moisture Conversion	
Crop Moisture	Moisture Fraction of Field Capacity
wet	1.1
abnormally moist	0.9
favorably moist	0.8
slightly dry	0.6
abnormally dry	0.5
excessively dry	0.4
severely dry	0.4

Table 6.1: Transition from crop moisture to moisture fraction of field capacity.

useful when a sub-grid-scale land surface parameterization is used. DEM (digital elevation model) data can be used to define terrain characteristics.

The USDA soil texture class used in the RAMS has been described in McCumber and Pielke (1981), Tremback and Kessler (1985), and Lee and Pielke (1992). The soil thermal and hydrological properties are defined using analytical functions when the soil texture class and soil moisture content are known. Following Cram (1990), the soil texture is translated from the global soil data described in Wilson and Henderson-Sellers (1985), and Henderson-Sellers et al. (1986). The soil types over the computational domain is shown in Figure 6.4. The soil surface roughness is specified in this study as 0.02 m throughout the entire computational domain.

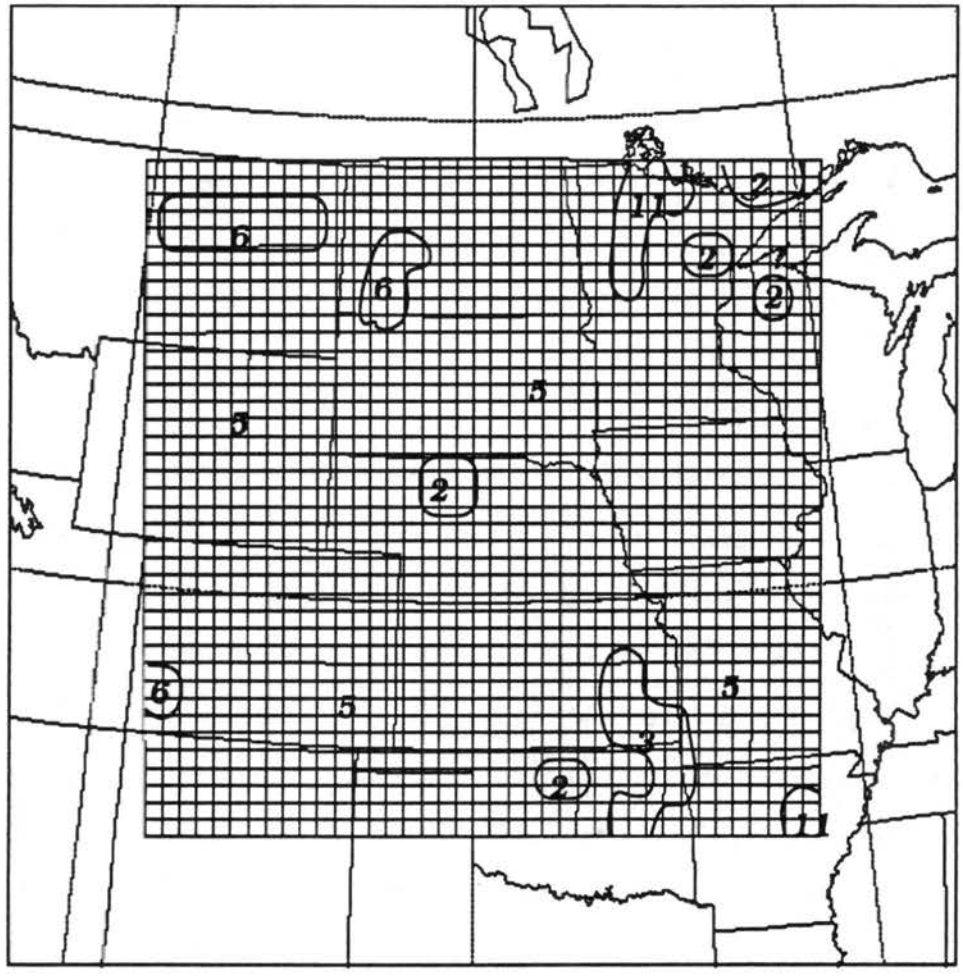

Figure 6.4: The USGS soil texture class over the computational domain.

The vegetation green Leaf Area Index (LAI), which is required by the model, is related to the Normalized Difference Vegetation Index (NDVI) observed from the NOAA-11 polar orbiting satellite. The relation between the NDVI and the LAI is

$$NDVI = 0.915\,(1.0 - 0.83\exp(-0.96LAI)) \tag{6.1}$$

and

$$NDVI = \ln(LAI/1.625) * 0.34 \tag{6.2}$$

for herbaceous vegetation (Asrar et al., 1984) and trees (Nemani and Running, 1989), respectively. The NDVI data is taken from the USGS 1990 conterminous U. S. AVHRR data set (Eidenshink, 1992). Figure 6.5 shows the NDVI over the domain of interest. The translated LAI is shown in Figure 6.6.

The USGS 1990 conterminous U. S. land-cover database (Loveland et al., 1991) is used to define surface vegetation type. The original data set has 167 land-cover types which had to be converted into the LEAF classes. Table 6.2 shows the translation from the USGS land surface cover types to the LEAF classes. Figure 6.7 shows the resultant vegetation types in the BATS classification. Recall that the conversion between the LEAF and the BATS classification has been shown in Table 3.2.

So far the LEAF model only handles three sub-grid scale surface types: water, bare surface, and vegetated surface. The percentage of the three surface covers is obtained by counting the pixels within a grid box and grouping the pixels into each of the three categories. For example, for the 1600 AVHRR pixels in a 40 km by 40 km grid box, there might be 1500/1600 covered by vegetation, 70/1600 covered by bare soil, and 30/1600 covered by water. The dominant vegetation type within a grid box is chosen as the representive vegetation type for that box.

Finally, the USGS 1 km pixel size DEM is used to define the model topography. The DEM is first averaged to the grid box value and then passed through a one-two-one filter to remove 2 Δx terrain forcing. The final topography for the coarse grid is shown in Figure 6.8.

Figure 6.5: The USGS conterminous U. S. 1990 NDVI data over the computational domain.

Figure 6.6: The LAI distribution translated from the USGS NDVI data.

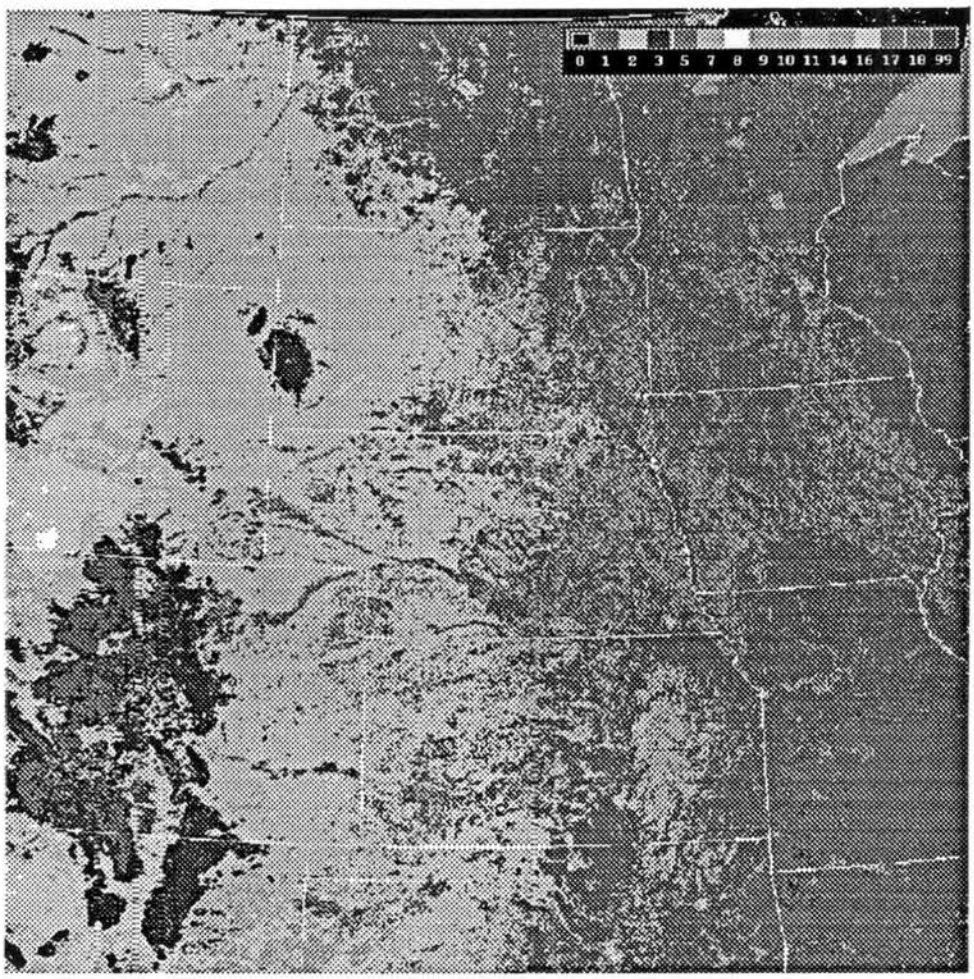

Figure 6.7: The BATS vegetation classes over the central Great Plains.

USGS vegetation class		LEAF vegetation class	
1	cropland	1	crop/mixed farming
2	cropland/grassland	9	irrigated crop
3	cropland	1	crop/mixed farming
4	cropland	1	crop/mixed farming
5	cropland	1	crop/mixed farming
6	cropland	1	crop/mixed farming
7	cropland	9	irrigated crop
8	cropland	1	crop/mixed farming
9	cropland	9	irrigated crop
10	cropland/woodland	1	crop/mixed farming
11	cropland	1	crop/mixed farming
12	cropland	1	crop/mixed farming
13	cropland	1	crop/mixed farming
14	cropland	9	irrigated crop
15	cropland	9	irrigated crop
16	cropland	9	irrigated crop
17	cropland	1	crop/mixed farming
18	cropland	1	crop/mixed farming
19	pasture/cropland	1	crop/mixed farming
20	cropland	9	irrigated crop
21	cropland/range	2	short grass
22	cropland	7	tall grass
23	cropland	1	crop/mixed farming
24	cropland	1	crop/mixed farming
25	cropland	9	irrigated crop
26	cropland	9	irrigated crop
27	cropland	1	crop/mixed farming
28	cropland	1	crop/mixed farming
29	cropland	9	irrigated crop
30	cropland	1	crop/mixed farming
31	cropland	9	irrigated crop
32	cropland	9	irrigated crop
33	cropland	1	crop/mixed farming
34	cropland	1	crop/mixed farming
35	cropland	9	irrigated crop

Table 6.2: Conversion table between USGS land-cover and LEAF land-cover. The original conversion between USGS land-cover to the BATS classification was provided by Jesslyn Brown of USGS EROS Data Center.

USGS vegetation class		LEAF vegetation class	
36	cropland/pasture	1	crop/mixed farming
37	cropland	9	irrigated crop
38	cropland	1	crop/mixed farming
39	cropland/grassland	9	irrigated crop
40	cropland/forest	9	irrigated crop
41	cropland/woodland	9	irrigated crop
42	cropland/woodland	1	crop/mixed farming
43	cropland/forest	5	deciduous broadleaf tree
44	cropland/woodland	1	crop/mixed farming
45	cropland/woodland	1	crop/mixed farming
46	cropland/woodland	8	tundra
47	cropland/woodlots	1	crop/mixed farming
48	woodland/cropland	1	crop/mixed farming
49	cropland/forest	1	crop/mixed farming
50	cropland/woodland	8	tundra
51	cropland/woodland	5	deciduous broadleaf tree
52	cropland/woodland	1	crop/mixed farming
53	woodland,crop,pasture	1	crop/mixed farming
54	cropland/woodland	1	crop/mixed farming
55	woodland/cropland	5	deciduous broadleaf tree
56	cropland/woodlots	1	crop/mixed farming
57	cropland/woodland	5	deciduous broadleaf tree
58	southern forest/crop	2	short grass
59	grassland	2	short grass
60	grassland	2	short grass
61	grassland	2	short grass
62	grassland	2	short grass
63	grassland	7	tall grass
64	desert shrubs	12	evergreen shrub
65	desert shrubs	12	evergreen shrub
66	desert shrubs	12	evergreen shrub
67	desert shrubs	12	evergreen shrub
68	desert shrubs	12	evergreen shrub
69	desert shrubs/grass	12	evergreen shrub
70	grassland	10	semi desert

Table 6.2: Continued.

USGS vegetation class		LEAF vegetation class	
71	desert shrubs/grass	12	evergreen shrub
72	savanna	12	evergreen shrub
73	desert shrubland	12	evergreen shrub
74	savanna	12	evergreen shrub
75	desert shrubs/grasses	12	evergreen shrub
76	desert shrubs/grass	12	evergreen shrub
77	desert shrubs/grass	12	evergreen shrub
78	desert shrubs/grass	12	evergreen shrub
79	desert shrubs/grass	2	short grass
80	grassland	2	short grass
81	desert shrub/grass	12	evergreen shrub
82	grassland/shrubland	2	short grass
83	grasslands/shrubs	2	short grass
84	grassland/shrubs	10	semi desert
85	desert shrubs/grass	12	evergreen shrub
86	grassland/pasture	2	short grass
87	desert shrubs/grass	12	evergreen shrub
88	cropland/grassland	2	short grass
89	cropland/grassland	2	short grass
90	western deciduous	9	irrigated crop
91	western deciduous	5	deciduous broadleaf tree
92	northern hardwoods	5	deciduous broadleaf tree
93	woodland/pasture	5	deciduous broadleaf tree
94	mixed hardwoods	5	deciduous broadleaf tree
95	coniferous	5	deciduous broadleaf tree
96	coniferous woodlands	5	deciduous broadleaf tree
97	southern pine/wetlands	3	evergreen needleleaf tree
98	northwest conifer/pasture	3	evergreen needleleaf tree
99	western pine forest	3	evergreen needleleaf tree
100	pine forest	3	evergreen needleleaf tree
101	western pine forest	3	evergreen needleleaf tree
102	western conifer	3	evergreen needleleaf tree
103	northwest forest	3	evergreen needleleaf tree
104	rocky mountain mixed forest	3	evergreen needleleaf tree
105	conifer forest	8	tundra

Table 6.2: Continued.

USGS vegetation class		LEAF vegetation class	
106	northwest conifer	3	evergreen needleleaf tree
107	coniferous forest	3	evergreen needleleaf tree
108	western pine forest	3	evergreen needleleaf tree
109	western conifer	3	evergreen needleleaf tree
110	western pine forest	3	evergreen needleleaf tree
111	northwest conifer	3	evergreen needleleaf tree
112	western conifer	3	evergreen needleleaf tree
113	western pine forest	3	evergreen needleleaf tree
114	northwest conifer	3	evergreen needleleaf tree
115	western conifer	3	evergreen needleleaf tree
116	northern forest/bogs	3	evergreen needleleaf tree
117	southern pine	3	evergreen needleleaf tree
118	southern pine	3	evergreen needleleaf tree
119	northwest forest	3	evergreen needleleaf tree
120	western mixed forest	3	evergreen needleleaf tree
121	conifer/mixed forest	14	mixed woodland
122	western mixed forest	14	mixed woodland
123	subalpine forest	14	mixed woodland
124	subalpine forest	14	mixed woodland
125	northern mixed forest	14	mixed woodland
126	western mixed forest	14	mixed woodland
127	western mixed forest	14	mixed woodland
128	subalpine forest	14	mixed woodland
129	northern forest	14	mixed woodland
130	northeast mixed forest	14	mixed woodland
131	northern forest	14	mixed woodland
132	rocky mountain mixed forest	14	mixed woodland
133	western mixed forest	14	mixed woodland
134	western mixed forest	14	mixed woodland
135	northern forest	14	mixed woodland
136	western mixed forest	14	mixed woodland
137	western mixed forest	14	mixed woodland
138	western mixed forest	14	mixed woodland
139	mixed forest	14	mixed woodland
140	western mixed forest	14	mixed woodland

Table 6.2: Continued.

USGS vegetation class		LEAF vegetation class	
141	northwest mixed forest	14	mixed woodland
142	subalpine forest,tundra	8	tundra
143	grassland/woodland	3	evergreen needleleaf tree
144	grassland/chapparel	2	short grass
145	desert shrubs/woodland	13	deciduous shrub
146	grassland/shrubs/wood	12	evergreen shrub
147	woodland	2	short grass
148	conifer woodland	14	mixed woodland
149	grassland/chapparel	3	evergreen needleleaf tree
150	grassland/chapparel	13	deciduous shrub
151	savanna	13	deciduous shrub
152	grassland/chapparel	2	short grass
153	cropland/woodland	13	deciduous shrub
154	pinyon/juniper woods	12	evergreen shrub
155	western woodlands	3	evergreen needleleaf tree
156	subalpine forest	3	evergreen needleleaf tree
157	subalpine forest	3	evergreen needleleaf tree
158	woodland/pasture	14	mixed woodland
159	water	17	inland water
160	coastal wetlands	11	bog or marsh
161	coastal wetlands	11	bog or marsh
162	coastal wetlands	11	bog or marsh
163	coastal wetlands	11	bog or marsh
164	barren	8	tundra
165	alpine tundra	8	tundra
166	alpine	8	tundra
167	alpine tundra	8	tundra

Table 6.2: Continued.

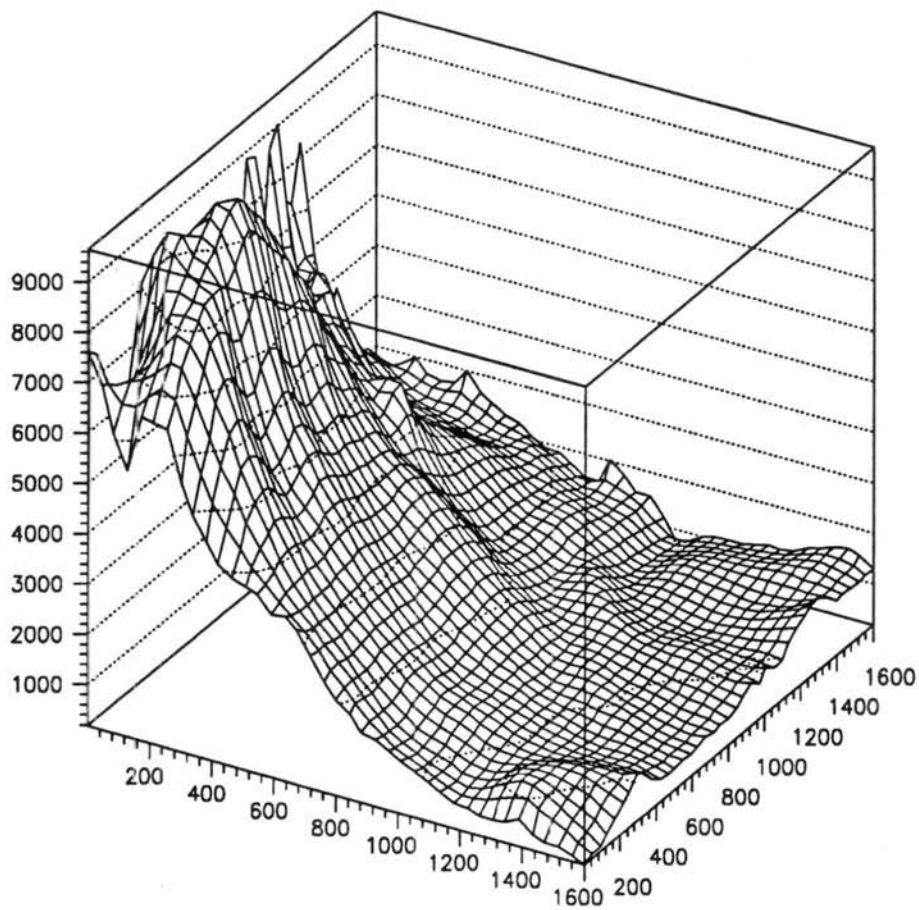

Figure 6.8: The final topography for the coarse grid. Units are in km for horizontal axes and in ft (1 ft = 0.3048 m) for the vertical axis. The view is from south-southwest of the grid.

6.4 Three-Dimensional Simulations

As stated previously three experiments are performed with and without real vegetation cover. The three experiments are initialized and setup exactly the same except for the surface data. The first simulation is with complete bare soil coverage. The RAMS is initialized as described in the previous two Sections and integrated for 14 hours. Figure 6.9 shows the simulated infrared temperature as estimated by the RAMS at 1500 UTC, 1800 UTC, 2100 UTC, and 0000 UTC as would be seen from a stationary satellite. At 1500 UTC, the MCS over Kansas and Nebraska has moved out to Iowa, the convection associated with the synoptic scale cold front is located near Kansas and Oklahoma, a shallow convective system is moving into South Dakota, and shallow boundary layer cloud covers northeastern Colorado. AT 1800 UTC, the MCS over Iowa and the cold frontal convection near Oklahoma is dissipating, some of the low clouds over eastern Colorado have dissipated, and no other significant convective activity is found at this time. These features are well verified by surface synoptic maps. Convection first developed around 1900 UTC near Cheyenne, Wyoming, while at 2100 UTC the first Colorado storm has developed between Colorado Spring and Limon moving northeast. At 0000 UTC, June 7, a line of convection has developed and the high cirrus clouds (anvil) has covered most of the northeastern Colorado, southeastern Wyoming, and western Nebraska. The convective precipitation at these four times are shown in Figure 6.10.

Figure 6.11 shows the analysis of convective available potential energy (CAPE) at these four time periods. The high CAPE region near the south boundary of the domain is associated with the cold front. As expected CAPE gradually builds up along the Colorado Front Range due to surface heating. The air mass that covers most of Nebraska and Kansas is mostly rain-cooled (Weaver et al., 1992) and is too stable to release the convective instability. This rain–cooled air mass also acts to suppress surface heating and thus reduces the possibility to trigger convection. Figure 6.12 shows low level stream lines and the water vapor mixing ratio field. The high pressure behind the cold front is gradually pushing into central Nebraska from the northwest. The low level flow over eastern Colorado is generally from the northeast and southeast direction. Recall that the upper level flow is

generally from the west (Figure 6.1) and is a good setting for severe storm to develop for eastern Colorado (Weaver and Dosken, 1991). For most of the day the mixing ratio over eastern Colorado remains nearly constant with some evidence of low level advection at 1800 UTC. Recall that the soil surface moisture is initialized at 0.25 of the field capacity and is quite low for evaporation, if any, to occur.

The next experiment has the same model configuration as the bare soil experiment but the surface is covered by observed vegetation (see Section 6.3). The LEAF parameterization is fully utilized in this simulation. The IR temperature fields (Figure 6.13) at 1500 UTC and 1800 UTC basically show the same features as shown in the bare soil experiment. However, convective activity at 1800 UTC and 0000 UTC are more concentrated near Denver and northeastern Colorado as evidenced in Figures 6.13 and 6.14. This result agrees well with satellite observations and the surface analysis. However, the convective cell is too far north (about one coarse grid cell) when compared to the satellite observation. Also, the convection was initiated by the convergence near the continental divide. Based on the analysis performed by Weaver et al. (1992), the first convection initiated along the Denver Convergence and Vorticity Zone (DCVZ) and this convergence zone is not resolved by either the coarse and fine grids.

Nevertheless, the fields of CAPE (Figure 6.15) show more spatial structure than the simulation without vegetation. Also, the CAPE is larger than the previous case because of the extra moisture that is put into the atmospheric boundary layer by transpiration. The lack of CAPE in southeastern Colorado is due to the low vegetation cover which results in less latent heat flux into the air and smaller CAPE. As evidenced in Figure 6.16, the surface water vapor mixing ratio increased significantly (from nearly 8 g $kg^{-1}$to 11 g kg^{-1}) over eastern Colorado which is a combined effect of horizontal advection and the local evapotranspiration.

It has been suspected that large scale agricultural practices can alter the local weather and possibly the local climate. The final experiment is designed to have the same model configuration as the actual vegetation experiment but the agricultural area is replaced by natural wild short grass. Specifically, the LEAF surface covers of crop/mixed farming and

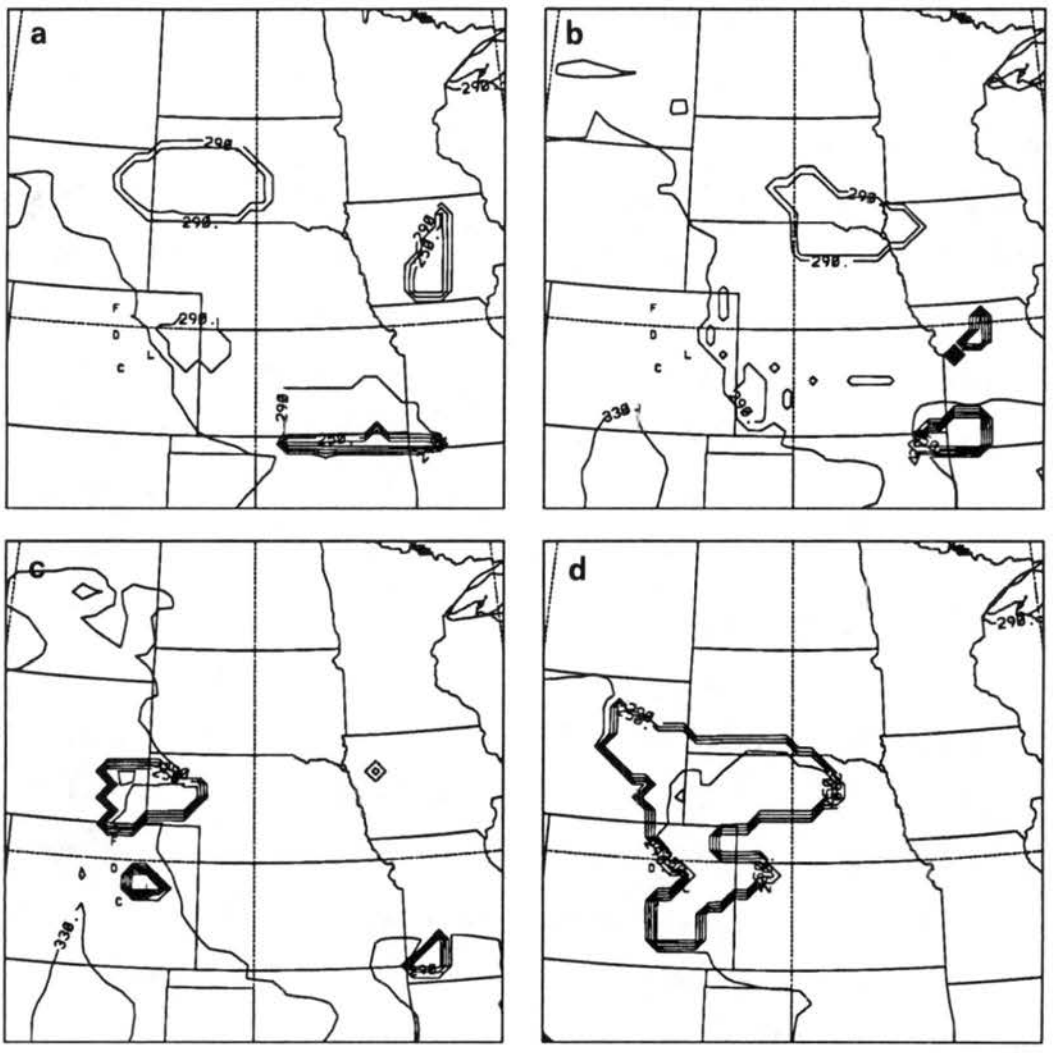

Figure 6.9: RAMS model estimated infrared temperature at (a) 1500 UTC, (b) 1800 UTC, (c) 2100 UTC, June 6, and (d) 0000 UTC, June 7, 1990. Bare soil is used for the entire computational domain.

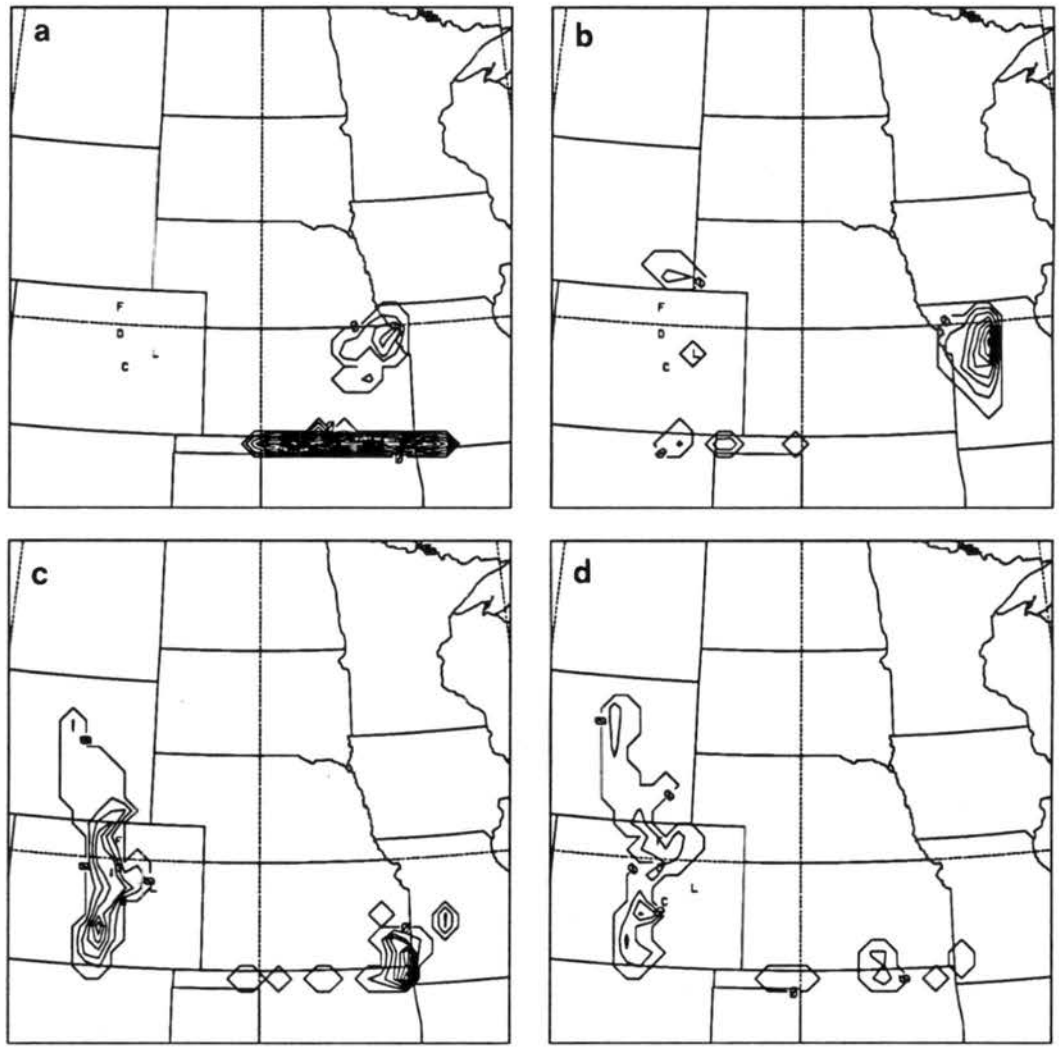

Figure 6.10: RAMS model simulated location of convective precipitation at (a) 1500 UTC, (b) 1800 UTC, (c) 2100 UTC, June 6, and (d) 0000 UTC, June 7, 1990. Bare soil is used for the entire computational domain. The contour interval is 0.1 mm s^{-1}.

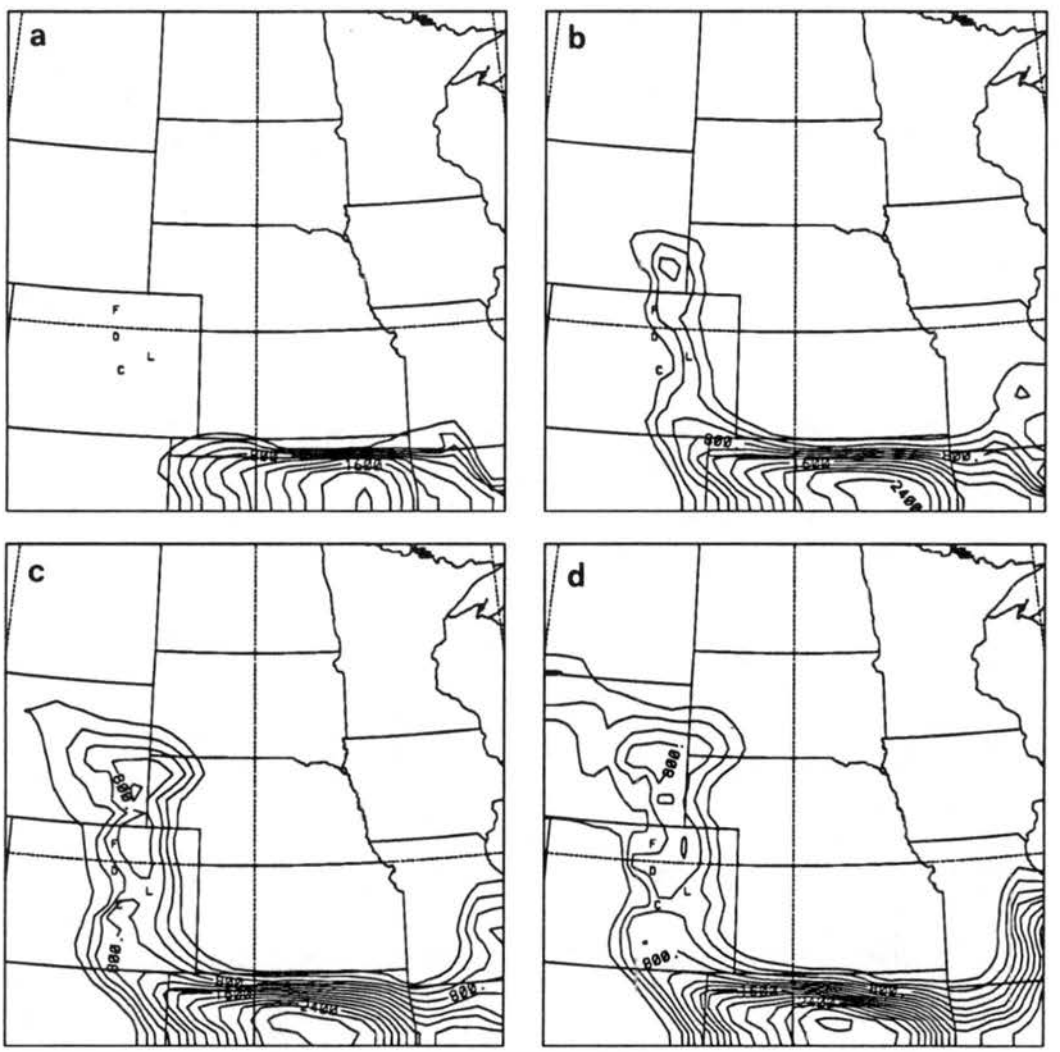

Figure 6.11: RAMS model simulated convective available potential energy (CAPE) assuming a air parcel at the surface is lifted upward. Bare soil is used for the entire computational domain.

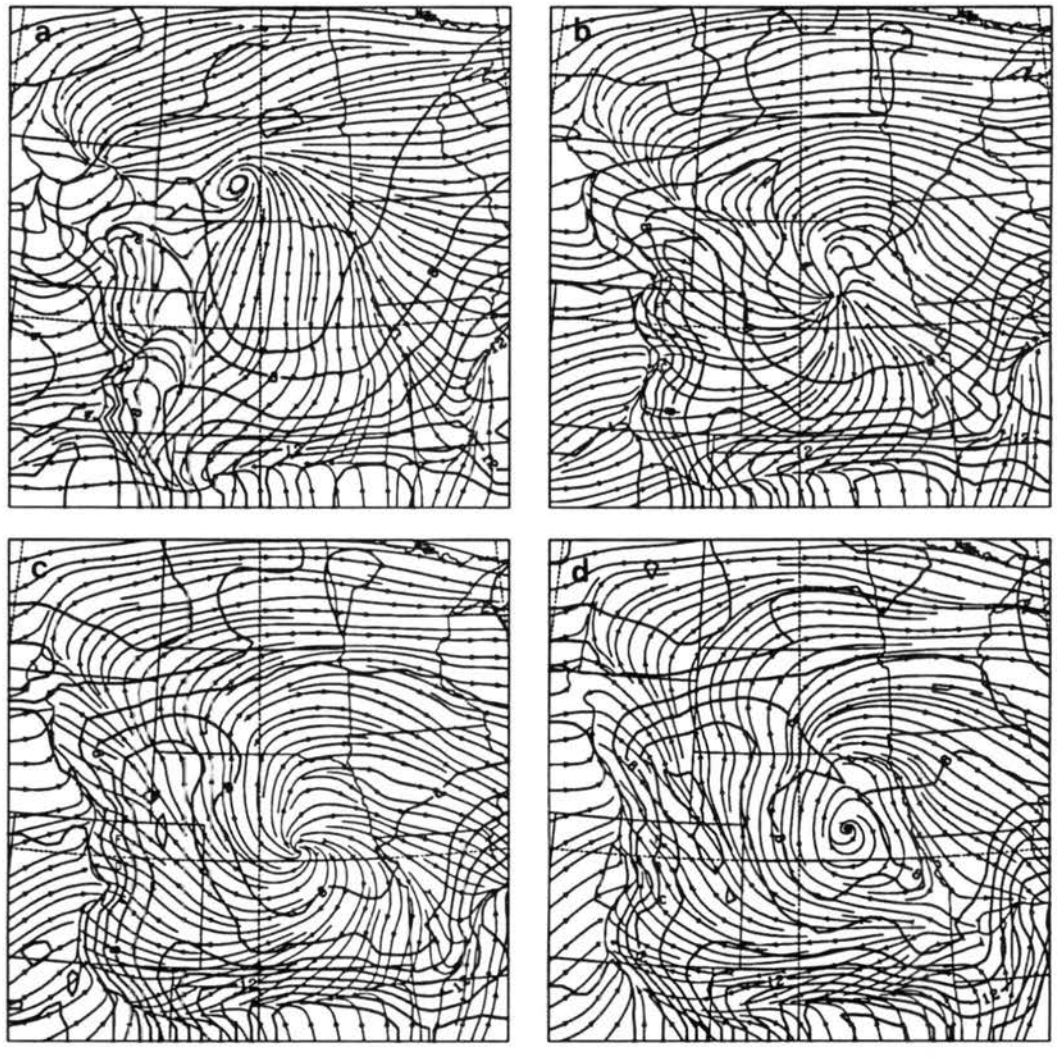

Figure 6.12: RAMS model simulated streamline at the lowest atmospheric level. The thick contour lines are water vapor mixing ratio. Bare soil is used for the entire computational domain.

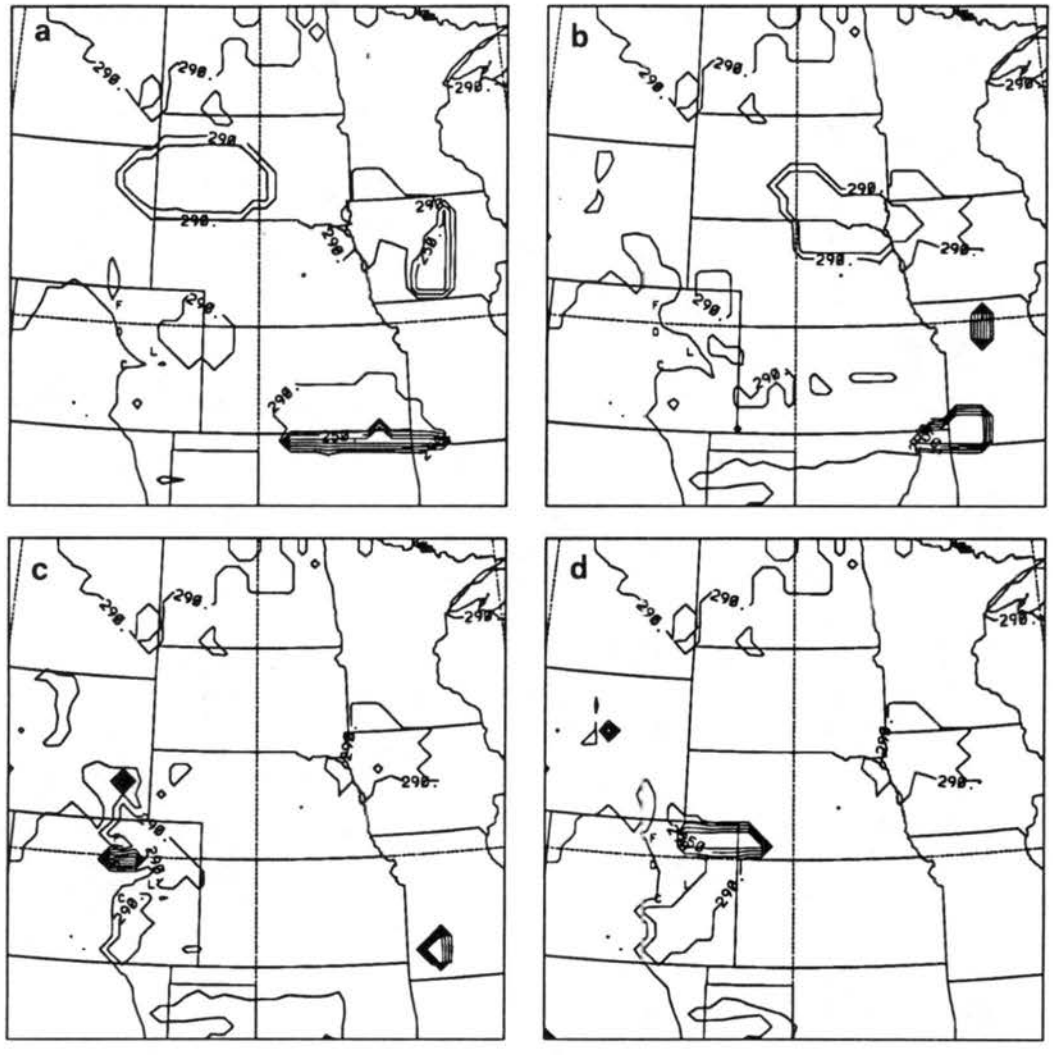

Figure 6.13: Same as Figure 6.9 but for a vegetation covered surface.

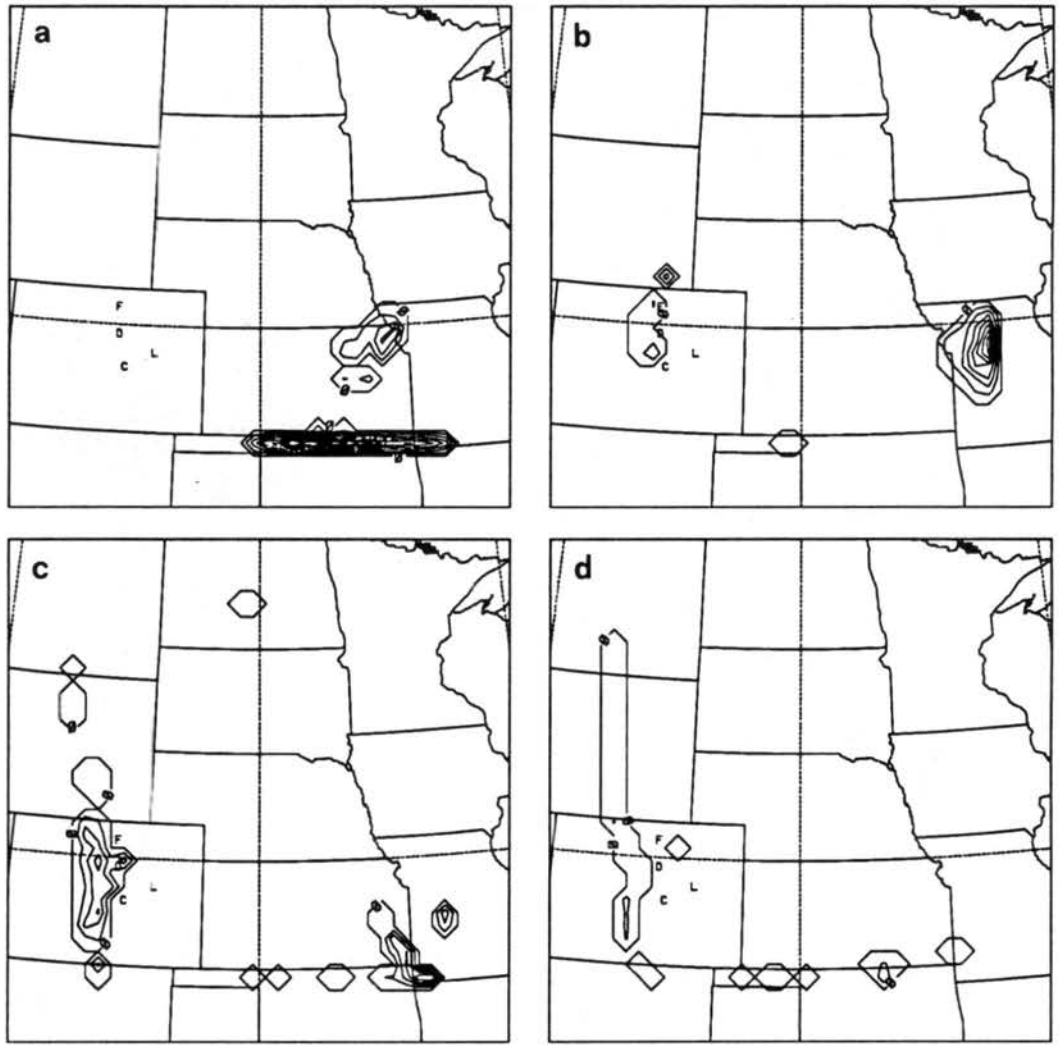

Figure 6.14: Same as Figure 6.10 but for a vegetation covered surface.

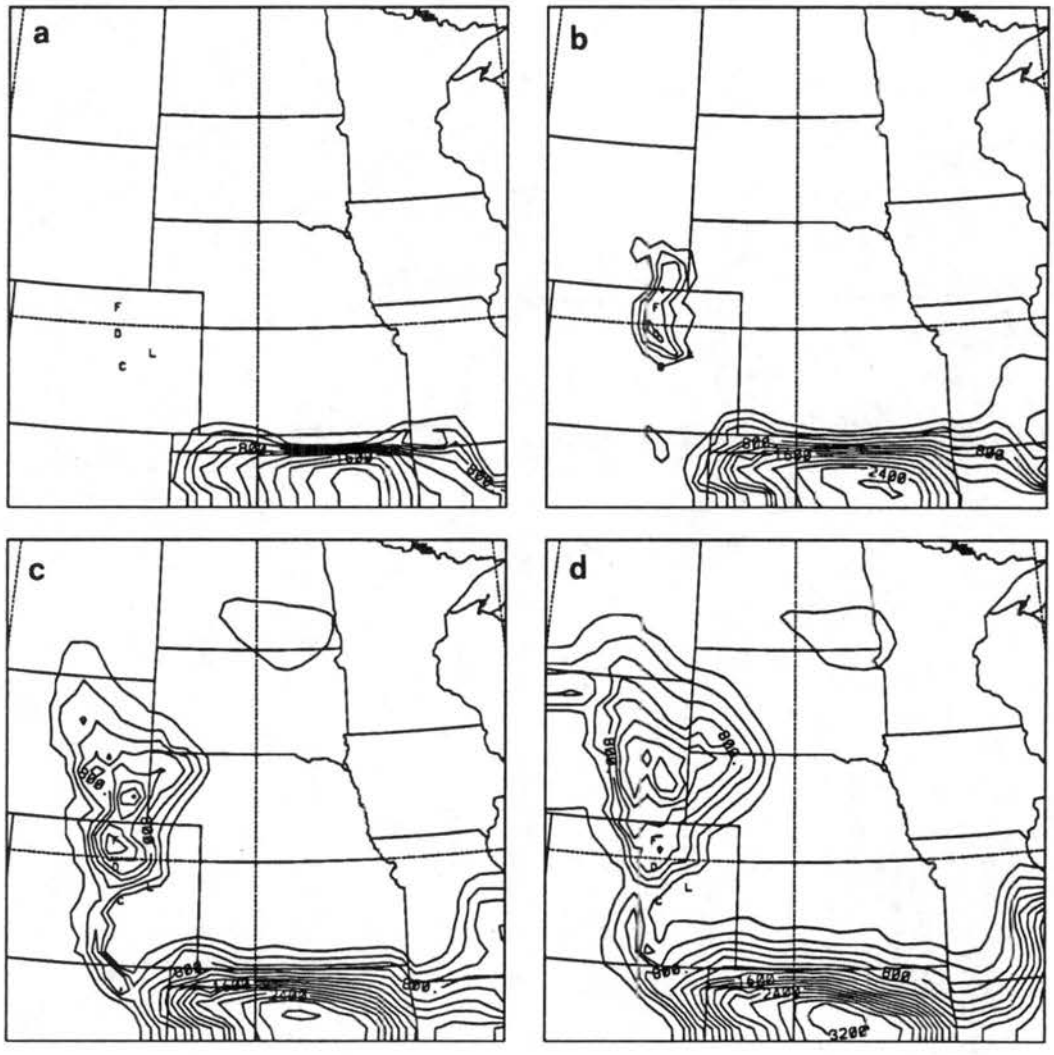

Figure 6.15: Same as Figure 6.11 but for a vegetation covered surface.

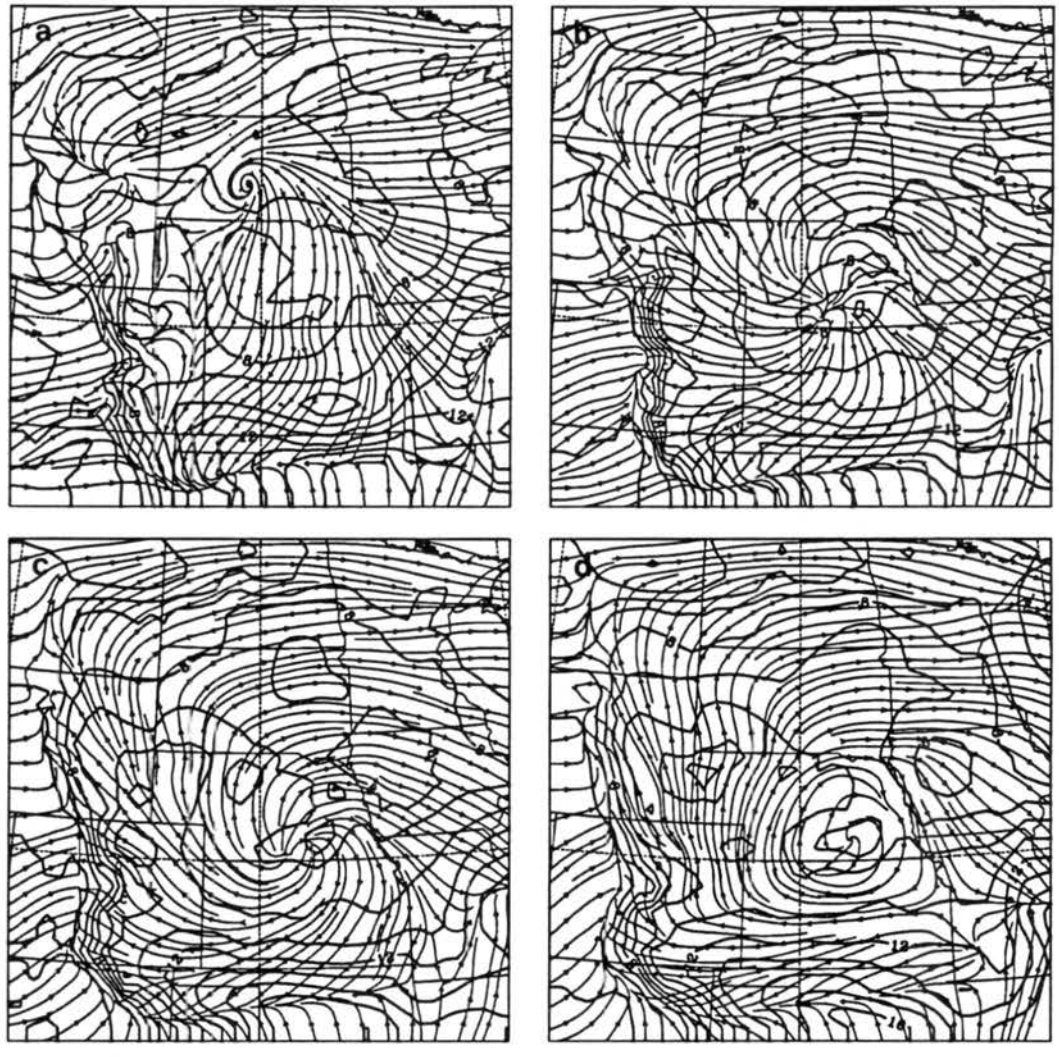

Figure 6.16: Same as Figure 6.12 but for a vegetation covered surface.

irrigated crop are turned into short grass. A LAI of 0.7 is assigned to the converted area. This number is actually higher than what it was with agricultural area since at this time of the year the crop has not yet fully matured and a considerable area of the substrate is exposed to the atmosphere. Again, the LEAF parameterization is fully utilized in this simulation.

Over all, the IR temperature (Figure 6.17) fields show similar features as shown in the bare soil experiment. Convective activity at 1800 UTC and 0000 UTC are more wide spread that the simulation with real vegetation. The convection over Colorado is also more organized along the Front Range when Figures 6.18 and 6.14 are compared. Much higher CAPE over the Colorado Front Range and southeastern Wyoming is shown later in the day (see Figure 6.19) due to the excess amount of transpiration. This is also evident in surface water vapor mixing ratio (Figure 6.20) where the value over eastern Colorado is more than 12 $g\,kg^{-1}$. There is another area that shows a substantial impact. The surface cover in eastern Nebraska and most of Iowa has been turned into grassland in this simulation. Since a higher LAI is assigned to the grass, more transpiration is found in this area and results in higher surface humidity (see Figures 6.20 and 6.16). This further demonstrates that large scale agricultural activity could potentially alter the local weather and the climate.

In a summary, the simulation with current vegetation shows better results when compared to the simulations with only bare soil and with "historical" vegetation converge. This demonstrates that the existence of surface heterogeneities resulting from man's agricultural activities has substantially altered the local weather for this particular case. Although the simulations with vegetation coverage produce a lower atmosphere that is too moist, the results can probably be improved using better soil moisture and soil texture data. In any case, the sensitivity of the regional meteorological conditions to the surface landscape has been convincingly illustrated.

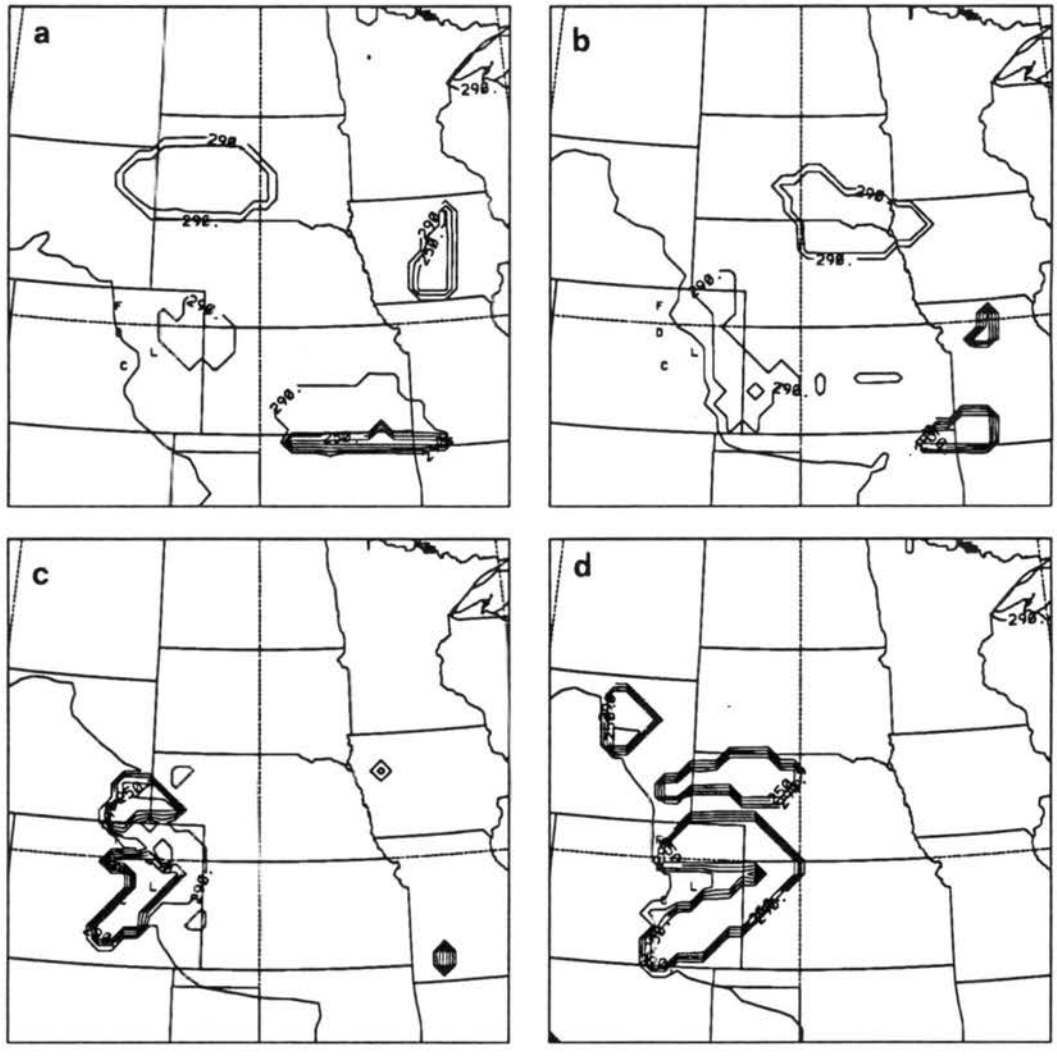

Figure 6.17: Same as Figure 6.9 but for a vegetation covered surface with agricultural area replaced by wild short grass.

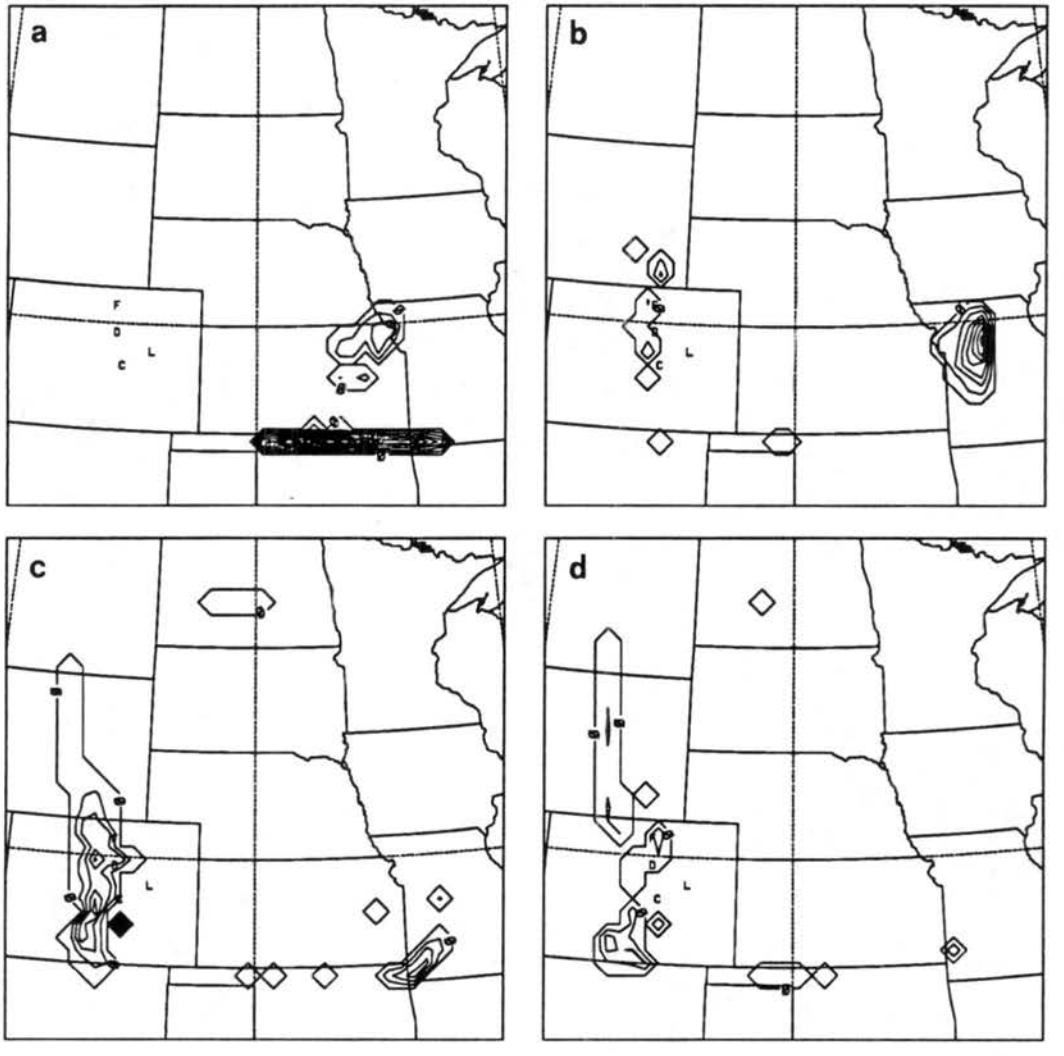

Figure 6.18: Same as Figure 6.10 but for a vegetation covered surface with agricultural area replaced by wild short grass.

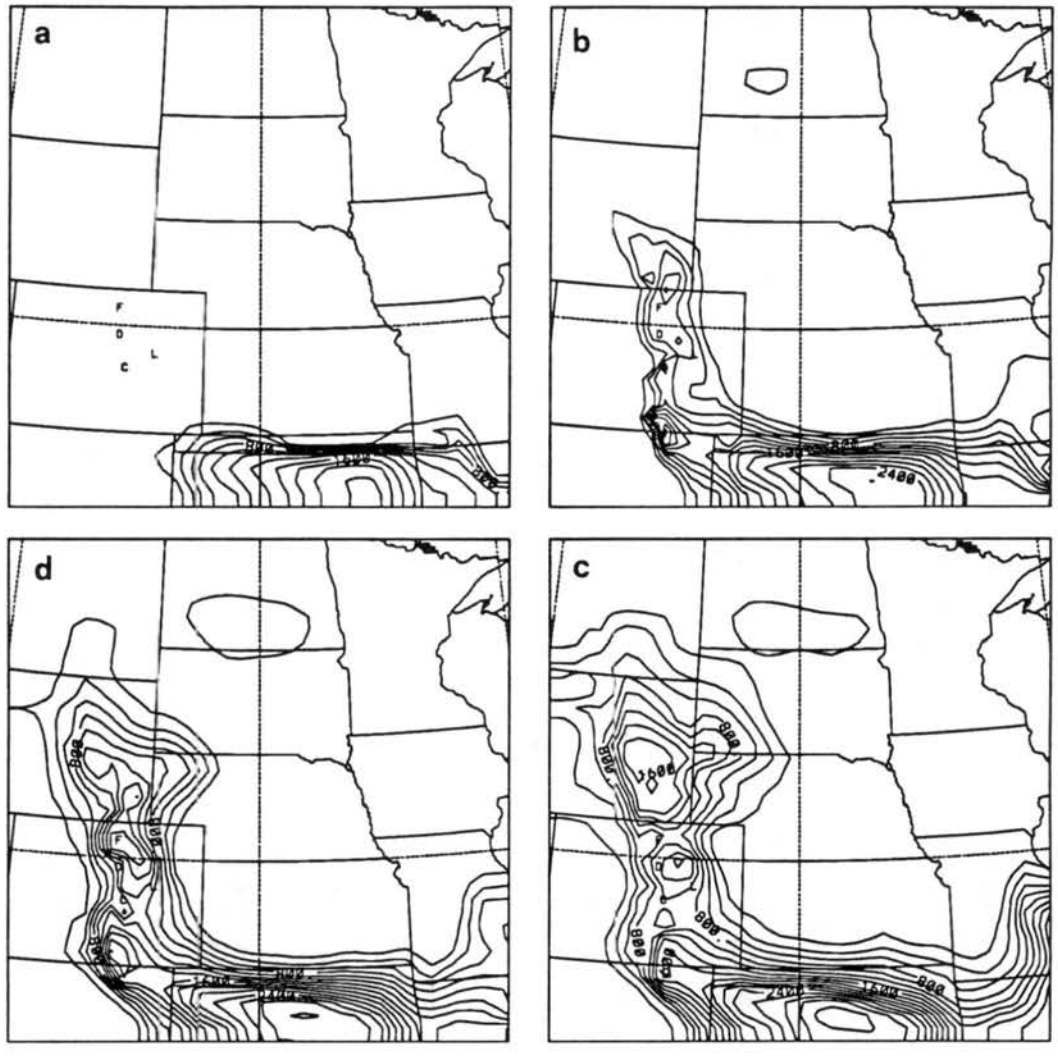

Figure 6.19: Same as Figure 6.11 but for a vegetation covered surface with agricultural area replaced by wild short grass.

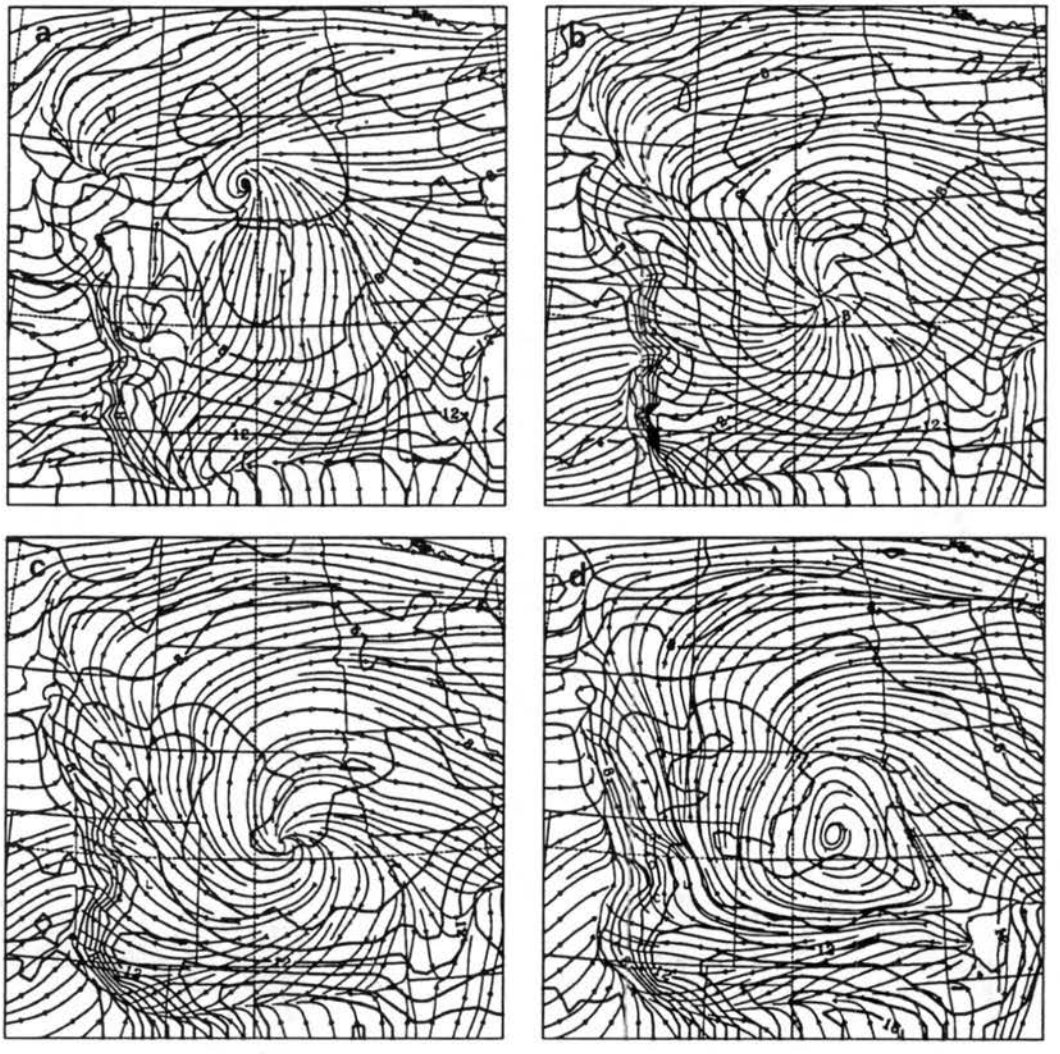

Figure 6.20: Same as Figure 6.11 but for vegetation covered surface with agricultural area replaced by wild short grass.

Chapter 7

SUMMARY, CONCLUSION AND SUGGESTIONS FOR FURTHER RESEARCH

7.1 Summary and Conclusions

A new and extended vegetation model for use in a mesoscale meteorological model has been developed based on Avissar and Mahrer (1988). The Land Ecosystem-Atmosphere Feedback (LEAF) model uses an elevated canopy structure, an above–canopy aerodynamic resistance, two in–canopy aerodynamic resistances, and one stomatal conductance functions. The air temperature and humidity are assumed to be constant in the canopy whereas the wind and radiation follow specified vertical profiles. A simple dump-bucket method is used to parameterize the interception of precipitation and a multi-layer soil model is utilized to handle the vertical transfer of soil water. Evaporation from soil and wet leaves and transpiration from dry leaves are evaluated separately. The soil water uptake is based on soil water potential rather than on the length of roots. Separate energy budgets for vegetation and for the soil are used in order to remove unnecessary assumptions on energy partition between the vegetation and the substrate. Primary parameters are LAI, maximum stomatal conductance, and albedo. Secondary parameters include displacement height and environmental controls on stomatal function.

The LEAF model has been implemented into the CSU-RAMS as an optional surface module. Due to the complexity of the LEAF model, statistical methods are used to improve LEAF model performance. The Multi-response Randomized Block Permutation (MRBP) procedure is used to guide the choice of model parameter values. The LEAF model is first "calibrated" using field observations and then tested against two independent data sets. The result shows the model can realistically re-produce the observed

latent and sensible heat fluxes with small error. The Fourier Amplitude Sensitivity Test (FAST) is applied to better understand the model behavior in response to the changes in model parameters. The most important conclusion from the FAST experiments is that the model responds to the changing environment quite differently for different situations which implies that a unique set of parameter can not be used for all environmental conditions. Nevertheless, when the observational data record is long enough, the model can be calibrated to work most of the time.

LEAF is then used to study the growth of boundary layer and local thermal circulations generated by surface inhomogeneities. Results show that the atmospheric boundary layer is substantially cooler and more moist over unstressed vegetation than over bare dry soil. The atmospheric boundary layer is shallower and more moist when above unstressed vegetation surface while it is deeper and drier when above stressed vegetation or a bare dry soil surface. Thermally forced circulation can result from the juxtaposition of two vegetation type due to different biophysical characteristics. When the turbulence in the atmospheric boundary layer is strong enough and the moisture is high enough, cumulus clouds are expected to form in response to the enhanced vertical mixing. Moreover, if the atmospheric is convectively unstable, cumulus convective clouds are expected to form and to be particularly enhanced within the convergence zones of the local thermal circulation which result from the juxtaposition of the different land surfaces.

Results from three-dimensional simulations show that the surface spatial heterogeneities made by vegetation play an important role in generating local convective storms. The simulation using real surface coverage data produced the best result in terms of storm location and size. However, the surface is too moist compared to the observation. This can be due to an error in the soil moisture profile. Methods to better evaluate soil moisture for input models with a vegetation surface need to be found. The simulation using "historical" vegetation cover produced a very different result than from the simulation with real vegetation cover. The lack of spatial distribution of near surface atmospheric moisture and the CAPE in this simulation indicated that human's agricultural practice has an important impact on local weather and may have already altered the local climate.

7.2 Suggestion for Further Research

Although this dissertation has attempted to resolve the problem of surface parameterization and link the surface exchange processes to the characteristics of the atmospheric boundary layer and convective storms, there is a lot more which could be done to make a better surface model. It has been a goal to use remotely sensed data when ever it is possible. However, during the course of this research several future research topics have been identified to improve the LEAF model, to improve the quality of input data, and to perform better model studies. These are

- There is an immediate need to collect data on atmospheric forcing, soil type, soil moisture and temperature, radiation, and surface fluxes for all types of vegetation. A better LEAF model parameter set that has more types of vegetation is needed if the model is to be extended to a ecosystem other than short grass prairie.

- The conversion between NDVI and LAI is not global. It varies from species to species. The two conversion formulations used in this study do not cover all the vegetation types that are observed over the central Great Plains. More work is needed to relate NDVI to LAI for different species.

- The recently proposed formulation for stomatal resistance by Sellers et al. (1992) is attractive. It relates the absorbed photosynthetically active radiation (APAR) to the respiration rate and thus the stomatal resistance.

- The effect of surface roughness length has not been investigated in detail. The range of surface roughness length and the height of vegetation used in sensitivity studies needs to be expanded.

- It has been suggested (Joe Berry, personal communication, 1992) that using a "scaled" VPD function for stomatal resistance calculation may be better especially when the air temperature is high.

- The in-canopy aerodynamic resistance functions are locally defined. It does not consider the sweeping effect by large eddies.

- Finer resolution model simulation is needed to simulate the initiation of cumulus convection and to fully utilize the USGS land-cover data base.

- An improved RAMS surface data ingestion system is needed to process raster data such as NDVI and land-cover data. The system needs to re-map the data onto model grids and to extract information such as percentage land-surface coverage by counting pixels within a model grid box.

- A better soil moisture estimation can be made using antecedent precipitation index (API) from the rain gauge data. Better yet, the soil moisture could be updated routinely using a data assimilation technique. It would be possible to couple radar observed precipitation with a land surface model like LEAF to yield high resolution soil moisture data.

- Soil surface temperature could be initialized using IR temperatures over cloud-free areas. A simple force-restore model could be used to define vertical soil temperature profiles.

- A finer resolution soil texture map is needed to better define the surface heterogeneities. A "potential" vegetation type (McGuire et al., 1992) could be deduced using soil and terrain data. This potential vegetation could be used to study the impact of human agricultural activity on local climate and weather.

- Finally, it would be possible to overlay "layers" of information (e.g. IR temperature, NDVI, land-cover class, DEM, and wind) using Geographic Information Systems (GIS) to find the "hot spots" of cumulus initiation.

Bibliography

Allaway, W. G. and F. L. Milthorpe, 1976: Structure and functioning of stomata. In *Water Deficits and Plant Growth*, Kozlowski, T. T., Editor, Academic Press, New York, 57–102.

André, J.-C., J.-P. Goutorbe, and A. Perrier, 1986: HAPEX–MOBILHY: A hydrologic atmospheric experiment for the study of water budget and evaporation flux at the climatic scale. *Bull. Amer. Meteor. Soc.*, **67**, 138–144.

Anthes, R. A., 1984: Enhancements of convective precipitation by mesoscale variations in vegetative covering in semiarid regions. *J. Climate Appl. Meteor.*, **23**, 541–554.

Argentini, S., P. J. Wetzel, and V. M. Karyampudi, 1992: Testing a detailed biophysical parameterization for land-air exchange in high-resolution boundary-layer model. *J. Appl. Meteor.*, **31**, 142–156.

Arritt, R. W., 1985: *Numerical studies of thermally and mechanically forced circulations over complex terrain.* Ph.D. dissertation, Colorado State University, Fort Collins, Colorado, 201 pp.

Asrar, G., M. Fuchs, E. T. Kanemasu, and J. L. Hatfield, 1984: Estimating absorbed photosynthetic radiation and leaf area index from spectral reflectance in wheat. *Agron. J.*, **76**, 300–306.

Avissar, R., 1992: Scaling up leaf stomatal conductance for the parameterization of land surface in atmospheric models. *Boundary-Layer Meteor.* (submitted).

Avissar, R., P. Avissar, Y. Mahrer, and B. A. Bravdo, 1985: A model to simulate response of plant stomata to environmental conditions. *Agric. For. Meteorol.*, **34**, 21–29.

Avissar, R. and Y. Mahrer, 1982: Verification study of a numerical greenhouse microclimate model. *Trans. Amer. Soc. Agric. Eng.*, **25**(6), 1711–1720.

Avissar, R. and Y. Mahrer, 1988: Mapping frost-sensitive areas with a three-dimensional local-scale numerical model. Part I: Physical and numerical aspects. *J. Appl. Meteor.*, **27**, 400–413.

Avissar, R. and R. A. Pielke, 1989: A parameterization of heterogeneous land surface for atmospheric numerical models and its impact on regional meteorology. *Mon. Wea. Rev.*, **117**, 2113–2136.

Avissar, R. and R. A. Pielke, 1991: The impact of plant stomatal control on mesoscale atmospheric circulations. *Agric. For. Meteor.*, **54**, 353–372.

Barry, R. G., 1969: Evaporation and transpiration. In *Water, Earth, and Man*, Chorley, R. J., Editor, Methuen and Co., New York, 169–184.

Brooks, C. E. P., 1928: The influence of forests on rainfall and run-off. *Quart. J. Roy. Meteor. Soc.*, **54**, 1–17.

Businger, J. A., J. C. Wangaard, Y. Izumi, and E. F. Bradley, 1971: Flux profile relationships in the atmospheric surface layer. *J. Atmos. Sci.*, **28**, 181–189.

Camillo, P. J., 1991: Using one- or two-layer models for evaporation estimation with remotely sensed data. In *Land Surface Evaporation: Measurement and Parameterization*, Schmugge, T. J. and A. J.-C., Editors, Springer-Verlag, New York, 183–197.

Chang, J.-T. and P. J. Wetzel, 1991: Effects of spatial variations of soil moisture and vegetation on the evolution of a prestorm environment: A case study. *Mon. Wea. Rev.*, **119**, 1368–1390.

Charney, J. G., W. J. Quirk, S. H. Chow, and J. Kornfield, 1977: A comparative study of the effects of albedo change on drought in semi-arid regions. *J. Atmos. Sci.*, **34**, 1366–1385.

Chen, C. and W. R. Cotton, 1983a: Numerical experimants with a one-dimensional higher order turbulence model: Simulation of the Wangara Day 33 case. *Boundary-Layer Meteor.*, **25**, 289–321.

Chen, C. and W. R. Cotton, 1983b: A one-dimensional simulation of the stratocumulus capped mixed layer. *Boundary-Layer Meteor.*, **25**, 289–321.

Chen, J., 1984a: *Mathematical analysis and simulation of crop micrometeorology.* Ph.D. dissertation, University of Utrecht, the Netherlands, Wageningen, the Netherlands, 116 pp.

Chen, J., 1984b: Uncoupled multi-layer model for the transfer of sensible and latent heat flux densities from vegetation. *Boundary-Layer Meteor.*, **28**, 213–225.

Cionco, R. M., 1972: Intensity of turbulence within canopies with simple and complex roughness elements. *Boundary-Layer Meteor.*, **2**, 435–465.

Clapp, R. B. and G. M. Hornberger, 1978: Empirical equations for some soil hydraulic properties. *Water Resour. Res.*, **14**(4), 601–604.

Clarke, R. H., A. J. Dyer, R. R. Brooke, D. G. Reid, and A. J. Troup, 1971: The Wangara experiment. Boundary-layer data. Paper no. 19. Technical report, Division of Meteor. Phys. CSIRO, Australia, 21 pp. plus data.

Collatz, G. J., J. T. Ball, C. Grivet, and J. A. Berry, 1991: Physiological and environmental regulation of stomatal conductance, photosynthesis and transpiration: a model that includes a laminar boundary layer. *Agric. For. Meteorol.*, **54**, 107–136.

Cram, J. M., 1990: *Numerical simulation and analysis of the propagation pf a prefrontal squall line.* Ph.D. dissertation, Colorado State University, Fort Collins, Colorado, 332 pp.

Cram, J. M., R. A. Pielke, and W. R. Cotton, 1992: Numerical simulation and analysis of a prefrontal squall line. Part I: Propagation of the squall line as an internal gravity wave. *J. Atmos. Sci.*, **49**, 189–208.

Deardorff, J. W., 1978: Efficient prediction of ground surface temperature and moisture, with inclusion of a layer of vegetation. *J. Geophys. Res.*, **83**(C4), 1889–1903.

Dickinson, R. E., A. Henderson-Sellers, P. J. Kennedy, and M. F. Wilson, 1986: Biosphere-atmosphere transfer scheme for the NCAR community climate model. Technical Report NCAR/TN-275+STR, NCAR, Boulder, 69 pp.

Eidenshink, J. C., 1992: The 1990 Conterminous U. S. AVHRR data set. *Photo. Eng. Rem. Sens.*, **58**, 809–813.

Garratt, J. R., 1992: On the sensitivity of climate simulations to land-surface and atmospheric boundary-layer treatments in GCMs – A review. *J. Clim.* submitted.

Garrett, A. J., 1982: A parameter study of interactions between convective clouds, the convecti ve boundary layer, and a forest surface. *Mon. Wea. Rev.*, **110**, 1041–1058.

Gates, D. M., 1980: *Biophysical Ecology.* Springer-Verlag, New York, 611 pp.

Goudriaan, J., 1989: Simulation of micrometeorology of crops, some methods and their problems, and a few results. *Agric. For. Meteorol.*, **47**, 239–258.

Goudriaan, J. and P. E. Waggoner, 1972: Simulating both aerial microclimate and soil temperature from observations above the foliar canopy. *Neth. J. Agric. Sci.*, **20**, 104–124.

Graetz, R. D., 1991: The nature and significance of the feedback of changes in terrestrial vegetation on global atmospheric and climatic change. *Climatic Change*, **18**, 147–173.

Hadfield, M. G., W. R. Cotton, and R. A. Pielke, 1992a: Large-eddy simulations of thermally forced circulations in the convective boundary layer. Part I: A small-scale circulation with zero wind. *Boundary-Layer Meteor.*, **57**, 79–114.

Hadfield, M. G., W. R. Cotton, and R. A. Pielke, 1992b: Large-eddy simulations of thermally forced circulations in the convective boundary layer. Part II: The effect of changes in wavelength and wind speed. *Boundary-Layer Meteor.*, **58**, 307–328.

Heckman, S. T., 1991: Numerical simulation of cirrus clouds – FIRE case study and sensitivit y analysis. Master's thesis, Colorado State University, Fort Collins, Colorado, 132 pp.

Henderson-Sellers, A., M. F. Wilson, G. Thomas, and R. E. Dickinson, 1986: Current global land-surface data sets for use in climate related studies. Technical Report NCAR/TN-272+STR, NCAR, Boulder, 110 pp.

Idso, S., R. Jackson, B. Kimball, and F. Nakayama, 1975: The depandence of bare soil albedo on soil water content. *J. Appl. Meteor.*, **14**, 109–113.

Inoue, E., 1963: On the turbulent structure of airflow within crop canopies. *J. Meteor. Soc. Japan*, **41**, 317–326.

Izumi, Y., 1971: *Kansas 1968 Field Program Data Report.* Air Force Cambridge Res. Lab. AFCRL-72-0041, Envir. Res. Paper No. 379, Hanscom AFB, MA, 79 pp.

Izumi, Y. and J. S. Caughey, 1976: *Minnesota 1973 Atmospheric Boundary Layer Experiment Data Report.* Air Force Cambridge Res. Lab. AFCRL-TR-76-0038, Envir. Res. Paper No. 547, Hanscom AFB, MA, 28 pp.

Jarvis, P. G., 1976: The control of transpiration and photosynthesis by stomatal conductance found in canopies in the field. *Philos. Trans. R. S. London Ser. B*, **273**, 593–610.

Jarvis, P. G. and K. G. McNaughton, 1986: Stomatal control of transpiration: Scaling up from leaf to region. *Adv. Ecolog. Res.*, **15**, 1–49.

Jones, P. G., 1983: *Plans and the Microclimate: A Quantitative Approach to Environmental Plant Physiology.* Cambridge University Press, New York, 323 pp.

Kanemasu, E. T., U. D. Rosenthal, R. J. Raney, and L. R. Stone, 1977: Evaluation of an evapotranspiration model for corn. *Agron. J.*, **69**, 461–464.

Klemp, J. B. and D. R. Durran, 1983: An upper boundary condition permitting internal gravity wave radiation in mumerical mesoscale models. *Mon. Wea. Rev.*, **111**, 430–444.

Klemp, J. B. and R. B. Wilhelmson, 1978: The simulation of three-dimensional convective storm dynamics. *J. Atmos. Sci.*, **35**, 1070–1096.

Koster, R., J. Jouzel, R. Suozzo, and G. Russel, 1986: Global sources of local precipitation as determined by the NASA/GISS G CM. *Geophy. Res. Let.*, **13**, 121–124.

Kramer, P. J., 1949: *Plant and Soil Water Relationships.* McCraw Hill, New York, 347 pp.

Lakhtakia, M. D., 1991: *A comparison of simple and complex treatments of surface hydrology and thermodynamics suitable for mesoscale atmospheric models.* Ph.D. dissertation, Pennsylvania State University, State College, Pennsylvania, 126 pp.

Lee, T. J. and R. A. Pielke, 1992: Estimating the soil surface specific humidity. *J. Appl. Meteor.*, **31**, 480–484.

Lettau, H. H. and B. Davidson, 1957: *Exploring the Atmosphere's First Mile, Proceedings of the Great Plains Field Program 1 August to 8 September 1953, O'Nill, Nebraska*, volume I and II. Pergamon Press, New York, 578 pp.

Louis, J.-F., 1979: A parametric model of vertical eddy fluxes in the atmosphere. *Boundary-Layer Meteor.*, **17**, 187–202.

Loveland, T. R., J. W. Merchant, D. O. Ohlen, and J. F. Brown, 1991: Development of a land-cover characteristics database for the conterminous U. S. *Photo. Eng. Rem. Sens.*, **57**(11), 1453–1463.

Lovelock, J. E., 1979: *GAIA: A New Look at Life on Earth.* Oxford University Press, Oxford, 157 pp.

Lynn, B. H. and T. N. Carlson, 1990: A stomatal resistance illustrating plant vs. external control of transpiration. *Agric. For. Meteor.*, **52**, 5–43.

Mafhouf, J. F., E. Richard, and P. Mascart, 1987: The influence of soil and vegetation on the development of mesoscale circulations. *J. Climate Appl. Meteor.*, **26**, 1483–1495.

Mahfouf, J.-F., 1991: Analysis of soil moisture from near–surface parameters: A feasibility study. *J. Appl. Meteor.*, **30**, 1534–1547.

Mahrer, Y. and R. A. Pielke, 1977: A numerical study of the airflow over irrigular terrain. *Contrib. Atmos. Phys.*, **50**, 98–113.

Manabe, S. and J. Holloway, J. L., 1975: The seasonal variation of the hydrological cycle as simulated by a global model of the atmosphere. *J. Geophys. Res.*, **80**, 1617–1649.

Martin, P., N. J. Rosenberg, and M. S. McKenny, 1989: Sensitivity of evapotranspiration in a wheat field, a forest, and a grassland to changes in climate and direct effects of carbon dioxide. *Climatic Change*, **14**, 117–151.

McCumber, M. C., 1980: *A numerical simulation of the influence of heat and moisture fluxes upon mesoscale circulations.* Ph.D. dissertation, University of Virginia, 255 pp.

McCumber, M. C. and R. A. Pielke, 1981: Simulation of the effects of surface fluxes of heat and moisture in a mesoscale numerical model. Part I: Soil layer. *J. Geophys. Res.*, **86**(C10), 9929–9938.

McGuire, A. D., J. M. Melillo, L. A. Joyce, D. W. Wicklighter, A. L. Grace, B. I. Moore, and C. J. Vorosmarty, 1992: Interactions between carbon and nitrogen dynamics in estimating net primary productivity for potential vegetation in North America. *Global Biogeochem. Cycles*, **6**, 101–124.

Mielke, Jr., P. W., 1984: Meteorological applications of permutation techniques based on distance functions. In *Handbook of Statistics, Vol. 4*, Krishnaiah, P. R. and P. K. Sen, Editors, North–Holland Publishing Co., Amsterdam, 813–830.

Mielke, Jr., P. W., 1991: The application of multivariate permutation methods based on distance functions in the earth sciences. *Earth–Sci. Rev.*, **31**, 55–71.

Monin, A. S. and A. M. Obukhov, 1954: Basic laws of turbulent mixing in the atmosphere near the ground. *Tr. Akad. Nauk., SSSR Geophiz. Inst.*, **24**, 1963–1987.

Monteith, J. L., 1965: Evaporation and the environment. *Symp. Soc. Expl. Biol.*, **19**, 205–234.

Monteith, J. L. and M. H. Unsworth, 1990: *Principles of Environmental Physics*, 2. Edward Arnold, New York, 291.

Moran, M. D., 1992: *Numerical Modelling of Mesoscale Atmospheric Dispersion.* Ph.D. dissertation, Colorado State University, Fort Collins, Colorado.

Mylne, M. F. and P. R. Rowntree, 1992: Modelling the effects of albedo change associated with tropical deforestation. *Climatic Change*, **21**, 317–343.

Nemani, R. and S. W. Running, 1989: Testing a theoretical climate-soil-leaf area hydrologic equilibrium of forests using satellite data and ecosystem simulation. *Agric. Forest Meteorol.*, **44**, 245–260.

Noilhan, J. and S. Planton, 1989: A simple parameterization of land surface processes for meteorological models. *Mon. Wea. Rev.*, **117**, 536–549.

Ookouchi, Y., M. Segal, R. C. Kessler, and R. A. Pielke, 1984: Evaluation od soil moisture effects on the generation and modification of mesoscale circulations. *Mon. Wea. Rev.*, **112**, 2281–2291.

Otterman, J., 1974: Baring high–albedo soils by overgrazing: A hypothesized desertification mechanism. *Science*, **186**, 531–533.

Otterman, J., 1977: Anthropogenic impact on the surface of the earth. *Climatic Change*, **1**, 137–155.

Otterman, J., A. Manes, S. Rubin, P. Alpert, and D. O. Starr, 1990: An increase of early rains in southern Israel following land-use changes? *Boundary-Layer Meteor.*, **53**, 333–351.

Paulson, C. A., 1970: Mathematical representation of wind speed and temperature profiles in the unstable atmospheric surface layer. *J. Appl. Meteor.*, **9**, 857–861.

Penman, H. L., 1948: Natural evaporation from open water, bare soil, and grass. *Proc. Roy. Soc. London*, **A193**, 120–146.

Pielke, R. A., 1984: *Mesoscale Meteorological Modeling.* Academic Press, Orlando, Florida, 612 pp.

Pielke, R. A. and R. Avissar, 1990: Influence of landscape structure on local and regional climate. *Landscape Ecology*, **4**, 133–155.

Pielke, R. A., W. R. Cotton, R. L. Walko, C. J. Tremback, W. A. Lyons, L. D. Grasso, M. E. Nicholls, D. A. Moran, T. J. Lee, and J. H. Copeland, 1992: A comprehen[hsive meteorological modeling system – RAMS. *Meteor. Atmos. Phys.* accepted.

Pielke, R. A. and M. Segal, 1986: Mesoscale circulations forced by differential terrain heating. In *Mesoscale Meteorology and Forecasting*, Ray, P. S., Editor, American Meteorological Society, Boston, Massachusetts, 516–548.

Pielke, R. A., J. Weaver, T. Kittel, and T. J. Lee, 1990: Use of NDVI for mesoscale modeling. In *Proc. Workshop on the "Use of Satellite-Derivied Vegetation Indices in Weather and Climate Prediction Models"*, February 26–27, Camp Springs, Maryland, 83–85.

Pielke, R. A. and X. Zeng, 1989: Influence on severe storm development of irrigate land. *Nat. Wea. Dig.*, **14**, 16–17.

Pielke, R. A., X. Zeng, and R. L. Walko, 1991: The predictability of atmospheric features in response to heterogeneous surface heating. In *Proc. Ninth Conference on Numerical Weather Prediction*, October, American Meteorological Society, Boston, Massachusetts.

Rabin, R. M., S. Stadler, P. J. Wetzel, D. J. Stensrud, and M. Gregory, 1990: Observed effects of landscape variability on convective clouds. *Bull. Amer. Meteor. Soc.*, **71**, 272–280.

Raupach, M. R. and J. J. Finnigan, 1988: Single-layer models of evaporation from plant canopies are incorrect but useful, whereas multilayer models are correct but useless: Discuss. *Aust. J. Plant Physiol.*, **15**, 705–716.

Richardson, L. F., 1922: *Weather Prediction by Numerical Process.* Cambridge University Press, London, 236 pp.

Rind, D., 1982: The influence of ground moisture conditions in North America on summer climate as modeled in the GISS GCM. *Mon. Wea. Rev.*, **110**, 1487–1494.

Rowentree, P. R. and J. A. Bolton, 1983: Simulation of the atmospheric response to soil moisture anomalies over europe. *Quart. J. Roy. Meteor. Soc.*, **109**, 501–526.

Rutter, A. J., 1975: The hydrological cycle in vegetation. In *Vegetation and the atmosphere, Vol. I*, Monteith, J. L., Editor, Academic Press, New York, 111–154.

Schädler, G., 1990: Triggering of atmospheric circulations by moisture inhomogeneities of the earth's surface. *Boundary-Layer Meteor.*, **51**, 1–29.

Schadler, G., N. Kalthoff, and F. Fiedler, 1990: Validation of a model of heat, mass and momentum exchange over vegetated surfaces using LOTREX-10E/HIBE88 data. *Contrib. Atmos. Phys.*, **63**, 85–100.

Schukla, J. and Y. Mintz, 1982: Influence of land-surface evapotranspiration on the earth's climate. *Science*, **215**, 1498–1501.

Schwartz, M. D. and T. R. Karl, 1990: Spring phenology: Nature's experiment to detect the effect of "green-up " on surface maximum temperatures. *Mon. Wea. Rev.*, **118**, 883–890.

Segal, M., R. Avissar, M. C. McCumber, and R. A. Pielke, 1988: Evaluation of vegetation effects on the generation and modification of mesoscale circulations. *J. Atmos. Sci.*, **45**, 2268–2292.

Segal, M., W. Schreiber, G. Kallos, and R. A. Pielke, 1989: The impact of crop areas in northeast colorado on midsummer mesoscale thermal circulations. *Mon. Wea. Rev.*, **117**, 809–825.

Sellers, P. J., J. A. Berry, G. J. Collatz, C. B. Field, and F. G. Hall, 1992: Canopy reflectance, photosynthesis and transpiration, III: A reanalysis using enzyme kinetics-electron transport models of leaf physiology. *Rem. Sen. Env.* (submitted).

Sellers, P. J., F. G. Hall, G. Asrar, D. E. Strebel, and R. E. Murphy, 1988: The First ISLSCP Field Experiment (FIFE). *Bull. Amer. Meteor. Soc.*, **69**, 22–27.

Sellers, P. J., Y. Mintz, Y. C. Sud, and A. Dalcher, 1986: A simple biosphere model (SiB) for use within general circulation models. *J. Atmos. Sci.*, **43**, 505–531.

Sellers, W. D., 1965: *Physical Climatology.* University of Chicago Press, Chicago, 272 pp.

Shuttleworth, W. J. and J. S. Wallace, 1985: Evaporation from sparse crops – an energy combination theory. *Quart. J. Roy. Meteor. Soc.*, **111**, 839–855.

Smolarkiewicz, P. K. and T. L. Clark, 1985: Numerical simulation of the evolution of a three-dimensional field of cumulus clouds. Part I: Model description, comparison with observations and sensitivity studies. *J. Atmos. Sci.*, **42**, 502–522.

Sud, Y. C., W. C. Chao, and G. K. Walker, 1992: Dependence of convective rainfall on vegetation. *Science.* submitted.

Thom, A. S., 1972: Momentum, mass and heat exchange of vegetation. *Quart. J. Roy. Meteor. Soc.*, **98**, 124–134.

Thomas, G. and P. R. Rowntree, 1992: The boreal forest and climate. *Quart. J. Roy. Meteor. Soc.*, **118**, 469–497.

Tremback, C. J., 1991: *Numerical simulation of a mesoscale convective complex: Model development and numerical results.* Ph.D. dissertation, Colorado State University, Fort Collins, Colorado, 247 pp.

Tremback, C. J. and R. Kessler, 1985: A surface temperature and moisture parameterization for use in mesoscale models. In *Proc. Seventh Conference on Numerical Weather Prediction*, American Meteorological Society, Boston, Massachusetts, 355–358.

Tripoli, G. J., 1988: *A numerical investigation of aaan orogenic mesoscale convective system.* Ph.D. dissertation, Colorado State University, Fort Collins, Colorado, 290 pp.

Tripoli, G. J. and W. R. Cotton, 1989a: A numerical study of an observed orogenic mesoscale convective system. Part I: Simulated genesis and comparison with observations. *Mon. Wea. Rev.*, **117**, 273–304.

Tripoli, G. J. and W. R. Cotton, 1989b: A numerical study of an observed orogenic mesoscale convective system. Part II: Analysis of governing dynamics. *Mon. Wea. Rev.*, **117**, 305–328.

Uliasz, M., 1988: Application of the FAST method to analyze the sensivity-uncertainty of a Lagrangian model of sulphur transport in Europe. *Water, Air and Soil Pollution*, **40**, 33–49.

Verma, S. B., J. Kim, and R. J. Clement, 1989: Carbon dioxide, water vapor, and sensible heat fluxes over a tall grass prairie. *Boundary-Layer Meteor.*, **46**, 53–67.

Walker, J. and P. R. Rowntree, 1977: The effect of soil moisture on circulation and rainfall in a tropical mod el. *Quart. J. Roy. Meteor. Soc.*, **103**, 29–46.

Walko, R. L., W. R. Cotton, and R. A. Pielke, 1992: Large-eddy simulations of the effects of hilly terrain on the convective boundary layer. *Boundary-Layer Meteor.*, **58**, 133–150.

Walko, R. L. and C. J. Tremback, 1992: *RAMS– The Regional Atmospheric Modeling System, Version 2C: User's Guide.* ASTeR, Inc., P.O. Box 466, Fort Collins, Colorado, 86 pp.

Wallace, J. S., J. M. Robert, and M. V. K. Sivakumar, 1990: The estimation of transpiration from sparse dryland millet using stomatal conductance and vegetation area indices. *Agric. For. Meteorol.*, **51**, 35–49.

Weaver, J. F. and N. J. Dosken, 1991: High Plains severe weather – ten years after. *Wea. Forecasting*, **6**, 411–414.

Weaver, J. F., J. F. W. Purdom, and E. J. Szoke, 1992: Analysis of the 6 June 1990 Limon, Colorado tornado case. *Wea. Forecasting.* submitted.

Wetzel, P. J. and S. Argentini, 1990: The sensivity of daytime low cloud amount to vegetation cover, soil moisture and pre-dawn sounding – Two case studies. In *Proc. Eighth Conference on Hydrometeorology*, AMS, American Meteorological Society, Boston, Massachusetts, 12–17.

Wilson, M. F. and A. Henderson-Sellers, 1985: A global archive of land cover and soils data for use in general circulat ion climate models. *J. Climatology*, **5**, 119–143.

Winkel, T. and S. Rambal, 1990: Stomatal conductance of some grapevines growing in the field under a mediterranean environment. *Agric. For. Meteor.*, **51**, 107–121.

Yan, H. and R. A. Anthes, 1987: The effect of variations in surface moisture on mesoscale circulations. *Mon. Wea. Rev.*, **116**, 192–208.

Zeng, X., 1992: *Chaos Theory and its Application in the Atmosphere.* Ph.D. dissertation, Colorado State University, Fort Collins, Colorado, 178 pp.